Publishing Office: *Department of Industrial Engineering, Engineering Faculty, King Abdulaziz University, P.O. Box: 80204 Jeddah 21589 Saudi Arabia*; Tel: +966 533 107628; Fax: +966 2 2486695.

Frequency: Journal of International Environmental Application and Science (ISSN 2636-7661) is published 4 times per year.

Aims and Scope: Journal of International Environmental Application and Science is dedicated to detailed and comprehensive investigations, analyses and appropriate reviews of the interdisciplinary aspects of renewable sources, municipal and industrial solid wastes, waste disposal, environmental pollution, environmental science and education, biomass, agricultural residues, energy sources, hazardous emissions, incineration, environmental protection topics included experimental, analytical, industrial studies, hydrological recycling, water pollution, water treatment, air pollution, gas removal and disposal, environmental pollution modelling, noise pollution and control. Suitable topics are also included regarding the efficient environmental management and use of air, water and land resources.

Publication information: Please address all your requests regarding orders and subscription queries to: *Dr. S. Dursun*, Environmental Engineering Department, Engineering Faculty, Konya Technical University, Konya, TURKEY. Tel: +90 3332 2051559, Fax: +90 332 2410635, Mobil: + 90 536 5954591.
E-mail: jieas@jieas.com

Guide for Authors

Submission of Papers: Manuscripts for publication may be sent to the Editor-in-Chief, a member of the Editorial Board. Submission address is: Editor-in-Chief, Dr. S. Dursun, Environmental Engineering Department, Engineering & Natural Science Faculty, Konya Technical University, Konya, TURKEY. Manuscripts can also be sent to any member of the Editorial Board (see inside front cover for addresses). Although this journal is international in scope, all articles must be in the English language. Potential contributors whose first language is not English are urged to have their manuscript competently edited prior to submission. Papers should be written in the third person in an objective, formal and impersonal style.

Manuscript Preparation:

General: Manuscripts must be typewritten, double-spaced with wide margins on one side of white paper. Good quality printouts with a font size of 12 pt are required. The corresponding author should be identified (include E-mail address, Telephone and Fax number). Full postal addresses must be given for all co-authors. Two hard copies of the manuscript should be submitted by regular mail.

Abstracts: Each manuscript must be including a brief abstract and a short list of keywords.

Text: Follow this order when typing manuscripts: Title, Authors, Affiliations, Abstract, Keywords, Introduction, Main text, Conclusion, Acknowledgements, Appendix, References, Vitae and Figure Captions followed by the Figures and Tables. Pages should be numbered consecutively. The corresponding author should be identified with an asterisk and footnote.

Symbols and Units: All Greek letters and unusual symbols should be identified by name in the margin, the first time they are used. SI units should be used wherever possible, as recommended in ISO 1000 and BS 5555.

References: All publications cited in the text should be presented in a list of references following the text of the manuscript. In the text refer to the author's name (without initials) and year of publication (*e.g.* "since Dursun (1993) has shown that..." or "This is in agreement with results obtained later (Boddy, 1984)". For three or more authors use the first author followed by "*et al.*", in the text. The list of references should be arranged alphabetically by authors' names. The manuscript should be carefully checked to ensure that the spelling of authors' names and dates are exactly the same in the text as in the reference list.

References should be given in the following form:

Boddy L, (1984) The micro-environment of basidiomycete mycelia in temperate deciduous woodlands. In: *The Ecology and Physiology of the Fungal Mycelium* (Ed. by D.H. Jennings & A.D.M. Rayner), pp. 261-289. British Mycological Society Symposium 8, Cambridge University Press, Cambridge.

Dursun S, Ineson P, Frankland JC, Boddy L, (1993) Sulphite and pH effects on CO_2 evolution from decomposing angiospermous and coniferous tree leaf litters. *Soil Biology & Biochemistry* **25**, 1513-1525.

Ergas SJ, Schroeder E, Chang D, Scow K, (1994) Spatial distributions of microbial populations in biofilters. In: Proceedings of the *78th Annual Meeting and Exhibition of the Air and Waste Management Association*, pp. 19-24, Cincinnati, OH.

Hickey M, King C, (1988) *100 Families of Flowering Plants*. Cambridge University Press, Cambridge.

Littlejohn D, Wang Y, Chang S-G, (1993) Oxidation of aqueous sulphite ion by nitrogen dioxide. *Environmental Science & Technology* **27**, 2162-2167.

Illustrations: All illustrations should be provided in camera-ready form, suitable for reproduction (which may include reduction) without retouching. Photographs, charts and diagrams are all to be referred to as "Figure" and should be numbered consecutively in the order to which they are referred. They should be accompanying the manuscript, should be included within the text.

Tables: Tables should be numbered consecutively and given a suitable caption and each table should be included within the text. Footnotes to tables should be typed below the table and should be referred to by superscript lowercase letters.

Electronic Submission: Authors may submit electronic copy of their manuscript by e-mail or online submission on WEB site of the JIEAS. The final version of the manuscript should be submitted on floppy disk or CD. The electronic copy should match the hardcopy exactly. MS Word is recommended for software for article submission.

Proofs: Proofs will send to the author and should be returned 48 hours of receipt. Corrections should be restricted to typesetting errors; any others may be charged to the author. Any queries should be answered in full.

Subscription: Subscription for the issue contains author's article published in "*Journal of International Environmental Application and Science*" is €100.00 which will be sending to the corresponding author.Journal of International Environmental Application and Science (ISSN 1307-0428) is published since 2006. Subscription rates for a year are: Institutions: € 300.00 (four issues per a year) Individuals: € 150.00 (four issues per a year)

Correspondence: Papers should be sent to: *Dr. S. Dursun*, *Environmental Engineering Department, Engineering Faculty, Selcuk University, Konya, Turkey*. It may also be sent by e-mail to jieas@jieas.com in Microsoft Office Word 2007 format.

Website**:** *http://www.jieas.com;* ***E-Mail****: jieas@jieas.com, info@jieas.com*

"Journal of International Environmental Application and Science" is indexed in:
"**Global Impact Factor**, **EBSCO, CAS Source Index (A Division of the American Chemical Society), Index Copernicus, ProQuest, CABI, Ulrich's™ Serials Analysis System, SCIRUS, ArgosBiotech, NAAEE, The University of Queensland's Institutional, The NAL Catalog (AGRICOLA), WORLDCAT Catalog, LexisNexis, The National Library of Finland, National Library of Australia, DergiPark Turkey"** *Journal Indexing List.*

C O N T E N T S

J. Int. Environ. Appl. & Sci., Vol. 15 No. 2 pp: 41-140 June, 2020

J. Int. Environmental Application & Science, Vol. 15(2): 41-47 (2020)

Research Paper

The Geological Setting of Durrës - Rodon Region in Albania

Arjol Lule*, Shaqir Nazaj

Faculty of Geology and Mining, Tirana, Albania; Faculty of Geology and Mining, Tirana, Albania.

Received March 04, 2020; Accepted April 21, 2020

Abstract: The object of this paper are some considerations on the geologic features of the region north to Shkumbin river in Albania based on the latest data from the complex studies on the relations of Kruja and Ionian zones with the South Adriatic basin. The paper highlights the tectonic features of the prognosis deep structures, facies types etc. The folding phases for this region are of Chattian, Burdigalian and Tortonian when the structures of the eastern part of Kruja zone are folded at an earlier geologic time as compared to the structures foreseen to be encountered at the western part of region. The lower tectonic stage in the studied region, as compared to the know structures of Ionian zone to the south and of Kruja zone in the east, appear with less developed tectonics and less effected by the folding tectonic phases. The influence of these folding phases over Kruja and Ionian tectonic zones has been considerable causing a mighty folding of structures and at the same time their big overlapping to the west. These facts drive us to the conclusion that the Ionian zone structures and consequently the separate tectonic belts within this zone must not extent to the north.
***Key words**: Kruja and Ionian zone, tectonic, structures.*

Introduction

The study region represents a very complicated geological area, where three tectonic zones collides: 1- Kruja tectonic zone in the east; 2- Ionian tectonic zone in the south; 3- Southern extension of the Adriatic Basin, Fig.1. There have been various opinions about the interpretation of the tectonic style in this region, which have been the subject of discussion among geologists, such as the relationship between the orogeny and platform zones, the possibility of introducing the "Sazan" zone toward the east in the northern part of the Patos-Verbas structure. These problems still have not received a solution and their clarification in the future, requires the completion of additional works of wit some complex methods. This paper will provide some consideration on these problems. The solution of these problems has a great importance in the future for more accurate orientation of the research work on the limestone formation. The information from the previous works as well as the new geological data received from the geological study methods done in the area during the last years, have been used for the preparation of this paper.

The stratigraphy and the folding phases

The oldest deposits of the Upper Cretaceous outcropped in the eastern part of the study area over Kruja, Ishëm, Tirana and Dajti structures. These deposits are represented by dolomitic limestone and organogenous - detritic limestone. These deposits are documented from the wells drilled in this region. The Paleocene-Eocene micritic limestone are placed with hiatus over the Upper Cretaceous deposits through a bauxite horizon (Velaj, 2012).

The terrigenous deposits (flysch-flyschoidal formation) of Lower Oligocene to Burdigalian are normally placed over the carbonate deposits through the marls transitional package. Upper Oligocene sediments are transgressively placed over the deposits of lower tectonic stage (carbonate and flysch formation), as it is clearly seen in the Valeshi structure. (Valbona & Sadiku, 1984). We emphasize two important things about the character of carbonate and terrigenous deposits of the Kruja tectonic zone.
Firstly: The thickness of the pelagic deposits of the Lower and Middle Oligocene is big and decreases westward direction becoming much thinner in the Ionian tectonic zone. The lower Oligocene deposits thickness is 600-1500 m, while the Middle Oligocene is 1250 m thick (Velaj, 2012). These data clearly indicate that during this geological time and later, Kruja tectonic zone was deep basin environments.
Secondly: The outcropped carbonates, and the carbonate meet by the wells drilled in the study region, in general belongs to a shallow platformic facies. This continued until the beginning of the Eocene

Corresponding: E-Mail: arjol.lule@fgjm.edu.al; Tel: +355 696 061 263

series. We note that the presence or not of flysch formation is not an argument for the presence of the platform conditions.

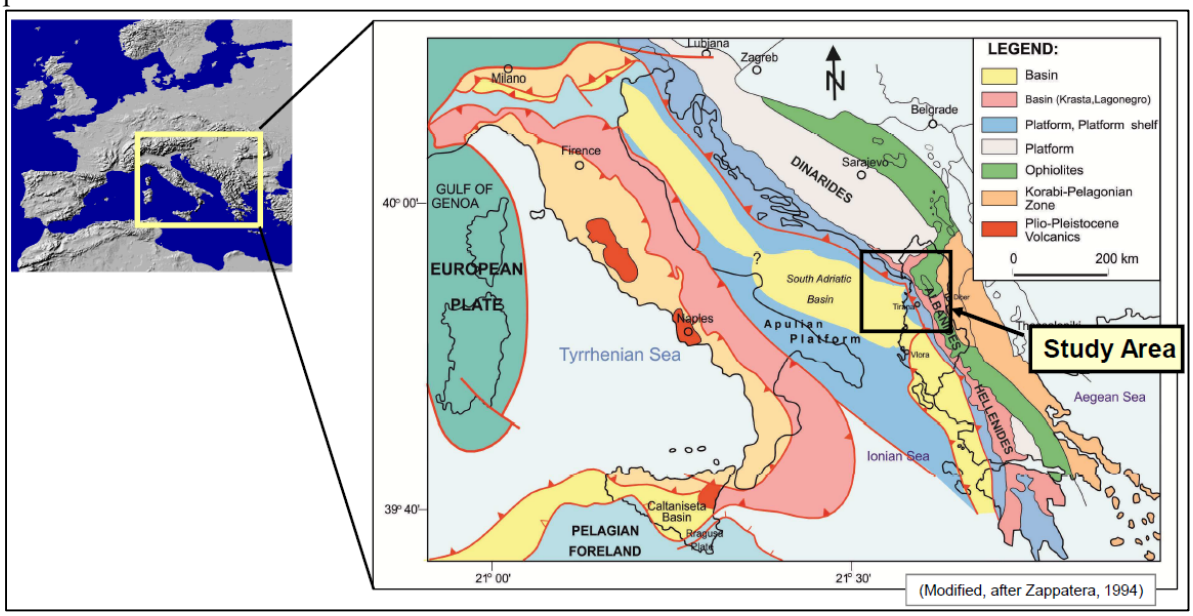

Figure 1.The location of the study region (Zappaterra, 1994)

The paleogeography conditions of the carbonate formation must be taken into consideration. Based on the sedimentation conditions, we believe that the Kruja tectonic zone existed as a platform until the beginning of the Paleocene-Eocene sedimentation, which later as a consequence of the dip, changed to a very deep basin. The Tortonian deposits (representing the Molasses Formation) along the eastern side of the Durrës basin (Peri-Adriatic Depression). (Dalipi & Kokobobo,1989). This deposit is placed transgressively over the older deposits of Kruja tectonic zone and over the eroded deposits of Upper Cretaceous. The thickness of the Tortonian deposits increases greatly from east to west (Valbona & Shaqir Nazaj, 1989) while the unconformity moves upward within the younger sediments in the same direction. This indicates that the most eastern structures of the Kruja tectonic zone were highly differentiated compared to the western ones expected to exist under the Durrës basin to the west of Kruja tectonic zone. Based on the lithological changes of the formations and the unconformity between them, it can be interpreted that the most powerful folding phases that transformed the area are those of Chattian, Burdigalian and Tortonian ages, which migrate in time from east to west. It means that the most eastern structures, which belongs to Kruja tectonic zone, have been affected by the earliest tectonic phases, while the most western structures, which belongs to the Ionian tectonic zone (clearly identified further to the south of the study area) are affected by the later folding phases. (Sadiku,*et al*.,1989) All the existing structures outcropped or proved by the drilled wells got the main features during the Burdigalian tectonic phase but their tectonic elements started since the Chattian time. It is believed that the tectonic contours of some big anticlinal folds, which existed since the Chattian time, correspond more or less with the tectonic boundaries of the existing outcropped anticlinal belts within the Ionian tectonic zone (Berati, Kurvelesh, and Çika anticlinal belts). Even the geological data show that the structures of the Kruja tectonic zone like Valesh-Letan, Makaresh, Tirana-Fushë Kruja, Petrela, Kozan and Ishëm (Sazhsanaku & Thomal, 1989) structures, were created before the Chattian time.

Tortonian deposits in the eastern part are transgressively placed on the Upper Cretaceous limestone, while to the west these deposits are placed on the younger deposits. The relationships between Kruja zone in the east and the Adriatic Basin in the west can be seen easily identified in F Figure 2.

The geological-tectonic model.

The eastern part of the study area is part of the Kruja tectonic zone, while the western part belongs to the Durrës basin (Adriatic Basin). The geological data from the wells show that the eastern part of this basin have two tectonic stage (Molasses formation transgressive placed over the flysch and carbonate formation). The data show also that the scale of structuring (folding) of the deposits under the

unconformity is more intensive comparing with the deposits above it (Xhomo,*et al*., 2002). From east to west direction the anticlinal structures are as following:

-Valesh-Letan-Dajt-Kakariq anticlinal structures
-Makaresh-Renc anticlinal structures
-Kozan-Petrela-Fushe Kruja-Tirana anticlinal structures
-Ishëm anticlinal structures

The eastern carbonate structures are very deformed, especially those found in the northern part of the study area. The eastern arms of carbonate structures can be seen in the surface, while their western arms are missing. This indicates the high coefficient of structuring compared to their low rate of folding.

The westernmost structure has the same characteristics as Ishmi structure, which is faulted along its western arms with a high amplitude and dips to the west. This fault is the main longitudinal fault with the highest amplitude in the region, which is related to the main western fault of the Dalmatia tectonic zone, meet by wells JJ-2 and JJ-1, further to the north in Montenegro (Bega, 2015).

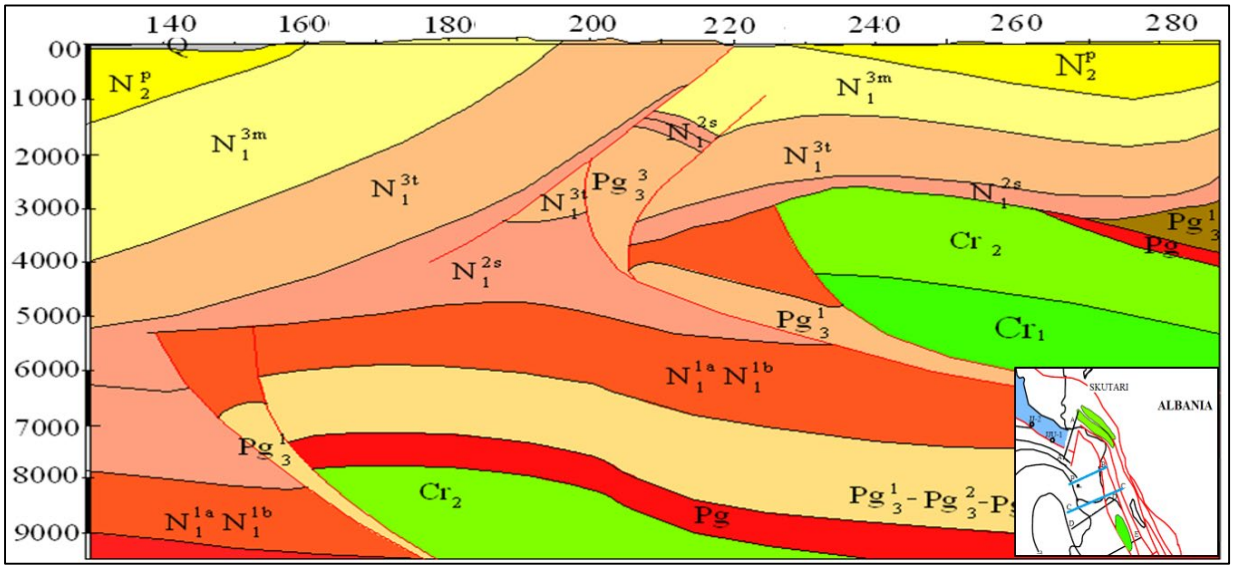

Figure 2. Seismic-geological cross section C-C & D-D.

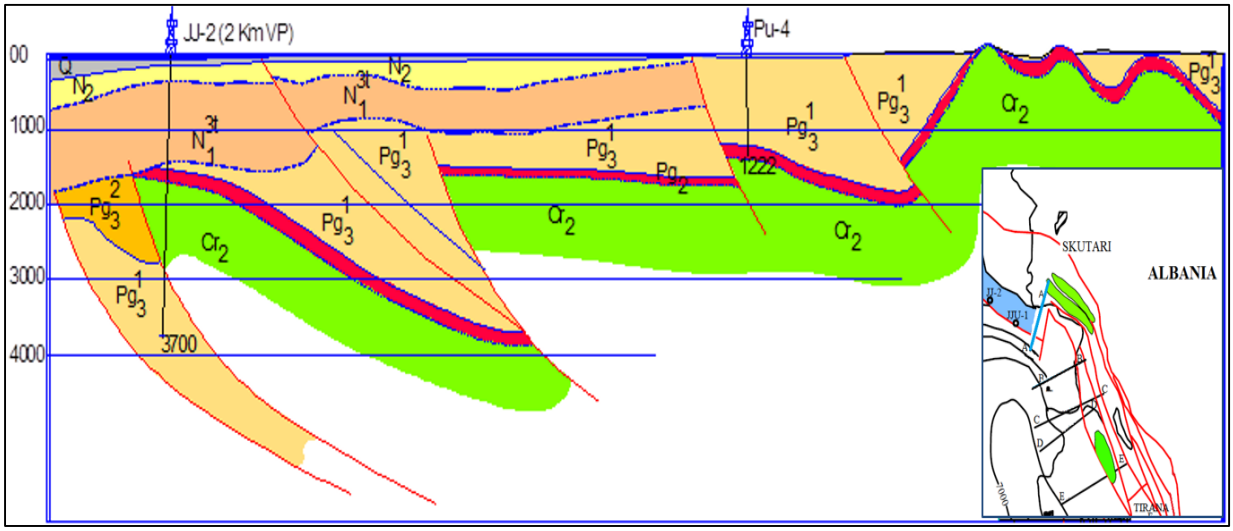

Figure 3. Seismic-geological section A-A

The seismic data show that the western fault of Kruja, which is linked to the north with the western fault of Dalmatia zone meet by the JJ-2 well in Montenegro (Figure 3).
Based on the seismic and well data the top carbonates are interpreted about 7000m deep and are covered by the overlap the structures of Kruja tectonic zone. (Velaj, 2012)

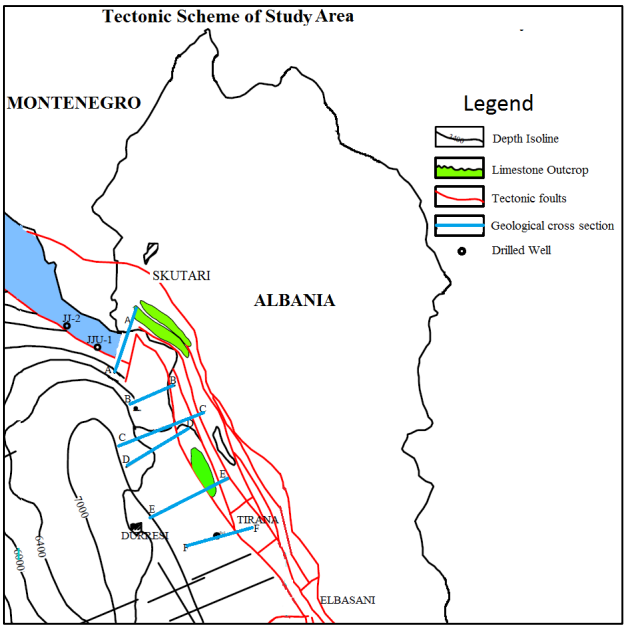

Figure 4. Tectonic scheme of study area

Another important discussion is the existence of Ionian tectonic zone further to the north and cover by the Peri Adriatic zone. Previous interpretations show different opinions. Based on geological data from the new seismic lines and wells we will give same consideration.

First - The gravimetric data indicate the presence of a large negative anomaly following from the - south (west of the Cika structure) to the north (west of the Kurveleshi structure) (Mëhillka,*et al*.,1986-1987) (Velaj,2015) which turns eastward near the Shkumbin river indicating that the tectonic belts do not extend towards the north of this river. ***Second-*** The data from the very depth Well-18 (Bega, 2010) proved the existence of this gravimetric anomaly. ***Third***- The seismic data and the correlation from the south to the north of the top of carbonate of the anticlinal structure of Patos-Verbas has shown that this structure does not continued further to the north of Vlora-Elbasan-Peshkopi fault. (Sadiku ,*et al.,*1989). Regarding to the continuation of this transverse fault to the east it is more possible that passes in the west of Paper and Rove anticlinal structures. In the depth this fault is join with the main west thrust of Kruja tectonic zone. This interpretation includes Paper and Rova structures (referring to the top carbonates) to the northern continuation of Ionian tectonic zone. (Thomai, 1987)

The seismic data registered down to 8 seconds (sections D-D, E-E, F-F; Figure 4) can be interpreted that the folding intensity of the carbonate structures in this region is less than the intensity of the known carbonate structures for the same tectonic stage for Ionian and Kruja tectonic zones.

Otherwise, the folding intensity looks to be the same for the Neogene structures from south to the north along the Kreshpan, Ardënica, Divjaka - Durrës (southern part) and Lushnja – Mlik - Shkoza (northern part). The axis orientation of these Neogene folds does not coincide with the orientation of the known carbonate structures. This means that the Neogene folds are the consequence of new tectonic phases, mainly after Tortonian time, which tells for the presence of the same sedimentation conditions for both the Ionian tectonic zone and Durrës. Basin during this time. The impact of tectonic phases was different over the different areas of the Ionian tectonic zone and Durrës basin as well. It is understandable that the thrusting amplitude of the possible interpreted structures is decreasing from east to west towards the Sazani tectonic zone. This is also supported by studies conducted for the areas in surrounding countries (Franket *et al*., 1983.) Which interpret the Adriatic platform is composed of some tectonic blocks divided by a series of normal tectonic faults. These tectonic blocks are found deeper moving from west to east passing gradually from the platform to the southern Adriatic basin. (Figure 6.) (Gartner *et al*., 2002). The seismic data registered down to 8 seconds (Figure 7), seismic section E-E distinguish two seismic facies: one seismic facies containing strong intense seismic reflections from 0 to 2.8 seconds and the other with rare seismic reflections belonging to the deeper section. These seismic models of reflections show for different degrees of deformation during the folding phases. Unconformity between

Neogene and Mesozoic folds and the lower stage of folding of structures to the west of Kruja zone (Figure 5).

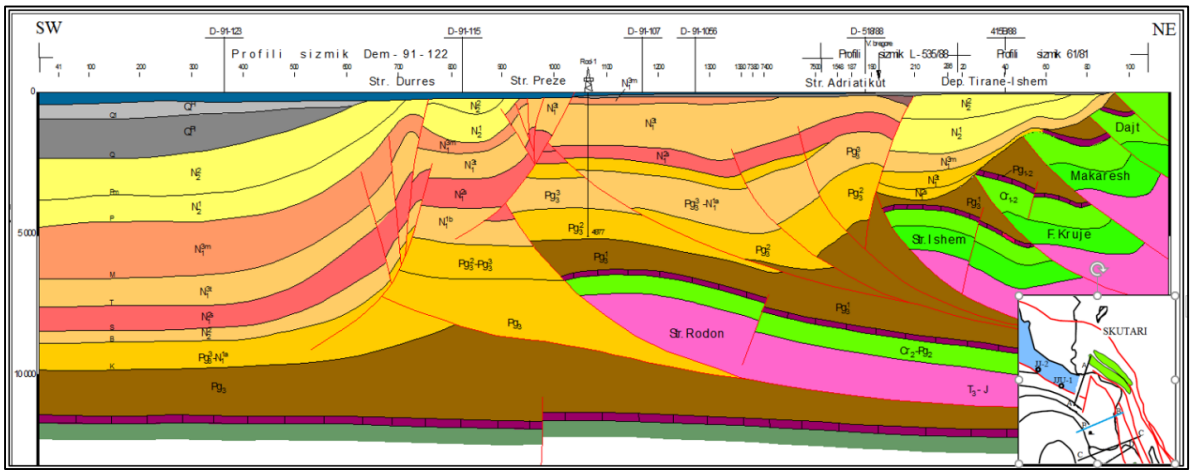

Figure 5. Seismic-geological section B-B

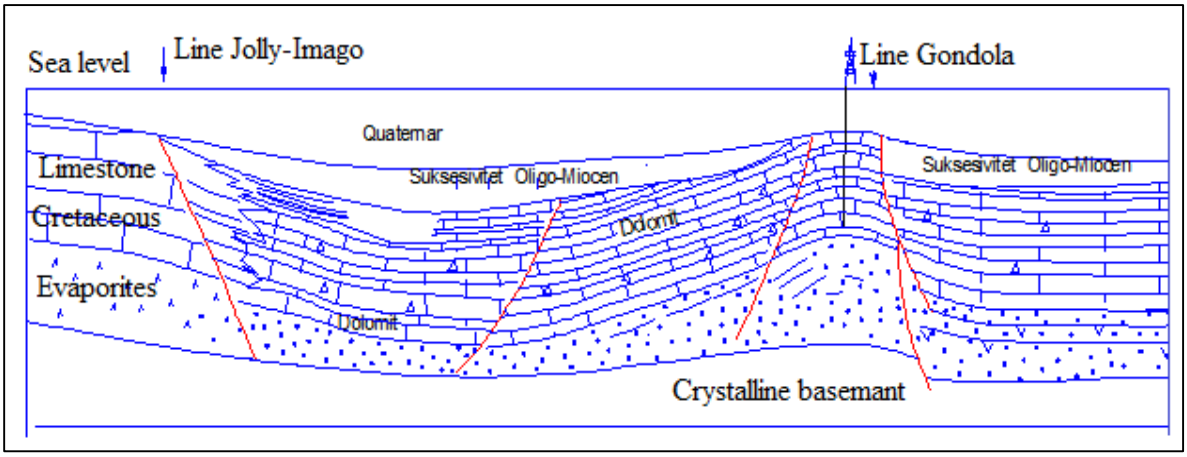

Figure 6. Geological profile according to line D-438. Gradual transition, through normal tectonic faults, from the platform to the Adriatic Basin.

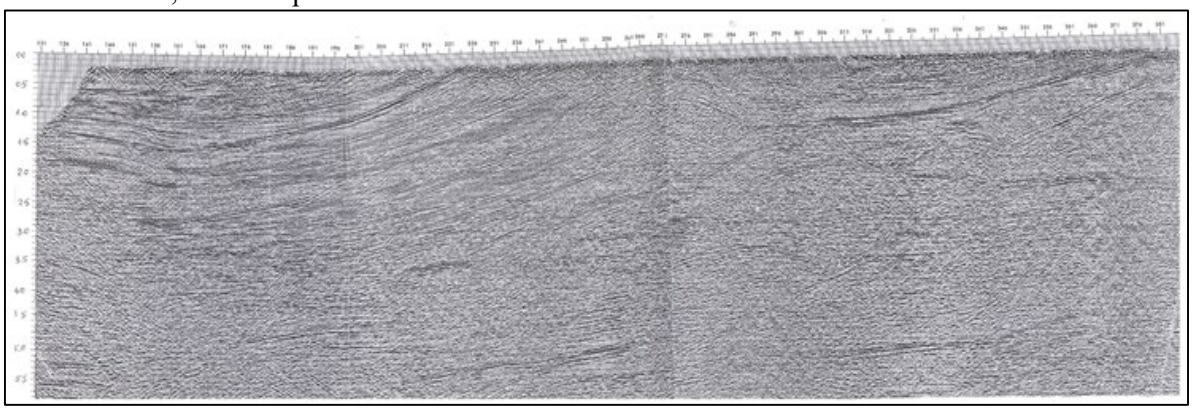

Figure 7. Seismic-geological section E-E.

Two seismic facies can be distinguished: One with plenty of reflections tractable up to 2.8 sec time and the other facies with rare reflections and preserved up to 5 seconds time. In the time 4.5-5 seconds we distinguish a steady reflection which rises to the west. This reflection belongs to the top of Mesozoic section. (Figure 7). The paleogeography changes that ha the Ionian zone from the south to the north and the decreasing of tectonic belts along this direction indicate the different tectonic style of the structures toward the north. Based on these facts we conclude that the study region represents a transitional zone,

where the structures of the lower tectonic stage (carbonate and flysch formations) are less folded and less fragmented. The top carbonate is shallower from east to west direction passing gradually in to the South Adriatic platform. It is also possible that during the Paleocene-Eocene time the South Adriatic basin and in the Ionian basin have been unified. The data mentioned above for the study area as wells as the data from the surrounding regions (Italy, Montenegro) suggest that for the Jurassic and possibly Cretaceous carbonates a platformic facies is expected. The tectonic style during this time was represented by a horst and graben model, which passes into the basin conditions in the later geologic time and was not affected or less affected by the tectonic phases. As a consequence, we think that the structures of the tectonic belts within the Ionian tectonic zone to the south do not extend along the study area towards the north with the same features. This fact is to be taken into consideration during the geological interpretations, structure prognosis and their depth.

Conclusion

The study region is not very folded and should belong to the Southern Adriatic zone. The structure of this are different from those we know today in the Ionian and Kruja tectonic zone. Expected structures in the region are thought to be large in size less tectonically complicated and with much lower folded structures.

Palegeographically the carbonate deposits of the Kruja zone in the Upper Cretaceous are platform facies whereas the Paleocene - Eocene and newer deposits are pelagic facies. Because during the Paleocene-Eocene age must have occurred the unification of the Ionian zone with the Kruja tectonic zone, at this time a single basin is created. Regarding to the type of the deposits in Southern Adriatic zone based on the geological phenomena observed in the surrounding units and regions the Eocene and Paleocene age are pelagic facie. At this time must have occurred the unification of the Southern Adriatic zone with Ionian zone.

Relations between the Kruja zone and the surrounding structural units are of a tectonic contact. The fault is thought to have a very large displacement amplitude in both vertically and horizontally direction. This fault is also confirmed by the work made outside the Albania borders. The carbonate structures of the Kruja tectonic zone appear tectonically complicated and eroded up to the level of Upper Cretaceous carbonate deposits. They have large size, with wide roofs, smooth eastern arms and no western arm with northwest-southeast extension.

Relationships between the Ionian Zone and the units in the west have tectonic character, where the fault is thought to have a much greater overlap amplitude and must pass in the west of the Patos-Verbas structure, arching further to the north, where in the vicinity of the Shkumbini river interrupts the continuation of this structure and further to the north.

The most powerful folding phases affecting the study area are those of the Hatian (Kugleri zone) Burdigalian and Tortonian.

References

Bega Z, (2010) Deep Seated Platform Carbonate Reservoirs as New Hydrocarbon Plays in the NW Albania–Montenegro Segment. *6th Workshop of the ILP Task Force on Sedimentary Basins,* (pp. 27-30). Tirana, Albania: ILP Task Force on Sedimentary Basins.

Dalipi H, Kokobobo A, (1989) *Përgjithësimi gjeologo – gjeofizik i rajonit të Durrësit (për Neogenin).* Fier: Instituti i naftes dhe gazit.

Frank G, Kriz J, Vlasic B, (1983.). Result and directions in hydrocarbon exploration of the Adriatic off-shore. *Nafta*, 387-396.

Gartner G, Morsilli M, Schlager W, Bosellini A, (2002) Toe-of-slope of a Cretaceous carbonate platform in outcrop, seismic model and offshore seismic data (Apulia, Italy). 91. . *International Journal of Earth Sciences.*, 315-330.

Mëhillka Ll, Generali Dh., Alia SH, (1986-1987). *Studim mbi ligjësitë tektonike, tektogjenezën e strukturave të brezit të Kurveleshit lidhur me orientimet e efektivitetit të kërkimeve.* . Fier: Insituti i Naftes dhe i Gazit.

Sadiku Y, Nazaj Sh. Mezini D, (1989). *Ndërtimi gjeologjik i rajonit Divjakë për katin e poshtëm tektonik dhe prespektiva naftë-gazmbajtëse.* . Fier : Instituti i naftes dhe i gazit .

Sazhsanaku F, Thomal L, (1989) *Përgjithësimi gjeologo – gjeofizik i rajonit Tiranë - Ishëm.* Fier : Instituti i naftes dhe gazit.

Thomal LNP, (1987) *Geological-geophysical generalization of the Papri region.* . Fier: Instituti i naftes dhe gazit.

Valbona Uk, Nazaj S, (1989) *Mbi ndërtimin gjeologjik dhe perspektivën naftë gazmbajtëse të rajonit Milk- Durrës - Rodon.* Fier: Instituti i naftes dhe i gazit .

Valbona Uk, Sadiku Y, (1984) *Ndërtimi gjeologjik dhe perspektiva naftë gazmbajtëse e rajonit Elbasan Llixha.* Fier: Instituti i naftes dhe i gazit .

Velaj T, (2012) Tectonic style and hydrocarbon evaluation of duplex Kruja zone in Albania., (pp. 236-242). Retrieved from https://hrcak.srce.hr/86219

Velaj, T. (2015) New ideas on the tectonic of the Kurveleshi anticlinal belt in Albania, and the perspective for exploration in its subthrust. . *Petroleum 1. SWPU*, 269-288.

Xhomo A, Dimo L., Xhafa, Nazaj Sh, Nakuci V, Yzeiraj D, Lula F., Sadushi P, Shallo M, Vranaj A, Melo V., Kodra A., Bakalli F., Meco S. (2002) *Gjeologjia e Shqiperise, Stratigrafia, Magmatizmi, Metamorfizmi, Tektonika dhe Evolucioni Paleogjeografik dhe Evolucioni Paleogjeografik dhe Gjeodinamik (Geology of Albania, text of geological mapo f Albania), scale 1:200 000).* Fier: Archive of National Agency of Natural Resources.

Zamir Bega (2015) Hydrocarbon exploration potential of montenegro – a brief review. *Journal of Petroleum Geology ,* **38***,* 317-330.

Zappaterra E, (1994) Source-rock distribution model of the periadriatic region. *AAPG Bulletin (American Association of Petroleum Geologists); (United States)*, 394-421.

J. Int. Environmental Application & Science, Vol. 15(2): 48-53 (2020)

Research Paper

SENTINEL-2 Imagery for Mapping and Monitoring Flooding in Buna River Area

Freskida Abazaj*

Departement of Geodesy, Faculty of Civil Engineering , Polytechnic University of Tirana, Albania

Received March 10, 2020; Accepted May 28, 2020

Abstract: Monitoring open water bodies accurately is an important and basic application in remote sensing. Various water body mapping approaches have been developed to extract water bodies from multispectral images. The method based on the spectral water index, especially the Normalized Difference Water Index (NDWI) calculated from the Green and Near Infrared (NIR) bands, is one of the most popular methods. The Sentinel-2 satellite can provide fine spatial resolution multispectral images. This new dataset is potentially of important significance for regional water bodies' mapping, due to its free access and frequent revisit capabilities. It is noted that the green and NIR bands of Sentinel-2 have same spatial resolutions of 10 m, respectively. In this paper NDWI was produced from Sentinel-2 at the spatial resolution of 10 m. This scheme provides the detailed information available at the 10-m resolution.

Keywords: *Flooding, NDWI, Sentinel-2, Image*

Introduction

Sentinel satellite constellation of the Copernicus program of the European Union (Berger, Moreno, Johannessen, Levelt, & Hanssen, 2012,) provides synthetic aperture radar (SAR) and multispectral data with global coverage. Every year, flood events cause great economic losses and victims (Ward, et al., 2013). For this reason, precise flood mapping and modelling are essential for flood hazard assessment (Moel, Alphen, & Aerts, 2009), damage estimation (Amadio, Mysiak, Carrera, & Koks, 2016) and sustainable urban planning to properly manage flood risk (Ran & Nedovic-Budic, 2016,). In such a context, satellite remote sensing is currently a low-cost tool that can be profitably exploited for flood mapping (Fayne, Bolten, Lakshmi, & Ahamed, 2017).

At present, remote sensing has become a routine approach for land surface water bodies' monitoring, because the acquired data can provide macroscopic, real-time, dynamic and cost-effective information, which is substantially different from conventional in situ measurements (Chen, Zhang, Ekroos, & Hallikainen, 2004) (Feng, et al., 2012,). Each remote sensing technique for flood mapping presents advantages and drawbacks (Malinowski, Groom, Heckrath, & Schwanghart, 2017) that must be evaluated on a case-by-case basis. The frequent passes of satellites and the availability of rapid processing chains allowed the development of services providing automatic and quasi-real time flood mapping such as, for example, the Copernicus Emergency Management Service (EMS) performed by the European Union (online:) (Ajmar, Boccardo, Broglia, Kucera, & Wania, 2017). However, these services provide rapid mapping products that can be affected by uncertainty and are not always validated (Revilla-Romero, et al., 2015,). Maps of flooded areas produced by official authorities and based on bespoke aerial photos and field surveys are more accurate, although they are time-consuming and require higher costs to be generated. Various methods, including single band density slicing (Work & Gilmer, 1976), unsupervised and supervised classification (Sivanpillai & Miller, 2010,) and spectral water indexes (Li, et al., 2013), were developed in order to extract water bodies from different remote sensing images. Among all existing water body mapping methods, the spectral water index-based method is a type of reliable method, because it is user friendly, efficient and has low computational cost (Ryu, Won, & Min, 2002). In this work, we present the Normalized Difference Water Index (NDWI) proposed by McFeeters (McFeeters, 1996), using the green and Near Infrared (NIR) bands of remote sensing images based on the phenomenon that the water body has strong absorbability and low radiation in the range from visible to infrared wavelengths. NDWI can enhance the water information effectively in most cases, but it is sensitive to built-up land and often results in over-estimated water bodies.

*Corresponding: E-Mail: fabazaj@hotmail.com; Tel: +355675121291

Open Street Map data were used for visual interpretation of the results. The image processing and analyses was carried out in ESA SNAP Desktop and QGIS Desktop.

Materials and Method

Study Site and Data Set

The River Buna runs in the last North-west segment of the Albanian Montenegrin border. This river springs from Lake of Shkoder, quite close to the city of Shkoder. Buna runs to the south, alongside Taraboshi up to its mouth in Adriatic Sea. The river has a length of 44 km. Lake Shkodra, Drin and Kir Rivers, drain into the Buna, which flows towards and empties into the Adriatic Sea. The combined flow from the other rivers and the lake into the Buna River can sometimes add up to more water volume than the Buna River can hold, causing it to overflow. It is of great interest to extract surface open water bodies and to monitor their changes in the Buna river area.

a)

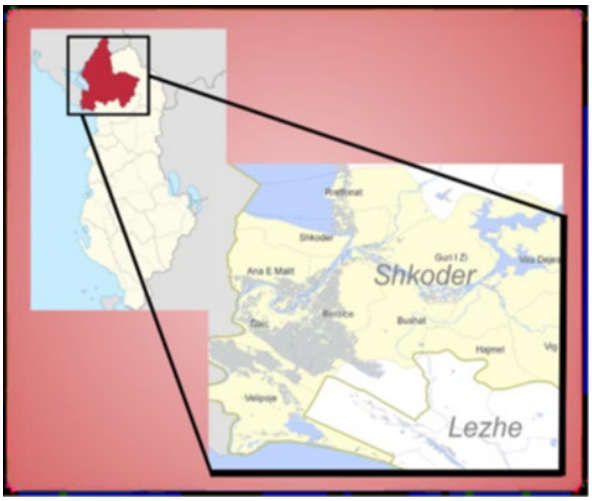

b)

Figure 1. a) Satellite image of the Drin and Buna rivers (Earth, 2020) **b)** Drin and Buna River Basin – overview (GIZ., 2015))

The dataset used in this study is the standard Sentinel-2A Level-2A product, which was produced by radiometric and geometric corrections, including ortho-rectification and spatial registration on a global reference system with sub-pixel accuracy. The Sentinel-2A Level-2A product is composed of 100 km × 100 km tiles in the UTM/WGS84 projection and provides the Bottom-Of-Atmosphere (BOA) reflectance. The UTM (Universal Transverse Mercator) system divides the Earth's surface into 60 zones. Each UTM zone has a vertical width of 6° of longitude and horizontal width of 8° of latitude. This study used a Sentinel-2 Level-2A image scene (date of acquisition: 28.03.2018). It was downloaded from the ESA Sentinel-2 Pre-Operations Hub (https://scihub.copernicus.eu/).

Open Street Map data were used for visual interpretation of the results. The image processing and analyses was carried out in ESA SNAP Desktop and QGIS Desktop

Sentinel-2 Imagery

SENTINEL-2 is a European wide-swath, high-resolution, multispectral imaging mission. The full mission specification of the twin satellites flying in the same orbit but phased at 180°, is designed to give a high revisit frequency of 5 days at the Equator. SENTINEL-2 carries an optical instrument payload that samples 13 spectral bands: four bands at 10 m, six bands at 20 m and three bands at 60 m spatial resolution. The orbital swath width is 290 km (ESA, 2020). SENTINEL-2 makes a significant contribution to Copernicus themes such as climate change, land monitoring, emergency management, and security. The false colour composite of the Sentinel-2 image at 10 m is shown in Figure 2a.

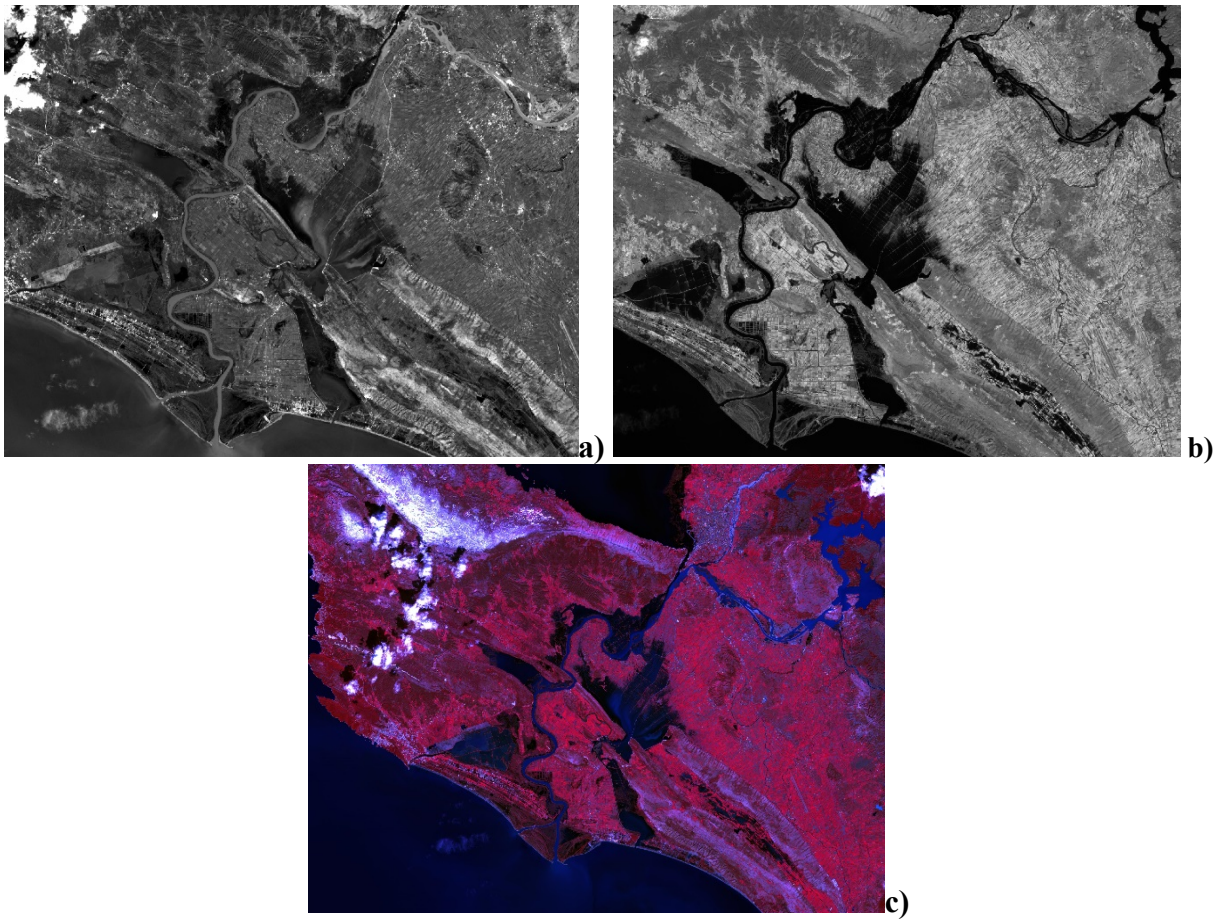

Figure 2. (**a**) 10-m green Band 3); (**b**) 10-m NIR Band 8; (**c**) Ten-meter false color map (R: Band 8; G: Band 4; B: Band 3);

Methodology

Spectral Water Indexes

The NDWI proposed by McFeeters (McFeeters, 1996) is designed to: (1) maximize the reflectance of the water body in the green band; (2) minimize the reflectance of water body in the NIR band (Sun, Sun, Chen, & Gong, 2012,), (Xu, 2006,). NDWI is calculated as:

$$\text{NDWI}=\frac{\rho Green-\rho NIR}{\rho Green+\rho NIR} \qquad (1)$$

Where ρGreen is the BOA reflectance value of the green band and ρNIR is the BOA reflectance value of the NIR band. Therefore, no additional pre-processing is required, and the NDWI for Sentinel-2 can be directly calculated as:

$$\text{NDWI}_{10m}=\frac{\rho 3-\rho 8}{\rho 3+\rho 8} \qquad (2)$$

Note that both Band 3 and Band 8 of Sentinel-2 have the spatial resolution of 10 m, and thus, the calculated NDWI in Equation (2) also has the spatial resolution of 10 m.
Afterwards, the NDVI was computed with the well-known method as follows: Then, impervious mask was obtain using threshold values for NDVI.

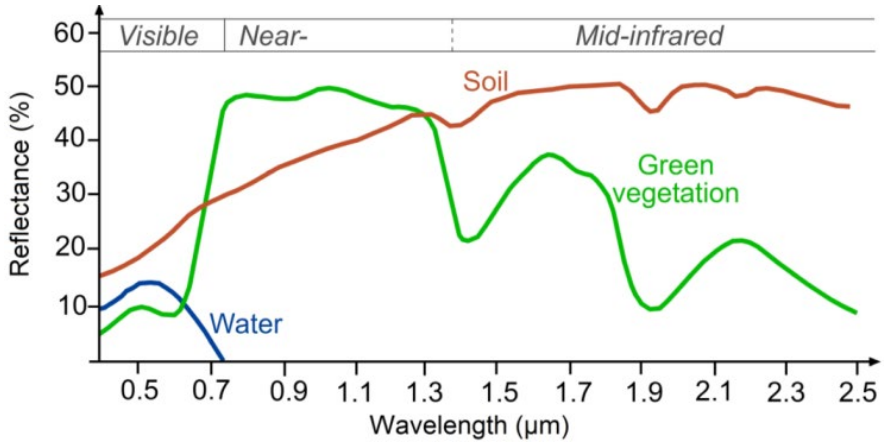

Figure 3. The spectral reflectance curves for water, soil and green vegetation;

Results

Sentinel-2 products contains 13 spectral bands in three different spatial resolutions.

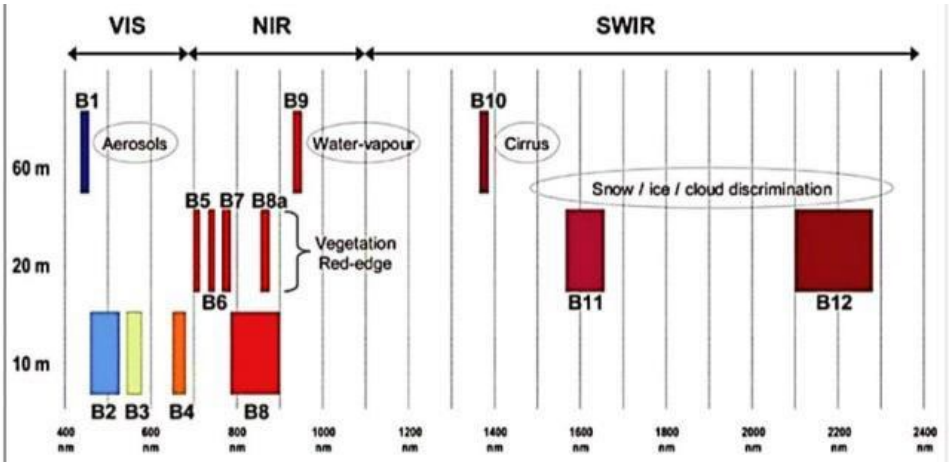

Figure 4: SENTINEL-2 spatial resolution bands **(ESA, 2020)**

The surface area measured on the ground and represented by an individual pixel. Many operators in SNAP toolbox do not support products with bands of different sizes so first we need to resample the bands to equal resolution. We define the size of resampled product by reference band B2.

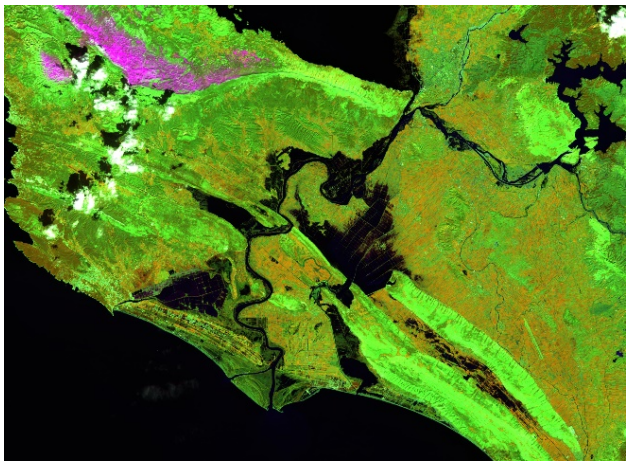

Figure 5: Ten-meter RGB image (R: Band 8; G: Band 11; B: Band 4);

To detect the water bodies we will use the Normalized Difference Water Index - NDWI it was proposed by McFeeters (McFeeters, 1996) and it is designed to: i) maximize the reflectance of the water body in the green band; ii) minimize the reflectance of water body in the NIR band. In figure 6 the open water pixels appear much brighter than other surfaces.

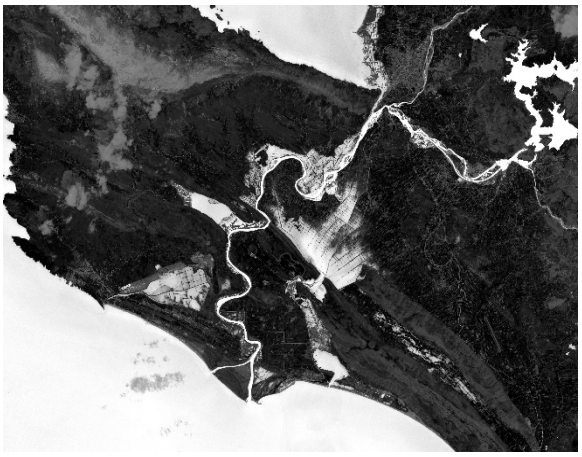

Figure 6. Image of the water bodies with Normalized Difference Water Index – NDWI

After detected the water bodies with NDWI, we create another new band that will only contain water surfaces. We will set the threshold for pixel to be classified as water to >= 0. In figure 7 we see the water mask.

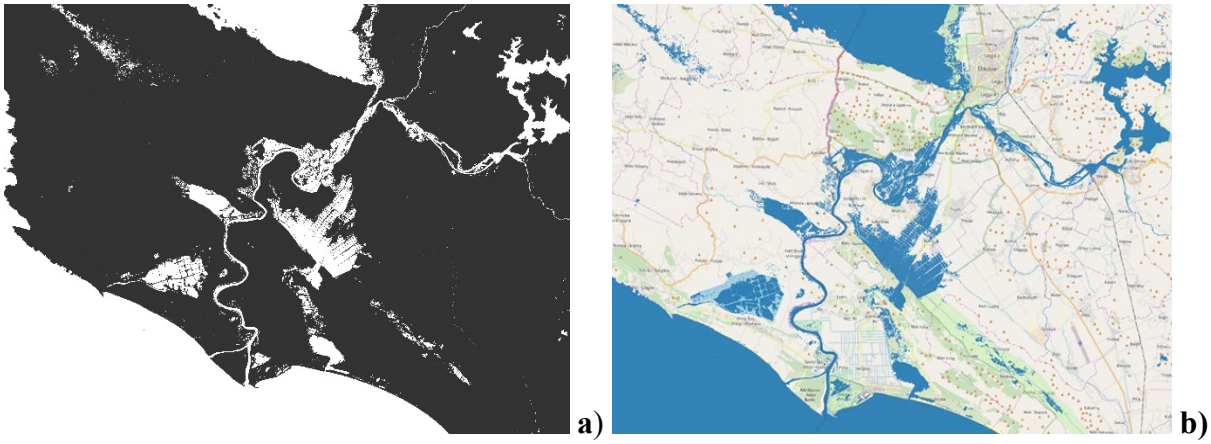

a) **b)**

Figure 7. a) The water mask of Buna river Area; **b**) The visualization of water mask in QGIS with base map the world map

Conclusions

The newly-launched Sentinel-2 can provide fine spatial resolution multispectral imagery at a fine temporal resolution, which makes it an important dataset for water bodies' mapping at the global scale. In this paper, a method is proposed for water bodies' mapping from the Sentinel-2 image by producing the 10-m NDWI image.

The experiment on the subset Sentinel-2 image located at Buna river area demonstrates that NDWI is efficient to enhance water bodies and to suppress built-up features than NDWI.

To estimate the flood water level, we developed a method that involves three steps, namely, To detect the water bodies we used the Normalized Difference Water Index - NDWI that was proposed by McFeeters2 and it is designed to maximize the reflectance of the water body in the green band and to minimize the reflectance of water body in the NIR band.

The implementation of this technique will provide invaluable information for water management and water security

References

Giz DG, (2015). doi:https://www.giz.de/en/downloads/giz2015-en-portfolio-albanien.pdf

Li EA, Won J, Min K, (2002) Waterline extraction from Landsat TM data in a tidal flat-A case study in Gomso Bay, Korea. . *Remote Sens. Environ*, **83**, 442–456.

Ajmar A, Boccardo P, Broglia M, Kucera J, Wania A, (2017) Response to flood events: The role of satellite-based emergency mapping and the experience of the Copernicus emergency management service. Flood Damage Surv. Assess. New Insights Res. Pract. 2017. *Flood Damage Surv. Assess. New Insights Res*, 213-228.

https://emergency.copernicus.eu/mapping/ems/response-flood-events-role-satellite-based-emergency-mapping-and-experience-copernicus-emergency

Amadio M, Mysiak J, Carrera L, Koks E, (2016) Improving flood damage assessment models in Italy. *Nat. Hazards*. **82**. 2075–2088.

Berger M, Moreno J, Johannessen J, Levelt P, Hanssen R, (2012) ESA's sentinel missions in support of Earth system science. *Remote Sens. Environ.* **120**, 84–90.

Chen, Q., Zhang, Y., Ekroos, A., & Hallikainen, M. (2004). The role of remote sensing technology in the EU water framework directive (WFD). *Environ. Sci. Policy*, **7**, 267–276.

Google Earth, (2020) Retrieved from https://www.google.com/earth/

ESA, Coop. (2020) Sentinel-2_User_Handbook. https://sentinel.esa.int/documents/247904/ 685211/ Sentinel-2_User_Handbook

Fayne J, Bolten J, Lakshmi V, Ahamed A, (2017) Optical and Physical Methods for Mapping Flooding with Satellite Imagery. In Remote Sensing of Hydrological Extremes;. *Remote Sens. Hydrol. Extremes; Springer:* pp. 83–103. doi:10.1007/978-3-319-43744-6_5

Feng L, Hu C, Chen X, Cai X, Tian L, Gan W, (2012,). Assessment of inundation changes of Poyang Lake using MODIS observations between 2000 and 2010. *Remote Sens. Environ.*, **121**, 80–92.

Li W, Du Z, Ling F, Zhou D, Wang H, Gui Y, Zhang X, (2013) A comparison of land surface water mapping using the normalized difference water index from TM, ETM plus and ALI. *Remote Sens.* **5**, 5530–5549.

Malinowski R, Groom GB, Heckrath G, Schwanghart WD, (2017) Remote Sensing Mapping Practices Adequately Address Localized Flooding? A Critical Overview,. *Springer Sci. Rev.*, **5**, 1–17. doi:https://doi.org/10.1007/s40362-017-0043-8

McFeeters S, (1996) The use of the normalized difference water index (NDWI) in the delineation of open water features. *Int. J. Remote Sens.* **17**, 1425–1432.

Moel, H., Alphen, J., & Aerts, J. (2009). Flood maps in Europe–methods, availability and use. *Nat. Hazards Earth Syst. Sci.*, **9**, 289–301.

online:, C. E. (n.d.). Retrieved 3 7, 2018, from http://emergency.copernicus.eu/mapping/list-of-components/EMSR120

Ran J, Nedovic-Budic Z, (2016) ntegrating spatial planning and flood risk management: A new conceptual framework for the spatially integrated policy infrastructure. . *Comput. Environ. Urban Syst.*, **57**, 68–79.

Revilla-Romero B, Hirpa FA, Pozo JT, Salamon P, Brakenridge R, Pappenberger F, De Groeve T, (2015) On the use of global flood forecasts and satellite-derived inundation maps for flood monitoring in data-sparse regions. . *Remote Sens.* **7**, 15702-15728.

Ryu J, Won J, Min KWA, (2002) Waterline extraction from Landsat TM data in a tidal flat-A case study in Gomso Bay, Korea. *Remote Sens. Environ.*, **83**, 442–456.

Sivanpillai R, Miller S, (2010) Improvements in mapping water bodies using ASTER data. . *Ecol. Inform.* **5**, 73–78.

Sun F, Sun W, Chen J, Gong P, (2012) Comparison and improvement of methods for identifying waterbodies in remotely sensed imagery. *Int. J. Remote Sens.* **33**, 6854–6875.

Ward P, Jongman B, Weiland F, Bouwman A, van Beek R,., Bierkens M, Winsemius H. (2013) Assessing flood risk at the global scale: Model setup, results, and sensitivity. *Environ. Res.. Lett*, **8**, 044019-10.

Work E, Gilmer D, (1976) Utilization of satellite data for inventorying prairie ponds and lakes. *Photogramm. Eng. Remote Sens*. **42**, 685–694.

Xu H, (2006) Modification of normalised difference water index (NDWI) to enhance open water features in remotely sensed imagery. *Int. J. Remote Sens.*, **27**, 3025–3033.

J. Int. Environmental Application & Science, Vol. 15(2): 54-61 (2020)

Research Paper

The Dynamic Role of Tectonic Faults in Geological Evolution of the Region in North - West Albania

Dhurata Ndreko[1,*], Shaqir Nazaj[2]

[1]*Geology and Mining Faculty, Tirana; Albania;* [2] *Geology and Mining Faculty, Tirana; Albania*

Received March 18, 2020; Accepted May 02, 2020

Abstract: The structural interpretation and the geological data allows us to give same consideration on the role of the longitudinal and transverse faults on the development of the structures. The object of this paper are the tectonic features and geological evolution of the north part of Albania. The study area is located in the sector between two old transverse tectonic faults of Shkoder – Peje in the north part and Vlore - Elbasan in the south. This region has very complicated geological features where combined of several facial structural zones. In the east is bounded by the Kruja (Gavrovo) tectonic zone and in the south by the Ionian tectonic zone and in the north western part by the Adriatic Sea waters. The Kruja (Gavrovo) and Ionian tectonic zones are intensively affected by orogenesis whereas Sazani (Apulia) and the Southern Adriatic Basin are partially affected. Longitudinal and transverse tectonic faults have played a very important role in facie sedimentation and in the structuring of tectonic zones and structures.

Keywords: *Longitudinal, tectonic, faults, Kruja, Folds*

Introduction

The study area is located in the north-western part of the Outer Albanides (part of the Dinarides - Albanides – Helenides structural belt). Outer Albanides are part of continental margin of the African edge and Ardia microplate) and are formed from sedimentary deposits and maybe metamorphic rocks. The study area is bordered to the east by the Kruja (Gavrovo) tectonic zone, in the south part from the Ionian tectonic zone and to the northwest by the Adriatic Sea water (Xhomo *et al,* 2020) (Figure 1). This area is located in the sector between two old transverse tectonic faults of Shkoder - Peje and Vlore - Elbasan and represents a region with complicated geological features where we have a combination of several facial structural zones. Studies made in this region have showed different opinions on the continuation of tectonic zones in north - west part of Albania and the relationships between them. This paper based on the structural interpretation and the geological data of the region, will give some consideration on the role of old and new tectonic faults in the geological evolution of the structures.

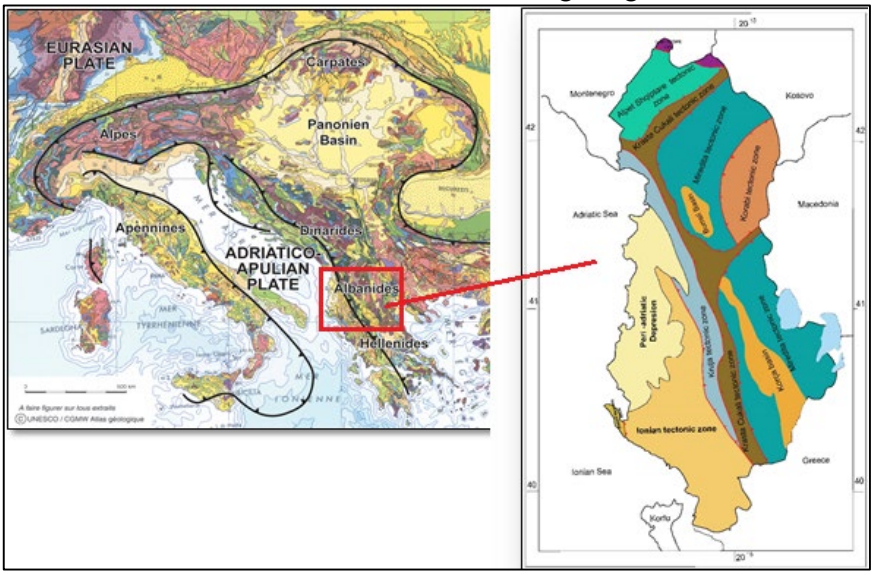

Figure 1. Location of the study area

**Corresponding: E-Mail: ndrekodhurata1216@gmail.com; Tel: +355 69 37 72 727*

Characteristics and the Role of Tectonic Faults

The Structural Units in the Outer Abanides have been created as a result of the continental collision between the Ardia microplates with the European plate. The structures units have generally south - west and north – east direction. The three tectonic zones of Kruja (Gavrovo), Ionian and Sazani (Apulia) in northern part dips and in this sector has its origin in the Pre-Adriatic Depression. The longitudinal and transverse tectonic faults have played a very important role in sedimentation and in the structuring of tectonic structures in the study area (Frashëri & Nishani, 1996) (Konomi, 2000). Based on the geological settings and in the change of the deposits thickness and their lithology in the Mlik-Rodon area and surrounding regions, the tectonic faults are grouped as follows:

The Longitudinal Faults

During the rifting phases (Liassic) a series of normal longitudinal faults have separated the tectonic zones and structures from each other (Roure, et al., 2004). These faults are not uniform everywhere and have different amplitudes in combination with transverse faults give different structures forms. Due to the combination of these faults in the study area and especially in the southern and eastern parts, horsts and grabens structures have been created, bounded with longitudinal and transverse faults from each other. (Figure 2). Generally these structures or tectonic zones have a longitudinal direction and the combination of normal longitudinal with transverse faults causes significant changes in the longitudinal direction. These faults throughout the time that the Outer Albanides margin had a distinctive regime are developed sinsedimentary. Such have been the western fault of the Kruja (Gavrovo) tectonic zone and some faults that border the Dajti, Tirana structure and Ionian tectonic zone (Frashëri & Nishani, 1996). We think that these faults have existed due to the fact that the thickness and lithology of the deposits have changed in the both sides of the faults, as well as the other fact that the same faults are found fossilized in Sazani (Apulia) tectonic zone evidenced by the field survey and seismic profiles in the Adriatic Sea and surrounding regions (Milia, *et al.,* 2017; Ndreko & Nazaj, 2019*)*.

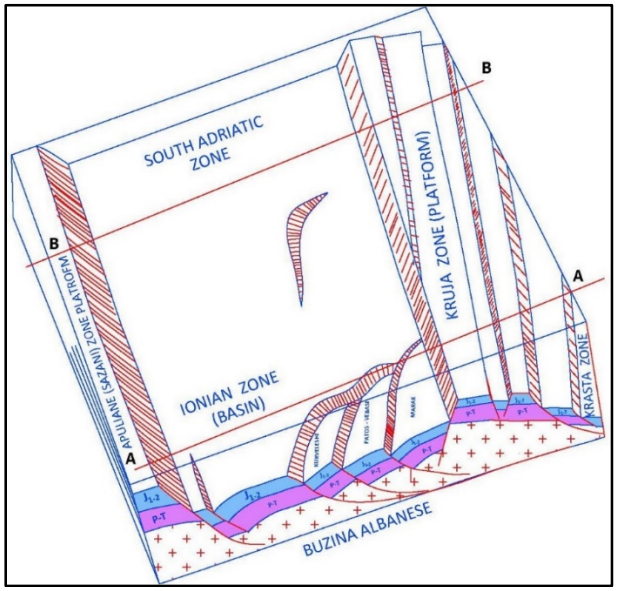

Figure 2. Scheme of tectonic zones during the rifting (Lower - Middle Liassic)

These normal faults separate the neritic deposits of the Sazani tectonic zone (Apulia platform) from the pelagic deposits of the Southern Adriatic Basin reference. Normal faults during the compression phases (orogenesis) begin to activate in the opposite direction according to these blocks and structures rotate. During the orogenesis process the compression resistance is small, so the deposits will be disconnected at their weakest point. The small resistance is exactly in the areas with existed normal fault due to this occurs inversion these faults. The amplitude of these faults depends on three factors:

The first factor: The amplitude of normal faults during lover Liassic age. The bigger the amplitude of these faults, the bigger is the overlapping amplitude of the structures, structural belts or different tectonic zones. Thus the fault of the Kruja (Gavrovo) tectonic zone in the north part has a very big overlapping amplitude of tens of kilometers (Roure *et al*., 2004). These are clearly evident in the seismic

profiles made in the Kruja (Gavrovo) tectonic zone (Figure 3). Which besides the top of limestone of this zone at 1.5-2 sec has another horizons almost parallel to the limestone top at 2.5-3 sec which dips northward direction. To the south direction this fault comes by reducing its amplitude (Nazaj & Valbona, 1990).

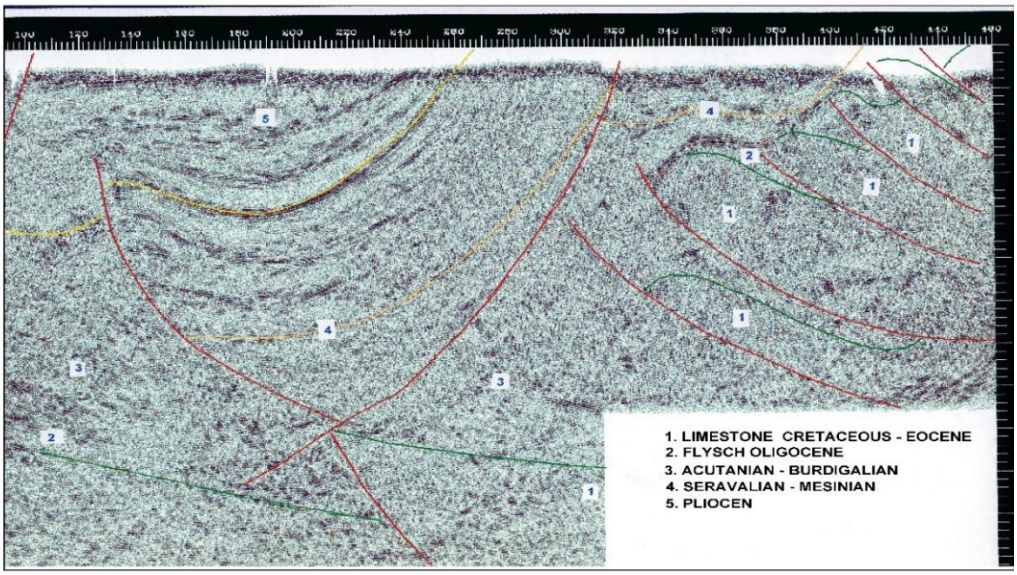

Figure 3. Seismic cross- section A-A

The second factor: The duration time of the normal fault that affect the overlapping amplitude of the structures, so how long does this normal fault continue to control the sedimentation. According to this model the tectonic inversion and overlap of the structure will occur where the normal fault has the bigger amplitude and time duration. The northern part had a bigger amplitude compared to the south part forming different structures. In the northern of the Kruja (Gavrovo) tectonic zone the folding phases is done with monoclines structure while Kozan-Tomorri structures in the south where the resistance is bigger (because the difference in deposit thickness is more gradual), the sedimentary formation responds creating structures with both arms. In some structures such as Dajti, Tirana, Rodoni perhaps and Mliku (Nazaj, 1995) where the amplitude of normal faults has been relatively small their overlapping amplitude is about several kilometers. These data show the dependence of the overlap by the amplitudes and the duration time of normal faults. At the south of the study region some structures of the Ionian tectonic zone have a very big overlapping amplitude to the north compared with the south of Ionian zone. In general, the movement direction of the structures is anti-clockwise.

The third factor affecting the structuring and the overlapping amplitude is the heterogeneity of the sedimentary formation as well as the horizons that serve as sliding horizons. The presence of incompetent horizons such as evaporate formation for the Ionian tectonic zone or different levels of the Schist of Jurassic, Cretaceous. The transition from the carbonate formation to the terrigenous formation and other horizons within the terrigenous formation play a very important role in the structuring and the overlapping amplitude. This is especially evident in the Ionian tectonic zone where most of the structures have in the west contact the outcrop of the evaporate formation (Velaj, *et al*., 1999) (Bega, 2017). These lubricating horizons have served as the basis for the sliding of the carbonate formation and fold them. It should be noted that in the northern part of the Ionian tectonic zone in the Mlik - Durres - Rodon region, based on the seismic data (Naco, *et al*., 2014), the region has flat geological construction with deep structures and small folding scale. This area forms the carbonate basement of the Southern Adriatic zone (basin). In the formation of structures in the study area has played an important role the combination of longitudinal and transverse normal faults.

Sinsedimentary Transverse Faults

In the study area other than longitudinal faults have existed and transverse faults that combined with the longitudinal faults have separated the study area into several structural blocks. Which have reacted

independently from each other during the orogenesis phases. In the study area are identified these main transverse tectonic faults:

- Transverse faults that interrupt the Ionian tectonic zone
- Transverse faults south of Durres – Fortuzaj
- Transverse faults of Rodoni area
- Transverse faults of Lezhe – Shkoder.

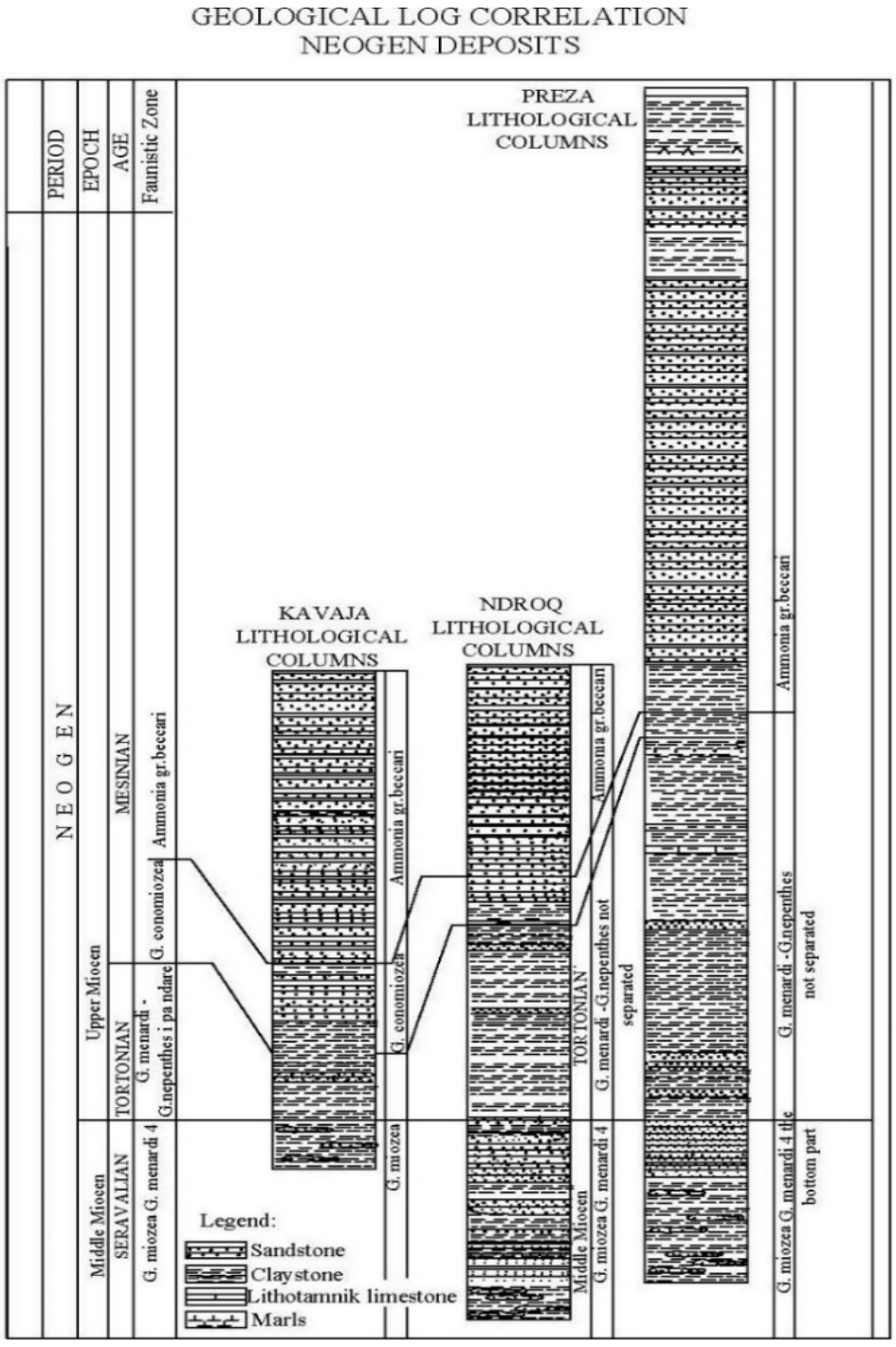

Figure 4. Geological correlation of the Kavaja, Ndroq and Preza outcrops

In these sectors is seen difference in thickness of the Burdigalian and Tortonian - Messinian deposition passing from north to the south part (Figure 4). At the same time the folding style and the rate of shortening of the structures in these sectors also changes. Transverse faults are also observed in the Kruja (Gavrovo) tectonic zone south of Tirana and in Elbasan - Tervolli sector and in the Tomorri anticline structure further to the south (Figure 5).

These transverse tectonic faults are combined with longitudinal faults. The existence of the transverse faults has made possible that today we can observe structures with different folding scale and with different dimensions. Further to the south part of the Kruja (Gavrovo) tectonic zone we have a gradual facial passing (Tomorri Structure) from neritic to pelagic facies for the Upper Cretaceous. Further to south in the anticlinal structure of Leskovik the deposition of Upper Cretaceous are pelagic facies. In this south sector of the Kruja (Gavrovo) tectonic zone the depositions are pelagic facies but belonging to the Ionian tectonic zone with the presence formation of the phosphate horizons. We think that the transition from the Kruja (Gavrovo) tectonic zone (neritic facies) to the Ionian tectonic zone (pelagic facies) e was made by some transverse paleofaults. Which combined with longitudinal faults have made the transition from neritic deposits in the northern area into mixed facies in the Tomorri anticline and in typical pelagic facies in the Melesin anticline and further in the south. As a result of these transverse tectonic faults, Kruja (Gavrovo) tectonic zone have different folding scale passing from north to south part. In the central area where the structures are monoclines (Tirana, Ishmi) and in the north and south direction the structures are anticlinal with the both arms and the number of structural belts in the south is reduced. In the sectors close to these faults as the compression resistance is smaller than is seen a greater structuring and overlapping scale. Regarding to the transverse faults that intersect the Ionian tectonic zone, is clearly seen the change of the folding style. Where the southern part is more folded and tectonically detached (Kreshpani, Verbasi and Maraku structures; Figure 5) while in the north part the structures have small folding scale for the lower tectonic level. This fault is not only one, but is a combination of western longitudinal faults of anticline belts and structures with the transverse faults. So this paleofaults has controlled in a transverse direction the sedimentation for the Triassic and Jurassic and possibly Cretaceous ages. North of the Ionian tectonic zone in Dumrea sector we have combination of longitudinal and transverse fault, we have also the outcrops of evaporate formations.

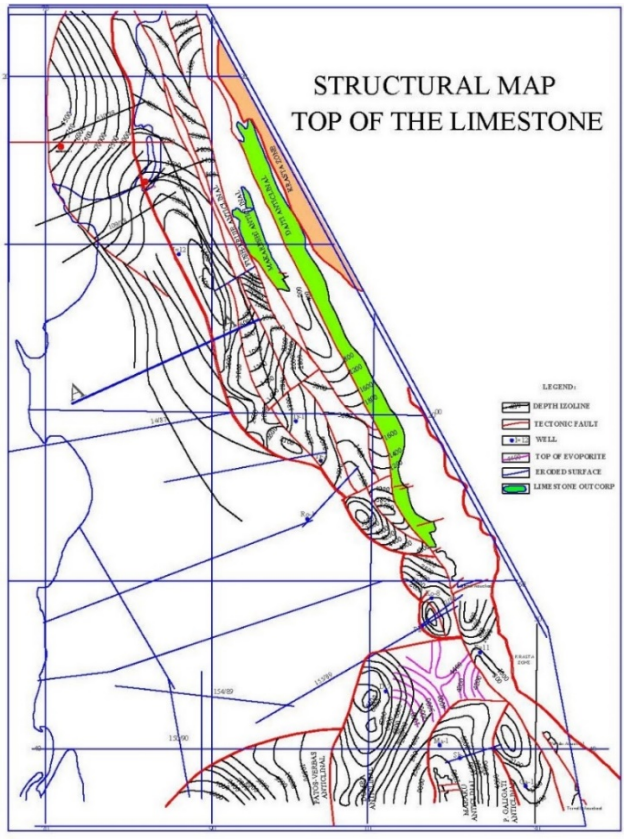

Figure 5. Structural map of the study region

Inter formational Faults and Their role in the Geological Evolution

General characteristic of the structures cover by flysch formation in the Kruja and Mlik-Rodoni structure is that in addition to the old faults that border the structures on the west arm that have continued their activity until the end of the Middle Oligocene new faults occur among the flysch formation (Nazaj, 1995). Carbonate structures are associated with flysch deposits until the Middle Oligocene and with the

continuation of the orogenesis phase cause the formation of new faults further to the west. The inter flysch faults are formed when the eastern arm of the extended structure is inserted under the handing structure. During this time the deposits fill the synclinal structure that separate the anticlinal structures. These faults have different ages in different structures. During the time of the formation of inter flysch faults which have smaller angel than older faults and usually act on the carbonate structures by moving the flysch formation of the synclines structure up to the axis of the structures. These faults are meet in Kozani, Fortuzaj and Mliku structure. In conclusion we can say that all the old structuring faults that affected the structures of the Kruja (Gavrovo) tectonic zone have ended the activity at the end of the Middle and Upper Oligocene. Then a new front of inter flysch faults has been opened in the west during the Upper Oligocene (Kugleri zone) according to these faults the carbonate structures have moved together with the flysch formation toward the west. This is seen in the big change of the thickness of the Upper Oligocene deposits (Kugleri zone) in the Kozani structure in the transverse direction on both side of the inter flysch fault. (Figure 6) (Sadiku & Nazaj, 1989) (Thomai & Nishani, 1987).

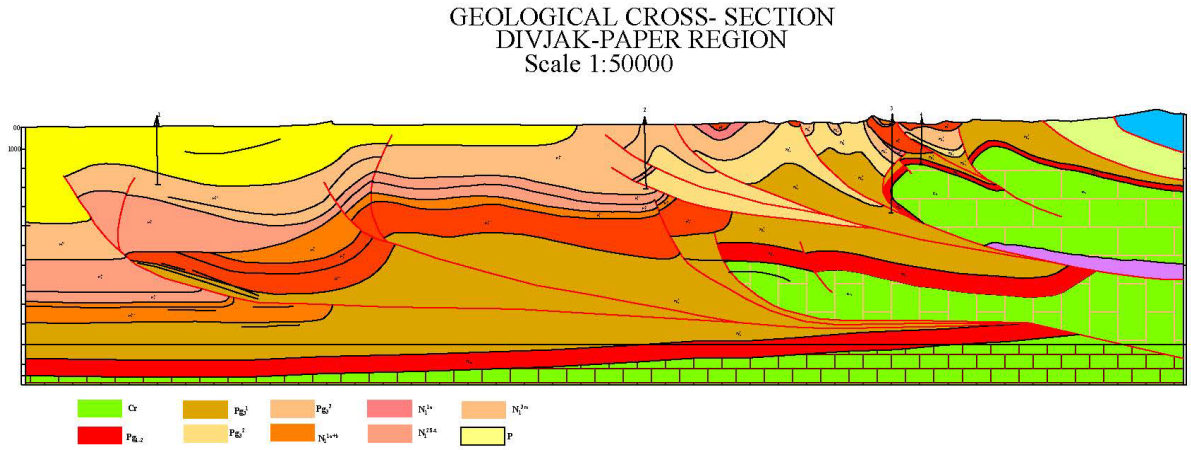

Figure 6. Geological cross- section

This phenomenon is accompanied by facial changes. During deposition of the Burdigalian sequence are formed several inter flysch faults further to the west direction in the Vrapi, Papri, Roves, and Mliku structures, all of these faults in the depth joined in one plan that dips eastward direction. Also during this sequence we have almost masked all the old faults and the new faults plan with small angles are formed further to the west. So the overlapping of the structures or the orogeny moves to the west direction according the new faults plans which in the depth join in the east direction with the old faults (Figure 6). During the Serravallian - Messinian sequence, the role of inter formational faults and their sinsedimentary character is more visible. During this time inter formational faults of Durresi, Shkoza and the Preza Monoclines are developed. In this area, from Kavaja in the south to Rodoni in the north, inter formational faults are active, this is related to the high seismic activity of this sector during the years 2019-2020. Where two powerful earthquakes with Magnitude M = 5.8 (September 2019) and M = 6.4 (November 2019) have their epicentre. This is accompanied with very high number of after aftershocks (Figure 7) (ASEM EMSC, 2019).

Characteristics for these inter formational fault is that the sedimentary prisms have large difference in depositional thickness on both sides of the faults in transverse direction and more gradual longitudinal direction. As in the Preza region where there are very large changes of depositions in transverse direction starting from the Burdigalian deposition up to the Pliocene and more gradual passage in longitudinal direction (Sazhdanaku & Thomai, 1988). This fact is important for determining the sedimentation and direction of orogeny movement. During the Pliocene sequence, the amplitude of longitudinal sinsedimentary faults continued increasing and masking of transverse faults continued. In the study area besides overlapping faults are also found faults with different direction and create the monoclines structures such as Thartori fault, Ishmi fault and Durresi fault (Figure 3). All of these faults are created as a result of orogenesis (Compression from the East) creating a triangular zones and flower structures. (Skrami, 2001). In the study area is also documented the transverse fault of Rodon which is active faults. Concerning to the origin and cause of the transverse fault of Rodon, we think that it was created as a result of the compressions forces acting differentiated in extent for the reason that to the south the

structures of the Kruja (Gavrovo) tectonic zone are shallow and passing to the north they extended excessively and as a result the resultant of the force operates at different depths. This is the cause for the creation of the shear forces of incompetent deposition and for this cause is formed the transverse fault of Rodoni and the monoclonal structure moves to the west direction. Another argument in support of this the development northward of the Neogene Adriatic uplift. There we have the intersection of the longitudinal fault of the Preza monoclines with the transverse fault of the Rodoni cape.

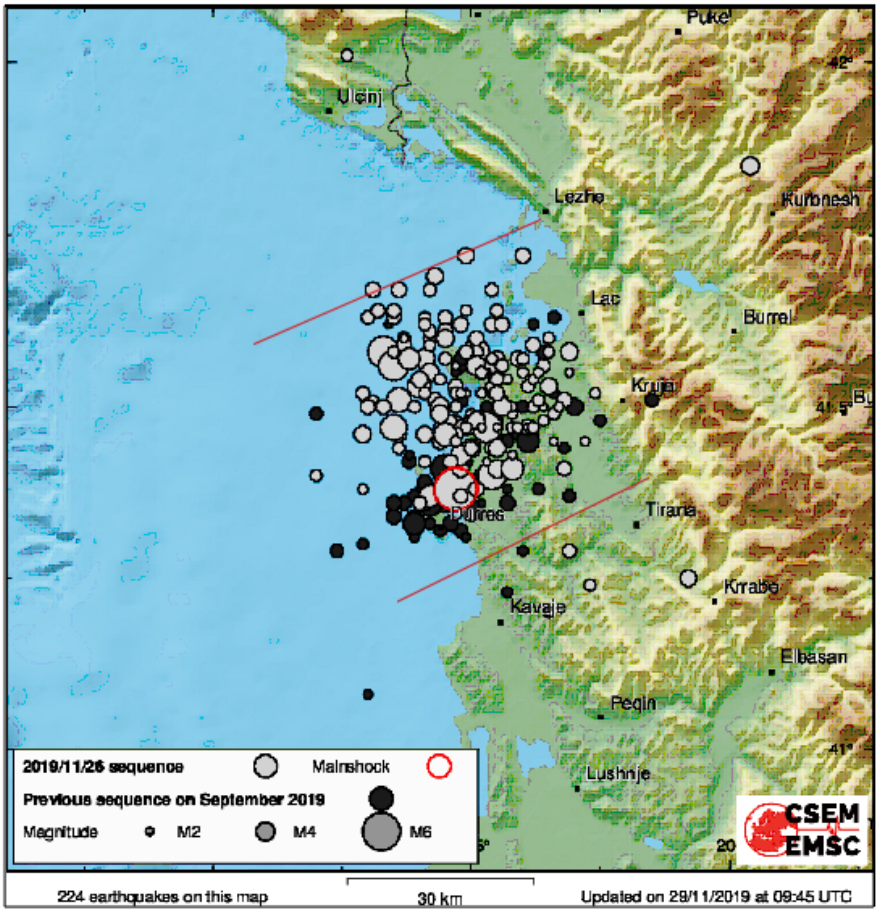

Figure 7. Durresi Earthquakes Epicentre (ASEM ESMSC, 29.11.2019)

Conclusions

1- The study region is located at the intersection of Kruja (Gavrovo), Ionian tectonic zones and Southern Adriatic zone.
2- Longitudinal tectonic faults combined with transverse faults have played a very important role in the formation of Neogene folds and have controlled the sedimentation. The facies in Kruja (Gavrovo) tectonic are neritic, while in Ionian tectonic zone and Southern Adriatic zone are pelagic facies in the southern direction (Tomorri) Kruja (Gavrovo) zone passes from neritic facies (northward) to pelagic facies (southward).
3- The tectonic style of the Southern Adriatic zone is different from Kruja (Gavrovo) and Ionian tectonic zone with big structures dimensions, low structuration scale and considerable depth.
4- The relationship between Kruja (Gavrovo) Ionian tectonic Zone with Southern Adriatic zone is tectonic where the overlap it's some tens kilometers. Some longitudinal and transversal tectonic fault are evident which combined with each other have given to the tectonic structures a certain independence in folding scale and over - thrusting.
5- The structuring tectonic fault that have reached the carbonates formation of Kruja (Gavrovo) tectonic zone have interrupted their activity during Globorotalia Kugleri time, from this time and later some new inter flysch faults have been formed in west direction. The inter flysch faults have controlled all sedimentary formation and tectonic evolution of Southern Adriatic Basin, sedimentation

environments and deposition thickness. These faults are unites and interlaced with each other and when one of them finish acting other younger fault begins to act.

6- The change of the lithology of the formation serve as sliding plans, like evaporates, different schist horizons into carbonate formation and the pass from the carbonate formation to the flysch formation.

7- The Ionian tectonic zone from the southwest to the northeast direction is tectonically faulted. So the Vlora – Elbasan tectonic fault it is not a single fault but an interlacing of western tectonic faults with transversal faults of the structures and structural belts of Ionian tectonic zone.

References

Bega Z, (2017). Chapter 24. In: J. F. Juan I. Soto., *Permo-Triassic Salt Provinces of Europe, North Africa and the Atlantic Margins* (pp. 517-538). Elsevier Science Publishing Co Inc.

Frashëri A., Nishani P. (1996). Relationship between tectonic zone of the Albanides based on results of geophysical studies. *In Ziegler & Hareath Ed.*, 485-511.

Konomi N, (2000). *Harta Gjeologo - Inxhinierike e Shqipërisë Sh 1:200 000.* Tiranë.

Milia A, Torrente MM., Iannace P. (2017). Pliocene-Quaternary orogenic systems in Central Mediterranean: The Apulia-Southern Apennines-Tyrrhenian Sea example. *Tectonics ,* **36**, 1614 - 1631.

Naco P, Kaza Gj, Doda V, Vilçani F, Cara F, (2014) Contribution of the reflected Waves Method in structural modeling of albanides,. *Jour J. Engein. Res. Appl.* **4**, 299-309.

Nazaj Sh., Valbona U, (1990) Relacion përgjithësues Gjeologo- Gjeofizikë për rajonin Mlik-Rodon dhe prespektiven Naftëgazmbajtëse.

Nazaj S, (1995). *Modeli Strukturor dhe evolucioni paleotektonik i rajonit Mlik- Rodon nën driten e koncepteve të teorisë Globale.* Fier.

Ndreko Dh., Nazaj Sh. (2019). Some considerations on tectonic relationship between Ionian and Sazani tectonic zones and their tectonic model. *KNOWLEDGE – Int. J.* **35**(3), 773-778.

Roure F., Nazaj Sh., Mushka K, Fili I, Cadet J.,Bonneau M, (2004) Kinematic Evolution and Petroleum System - An Apprasal of the Outer Albanides. *K.R. McClay, Thrust tectonic and hydrocarbon system.* AAPG Mem., **83**, 474-493.

Sadiku Y, Nazaj Sh., (1989) *Ndertimi gjeologjik i rajonit Divjak për katin e poshtëm tektonik dhe prespektiva naftëgazmbajtëse.* Fier.

Sazhdanaku F, Thomai L, (1988) *Përgjithësimi Gjeologo- Gjeofizikë i Rajonit Tiranë – Fushkruje.* Fier.

Skrami J, (2001) Structural and neotectonic features of the periadratic depression (Albania) detected by seismic interpretation. *Buletin of the Geological Society of Greece Vol. XXXIV*, 1601 - 1609.

Thomai L, Nishani P, (1987). *Përgjithësimi Gjeologo- Gjeofizikë i rajonit të Paprit.* Fier.

URL (2019) Retrieved from ASEM EMSC: November 29, https://www.emsc-csem.org/#2

Velaj T, Davison I, Serjani A., Alsop I, (1999) Thrust tectonic and the role of Evaporite in the Ionian zone of the Albanides. *AAPG Bulletin.* **83(**9), 1408-1425.

Xhomo A, Dimo L, Xhafa I, Nazaj Sh., Nakuci V, Yzeiraj D, Lula F, Sadushi P, Shallo M, Vranaj A, Melo V, Kodra A, Bakalli F, Meco S, (2002) *Gjeologjia e Shqiperise, Stratigrafia, Magmatizmi, Metamorfizmi, Tektonika dhe Evolucioni Paleogjeografik dhe Evolucioni Paleogjeografik dhe Gjeodinamik (Geology of Albania, text of geological mapo f Albania), scale 1:200 000).* Fier: Archive of National Agency of Natural Resources.

J. Int. Environmental Application & Science, Vol. 15(2): 62-67 (2020)

Research Paper

Electromagnetic Field Levels Associated with Selected Mobile Phones

Ekpuk Brown Owoh*, Kingsley Monday Udofia, Akaninyene Bernard Obot

Department of Electrical/Electronic and Computer Engineering, University of Uyo, P.M.B. 1017, Uyo, Akwa Ibom State, Nigeria

Received February 20, 2020; Accepted June 11, 2020

Abstract: This work was carried out to examine the possible potential health risks that result from the use of some commonly available mobile phones in Nigeria. The mobile phones subjected to test were Tecno S1, Touching T1, Infinix hot 6 and Itel 1701. Their electric field strength, magnetic field strength and power density varied significantly per call engagement mode at various varied distances of measurement. Also, their computed head SAR values were observed to be below the limit set by the International Conference on Non-Ionising Radiation Protection. From a potential health hazard point of view, Tecno S1 was found to be the safest for use.

Keywords: *Electric field strength, Health problem, Magnetic field strength, Power density, Specific absorption rate.*

Introduction

Without the use of mobile phones in this 21st century, the world of human activities would be dull and uncoordinated. This is very obvious when considering how the world is being turned into a global village as a result of using such devices for certain purposes. Bhargavi *et al*. (2013) posited that mobile communication involves signal transfer by electromagnetic wave (EMW) through radiofrequency and microwave signals. Based on observation, it has become a common knowledge nowadays that certain mobile phone categories can be employed for a wide range of applications in addition to making of voice calls and text messaging. For example, smartphones can be used to make video calls, schedule tasks, record audio and video signals, take snapshots, navigate locations, and also carry out internet and banking services as well as applications involving security and health. It is noteworthy that mobile phones are no longer the preserve of few wealthy individuals in any society. In other words, due to drastic reduction in cost prices, both young and old can now afford at least one phone for personal use. Eventually, there has been an astronomical increase in the number of phone users. This, in turn, makes the technological advancements in cellular technology/mobile phone applications to be one of the fastest in terms of growth in the last few decades.

Extensive new collection of digital 2019 reports reveals that about 5.11 billion people worldwide use mobile phones (Kemp, 2019). Although the device in question has become a must-own due to the aforementioned advantages, it has been reported that its use has some adverse health effects as a result of exposure to radiofrequency electromagnetic radiations from it. For instance, (Blank & Goodman, 2009) opined that in the course of using mobile phone, electromagnetic wave is transferred to human body with resultant health problems especially at the ear-skull region. Other research reports have it that in the said circumstance, such radiations interfere with the electrical impulses that connect two neurons with each other and can lead to deafness, migraines, high blood pressure, hot and itchy ears, burning skins, headaches and fatique (Bhargavi *et al*., 2013; Mitra *et al*., 2014). In an attempt to address the situation, several international and regional agencies have developed safety limits to serve as guidelines towards safe radiation exposures. However, there may be other cases of related health challenges reported by users but are yet to be scientifically verified and documented.

In recent times, it has been observed that there is unprecedented proliferation of many markets and homes with assorted mobile phones. The substandard or bad ones among them are even being falsely portrayed (by the specification in their user's manual) to possess features that can be utilised to guarantee safety on the part of their users. Also, very many people are in the habit of becoming mobile phone owner (or user) without caring to know about the compliance to safety standards in relation to their phone of interest. Since the utilization of substandard products can cause serious harm, there is no doubt that the radiations emitted in the process of using the said phones can interact with the user's body and cause health problem(s). When considering the activities of smugglers in by-passing

*Corresponding: E-Mail: brownekexcel@yahoo.com; Tel: 08020361602

regulatory authorities to circulate defective products that are not easy to identify by mere physical inspection, the current situation becomes so worrisome these days that public safety concern is expressed to the extent of requiring very urgent attention. This work is, therefore, designed to assess the level of electromagnetic field (EMF) radiations associated with some select low-cost mobile phones that are widely used in Nigeria, so as to ascertain their potential risks to user's health. It is hoped that the findings from this work will be of great benefit to relevant industry and potential users of different mobile phone types/models.

Method

This work was carried out inside a room in Uyo urban, South-South, Nigeria. Tecno S1, Touching T1, Infinix hot 6 and Itel 1701 were selected and then after removed from their case before each of them was used as the source of radiation in this work. Also, four call engagement modes such as Ringing and Answered call (RA), Ringing and Unanswered call (RU), Vibration and Unanswered call (VU), as well as Silent and Unanswered call (SU) were considered. In the experimental setup (Figure 1) used, the phone under test was clamped such that its transceiver maintained a good line of sight with the sensor of an electrosmog meter (TES-92) employed to measure (in tri-axis mode) the instantaneous values of EMF parameters of the phone. In order to avoid interference effect, the caller was always positioned at a distance of about 10 m from where the setup was mounted. Also, active sources of electromagnetic radiations were put off and kept away from the room. The measurement of every parameter was performed three times for each of the phones and at the same varied distances per call engagement mode. In each case, the mean values of the results were determined and analysed.

Based on the maximum values of electric field strength obtained at 5 cm, the localized specific absorption rate (SAR) of human head was calculated using the relation (Joanna *et al*., 2012; Kumar & Bhat, 2013)

Figure 1. Set-up for measurements of EMF parameters of the selected mobile phones.

$$\text{SAR} = \frac{\sigma |E|^2}{2\rho} \qquad 1$$

where σ is tissue conductivity, ρ is tissue density and E is electric field strength expressed as (Kumar and Pathak, 2011)

$$E = E_o \, exp\left|-z/\delta\right| \qquad 2$$

where E_o is incident electric field on the body surface, δ is skin depth and z is depth of tissue with respect to incident field (Figure 2).

For computation of skin depth, the following equation was used (Sallomi, 2012):

$$\delta = \sqrt{\frac{1}{\pi\mu\sigma f}} \qquad 3$$

where μ is tissue permeability ($4\pi \times 10^{-7}$ H/m) and f is frequency (900 MHz and 1800 MHz) of the electromagnetic radiations. The values of tissue density and conductivity used in this work were based on the data provided by Stankovic *et al*., (2017) as shown in Table 1.

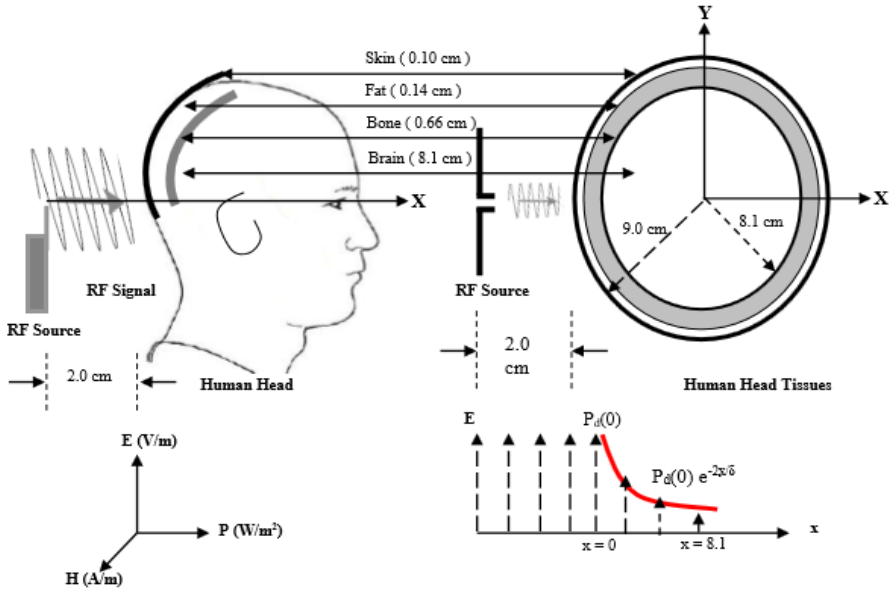

Figure 2. Human head model

Table 1. Characteristics of tissues at 900 MHz and 1800 MHz

Tissue	σ (S m^{-1})	ρ (kg m^{-3})
Skin	0.867[a]	1109
	1.180[b]	1109
Fat	0.109[a]	911
	0.190[b]	911
Bone	0.143[a]	1908
	0.275[b]	1908
Brain	0.7665[a]	1046
	1.710[b]	1046

Source: Stankovic et al. (2017).

Where: a is value at frequency of 900 MHz and b is value at frequency of 1800 MHz.

Results and Discussion

The mean values obtained from the measurements of the EMF parameters are registered in Table 2. Also, the computed values of head SAR and the regulated limits specified in electromagnetic guidelines by International Conference on Non-Ionising Radiation Protection (ICNIRP, 1998) are presented in Table 3.

From Table 2, it can be seen that the mean values of the EMF parameters for each call engagement mode decrease with increasing distance from the phone (source of radiation). This simply portrays the fact that even if there is a long-term exposure to the radiation, less effect of it would be experienced by a user whose body is usually at a distance that is reasonably far from the mobile phone used. As evident from the results, the recorded values of magnetic field strength are greater than those obtained under the same conditions for electric field strength. By implication, the selected phones are capable of emitting electromagnetic radiations with greater proportion of magnetic field effect than the electric field counterpart. Irrespective of the mode of engagement, it is crystally clear from the results that the least values of each EMF parameter at all varied distances are obtained with the use of P1. However, at the closest distance (being 5 cm in this study) from the mobile phone, the highest value of electric field strength is obtained in the case of P3 in all the engagement modes, whereas P2 shows such tendency for magnetic field strength except in VU and SU modes. For power density, the highest obtained value is associated with P3 in RA mode, P2 in RU mode and P4 in VU and SU modes. On the whole, the maximum mean power density value in this work (80.76 μW/cm^2) is observed to be far less than the minimum value of 0.3 μW/m^2 obtained by Shalangwa et al., (2011) for testing selected mobile phones of different models held at a distance of 0.01 m from the head. The disparity noticed in

the two results may be understood to be due to the twin factors of measurement distance, the type and model of phones involved in the study.

Though the results obtained in this work appear to differ across the engagement modes for each of the phones used, one-way analysis of variance performed at 0.05 level of significance shows that the differences are not significant. This implies that the possibility of experiencing negative health effect does not depend mainly on any of the call modes considered for the selected phones. However, for each of the engagement modes, the same statistical analysis reveals that the results of any of the measured parameters recorded for the phones are significantly different. This may be attributed to differences in the ages, types and/or qualities of the phones.

Table 2. Mean values of the measured EMF parameters of the tested phones

Oper. mode	Distance (cm)	Electric field strength (mV/m)				Magnetic field strength (μA/m)				Power density (μW/cm^2)			
		P1	P2	P3	P4	P1	P2	P3	P4	P1	P2	P3	P4
RA	5	8.542	18.92	26.82	22.23	20.96	53.74	46.75	44.26	25.97	48.20	52.12	51.11
RA	10	4.278	14.26	22.95	20.15	15.92	42.71	39.16	40.01	19.51	37.65	45.57	44.72
RA	15	3.208	12.54	20.97	19.12	12.85	36.01	35.95	35.45	12.97	34.08	36.95	35.52
RA	20	2.257	11.82	15.71	16.14	11.52	26.73	31.27	31.03	5.582	32.17	28.18	27.17
RA	25	2.097	8.746	12.56	12.52	8.537	23.46	23.93	22.89	4.621	24.51	22.24	20.33
RA	30	1.942	7.421	9.847	9.115	7.362	21.74	20.35	19.78	3.968	12.72	18.20	17.57
RA	35	1.834	6.624	7.950	7.023	5.399	19.23	18.18	17.58	2.711	7.785	16.93	15.96
RA	40	1.388	5.347	6.657	6.724	4.921	17.93	15.46	15.34	1.715	6.284	14.19	13.46
RA	45	1.276	5.170	4.891	4.512	4.382	13.16	14.61	13.99	1.315	3.383	11.46	11.24
RA	50	1.205	3.572	3.955	3.365	3.214	10.92	13.92	12.82	0.750	2.492	8.872	7.915
RU	5	7.943	14.83	28.97	25.42	19.24	73.91	48.13	59.04	11.42	80.79	43.15	63.23
RU	10	7.245	12.56	24.57	23.93	17.10	57.23	45.71	53.17	10.53	72.60	41.10	60.04
RU	15	5.097	10.45	21.11	20.59	15.83	30.56	43.79	49.14	7.415	51.32	39.11	55.11
RU	20	3.725	9.731	13.15	17.54	13.42	28.63	40.35	46.98	5.814	43.75	35.52	50.37
RU	25	2.915	8.063	12.53	16.01	10.31	26.45	37.41	38.52	4.171	30.97	30.15	41.88
RU	30	2.895	7.791	11.55	15.21	8.973	22.17	32.74	32.61	3.710	18.15	22.61	35.11
RU	35	2.091	7.588	10.73	13.02	8.357	19.01	30.58	28.29	3.058	11.81	16.53	30.42
RU	40	1.962	7.415	10.50	11.18	7.182	18.01	28.40	25.51	2.424	9.251	14.28	22.45
RU	45	1.752	6.672	9.725	10.01	6.573	12.91	25.56	23.34	2.409	7.650	11.36	15.77
RU	50	1.519	5.098	8.202	6.923	5.741	11.87	21.51	19.58	1.657	5.673	9.143	10.81
VU	5	11.42	12.68	19.34	14.74	24.46	33.41	31.07	34.80	34.18	42.32	41.23	43.59
VU	10	7.651	11.94	17.77	13.45	20.74	31.87	30.23	31.52	17.62	37.92	39.98	35.54
VU	15	5.827	10.59	16.65	12.75	16.87	27.41	28.91	30.34	12.72	35.12	37.83	32.72
VU	20	4.456	9.771	15.02	11.52	13.96	25.92	25.98	28.25	8.712	32.46	35.22	29.75
VU	25	3.742	8.769	14.16	10.84	10.15	24.54	23.45	27.91	5.002	28.35	32.98	28.73
VU	30	3.457	8.387	12.13	10.53	10.08	20.72	20.54	26.27	4.269	23.97	29.52	27.51
VU	35	3.214	7.793	10.98	10.25	9.157	18.99	19.01	23.34	3.749	17.60	25.76	20.82
VU	40	2.579	7.755	9.542	9.454	8.827	17.67	17.74	20.84	2.626	13.75	22.11	15.42
VU	45	1.779	7.054	9.154	9.342	7.679	12.61	15.09	19.80	1.568	10.03	19.06	10.46
VU	50	1.452	5.227	6.065	5.873	5.362	8.511	14.35	19.51	0.798	9.862	13.22	7.682
SU	5	8.505	12.92	12.97	12.34	24.05	34.57	32.72	30.65	25.92	41.72	41.27	42.72
SU	10	7.342	11.71	12.95	12.23	16.80	31.32	29.48	29.57	15.31	37.62	40.20	41.10
SU	15	3.804	10.52	12.84	12.11	12.94	29.46	27.34	27.21	10.54	32.05	39.52	40.22
SU	20	3.282	9.512	12.82	11.87	10.71	27.56	26.39	25.99	7.921	30.54	30.80	37.65
SU	25	2.814	8.302	12.72	11.36	10.01	24.72	24.08	25.12	4.452	25.41	28.95	33.54
SU	30	2.683	7.742	11.46	11.13	9.525	21.83	22.87	21.95	3.942	21.45	27.63	29.62
SU	35	2.584	6.751	10.85	9.959	7.201	18.75	20.53	19.64	3.668	15.52	25.58	25.33
SU	40	2.482	5.457	9.371	8.628	6.714	17.82	20.45	18.03	1.955	12.83	20.93	19.20
SU	45	1.747	4.207	7.674	7.453	5.363	15.63	19.63	16.16	1.446	9.213	17.52	15.09
SU	50	1.243	3.026	6.213	5.582	3.447	13.95	17.43	15.05	0.432	5.573	10.75	9.093

P1= Tecno S1, P2 = Touching T1, P3 = Infinix hot 6, and P4 = Itel 1701.

Figure 3 shows the plots of how the EMF parameters vary with the measured distances from the tested phones per engagement mode. It can be deciphered from them that the electric field strength, magnetic field strength and power density for each of the phones show exponential variations with increase in the distance in question notwithstanding the engagement mode of the phones. The seeming

similarity in the power density plots for VU and SU modes justifies the statistically verified fact earlier stated above that there is no significant influence of phone engagement mode on the EMF parameters.

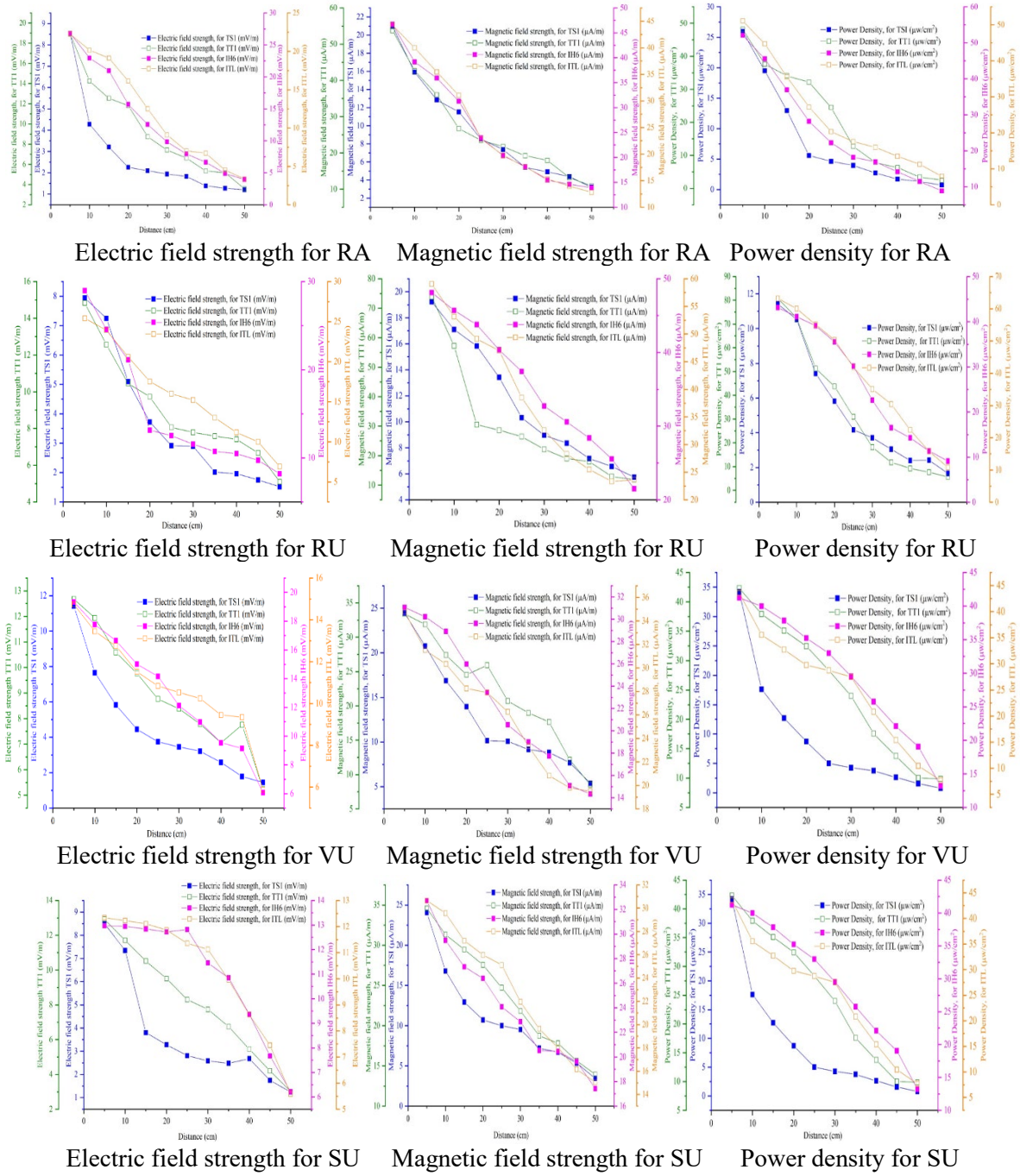

Figure 3. Variation of EMF parameters with distances from the tested phones for different call engagement modes (a) Electric field strength (b) Magnetic field strength (c) Power density.

Table 3. Computed head SAR values at different operating frequencies of the phones

Phone type/model	Frequency (MHz)	SAR (10^{-7} W/kg)
P1	900	0.97
P2	900	2.65
P3	900	6.21
P4	1800	6.84

It can be inferred from a careful observation of the results that the mean values of power density for VU mode are greater than those obtained for the SU mode with respect to the phones used. Moreover, at measurement distance of 5 cm from the phones, Table 3 entries show that the computed head SAR at 900 MHz ranges in value from 0.97×10^{-7} W/kg to 6.21×10^{-7} W/kg with P3 having the highest. Observably, this maximum value of head SAR at 900 MHz and the value of 6.84×10^{-7} W/kg obtained for P4 at 1800 MHz are less in the order of 10^{-4} than 1.8×10^{-3} W/kg head SAR value got by Shalangwa *et al*., (2011) and Kumar and Bhat, (2013) at a measured distance of 0.01 m from a 900 MHz mobile phone radiation source. This is, plausibly, due to differences in transmission power from the transmission tower as well as antenna quality. Also, though the calculated head SAR values at both frequencies are well below the regulated limit of 2.0 W/kg stipulated by (ICNIRP, 1998), P1 has the least value possible. This means that with its use, the user can be sure of being exposed to the least amount of radiofrequency radiation. It can be well said, based on equation 1 used in this work, that SAR value varies positively with that of electric field strength. On the strength of this consideration, it follows that the calculated head SAR value will only increase as the mobile phone is held closer to the user's head. This trend enjoys the support of, and resonates with the findings of (Kargel, 2005).

Conclusion

It was found in this work that electric field strength, magnetic field strength and power density vary significantly among Tecno S1, Touching T1, Infinix hot 6 and Itel 1701 phone types and models at same distances of measurement. Also, the results obtained revealed that variations in their call engagement modes have no significant effect on the emitted radiations. Again, by having the least value of head SAR, Tecno S1 could be rightly adjudged to be the safest, though all the phones used in this study have head SAR values that are less than the limit stipulated by ICNIRP. Above all, the findings from this work indicate that the selected phones cannot pose serious health problems to their users.

References

Bhargavi K, Balachandrudu KE, Nageswar P, (2013) Mobile Phone Radiation Effects on Human Health. *Int. J. Comput. Engin. Res.,* **3**, 196-203.

Blank M, Goodman R, (2009) Electromagnetic fields stress living cells. Pathophysiology: the official journal of the International Society for *Pathophysiology* **16**, 71-78.

ICNIRP International Conference on Non- Ionising Radiation Protection (1998). Health Physics, **74**, 494-522.

Joanna M, Arkadiusz M, Andrzej W, (2012) Numerical Analysis of high frequency electromagnetic field distribution and specific absorption rate in realistic breast models. *Przeglad Elektrotechniczny*, 97-99.

Kargel C, (2005) Infrared thermal imaging to measure local temperature rises caused by handheld mobile phones. IEEE transaction on instrumentation and measurement, 54, 1513-1519.

Kemp S, (2019) Digital 2019: Global Digital Overview. Accessed by web, URL (Accessed on 30 December 2019).

Kumar S, Pathak PP, (2011) Effect of electromagnetic radiation from mobile phone towers on human body. *Ind. J. Radio & Space Physics* **40**, 340-342.

Kumar V, Bhat MA, (2013) Calculation of SAR and measurement of temperature change of human head due to the mobile phone waves at frequencies 900 MHz and 1800 MHz. Ad. *Physics Theories & Appl*., **16**,

Mitra R, Mazumder M, Pal K, Jana S, (2014) A study on effect of mobile phone radiation on human health. *Explor. Animal Medical Res.,* **4**, 246-252.

Sallomi AH, (2012) A Theoretical Approach for SAR Calculation in Human Head Exposed to RF Signals. *J. Engin. & Develo*., **16**, 304-313.

Shalangwa DA, Vasira PG, Waba AS, (2011) Health risk of using Global System for Mobile Communication (GSM) mobile phone. *Int. J. Electro. & Appl.* **1**, 16-18. Doi: 10.5923/j.ijea.20110101.04.

Stankovic V, Jovanovic D, Krstic D, Markovic V, Dunjic M, (2017) Calculation of electromagnetic field from mobile phone induced in the pituitary gland of children head model. *Vojnosanit Pregl.* 854-861.

J. Int. Environmental Application & Science, Vol. 15(2): 68-80 (2020)

Research Paper

3D Modelling of the Wind Flow Trajectories and Its Characteristic Effects on Horizontal Axis Wind Turbine at Different Wind Regimes

Etuk Ekom Mike[1, *], Ikpe Aniekan Essienubong[2]

[1]Department of Production Engineering, University of Benin, Benin City, PMB 1154, Nigeria; [2]Department of Mechanical Engineering, University of Benin, Benin City, PMB 1154, Nigeria

Received March 18, 2020; Accepted May 01, 2020

Abstract: In this study, an overview of the effect of turbulence on wind turbine performance is presented. Flow Models with full description were generated to clearly illustrate Winfield plots, 3 Dimensional Spatial Wind Flow Directions, Wake Distribution Patterns behind the Rotors, and 3 Dimensional Spatial Turbulent Wind Distribution Patterns. The power and the coefficient of power were examined from the wake vortex simulation while the flow velocity cut plots at different wind speeds (2, 4, 6 and 8 m/s) and time steps (2, 4 and 6 s) were obtained using Q-Blade software. The results revealed that, while the power coefficient was observed to decrease and increase with increasing wind speed, the power output increased variably from 0.0416903 to 2.51354 kw as the wind speed also increased from 2 to 8 m/s at peak time step of 6s. It was also found that, while the wind influx towards a wind turbine can be displaced by extreme turbulence which subsequently displaces the wind directions, reduces turbine trust, power coefficient and the power output; the wake effect downstream can affect the wind speed and performance of other turbines downwind. The characteristics and complexity of a given terrain as well as the aforementioned factors should be considered while siting and operating a wind turbine or wind farm.

Keywords: *Modelling, Wind flow, Wind turbine, Wake vortices, Turbulence, Wind direction,*

Introduction

Atmospheric wind flow has a strong turbulence fluctuation and shows transient characteristics (Kim & Kim, 2012). Upon approaching a wind turbine, the wind speed decreases and turbulence increases. Consequently, rotation of the wind turbine blades results in turbulence, manifesting in the form of rotational vertical wakes which are sustained behind the rotors in a distance for several miles before being dissipated fully (Brand *et al*., 2011). The turbulence in the flow towards a wind turbine is modelled on the basis of similarity theory in combination with computational fluid dynamics (CFD) methods (Satoh, 2004). Mikkelsen (2013) investigated the effect of free stream turbulence on a model wind turbine's performance characteristics and the wake development downstream using a reference wind speed of 10 m/s. The wind turbine was found to operate most efficiently at TSR≈6, the peak power coefficient (C_p) without free stream turbulence was 0.461, while C_P of 0.45 was obtained with free stream turbulence. Hence, the power coefficient seemed to be slightly reduced with increased levels of turbulence, except at low tip speed ratios where the effect of stall dominated.

The effects of wind shear and inflow turbulence on the performance of a semisubmersible offshore floating wind turbine was investigated by Li *et al*. (2018). It was observed that the ultimate structural and fatigue damage loads at the blade root were augmented by inflow turbulence and wind shear. Both the ultimate and fatigue damage loads increased as a result of inflow turbulence and wind shear. The effect of inflow turbulence on the power generation was observed to depend on the operational state due to the control scheme of the wind turbine.

Existing wind farm wake models vary from low-fidelity empirical and semi-empirical approaches (Ainslie, 1988), to more complex high fidelity large-eddy simulations where the turbines are parameterized using either an actuator disc (Jimenez, 2007), or an actuator line approach (Troldborg *et al*., 2010, Troldborg *et al*., 2011). Actuator disk (Sanderse, 2000), and actuator line (Troldborg *et al*., 2010), methods have been employed in simulating the rotor and aerodynamic flow around a wind turbine by solving the NS equations, which enabled the CFD domain to cover the region extending from the

*Corresponding: E-Mail: alwaysetuk@gmail.com; Tel: +2348025276325; Fax: +23452602361

rotor plane to several diameters downstream, and to fully compute the near and far vortex wake elements.

Wußow et al. (2007) employed CFD model (ANSYS FLUENT 6.3 using the LES technique) to simulate a full meandering turbulent wake using an incoming wind field that matches the IEC-61400 requirements. Tip or nacelle vortices were only slightly present in the near wake region which was observed to meander horizontally and vertically. The relatively high velocity gradients experienced at either the outer and inner edges of the wake in conjunction with the meandering contributed significantly to the turbulence intensity observed on a ten-minute time scale. Zhang *et al*. (2012) investigated the near-wake flow structure downwind of a wind turbine in a turbulent boundary layer, and observed that the significant turbulence enhancement at a distance of three rotor diameters is associated with strong wind shear and high mechanical production of turbulent kinetic energy at the top-tip level. The spatial distribution of vorticity and swirling strength measured with High-resolution particle image velocimetry (PIV) also revealed the presence of top-tip vortices, which persist up to about 2-3 rotor diameters downwind of the turbine, longer than the hub/root vortices in the near wake region. The measurements also revealed intense flow rotation and a highly non-axisymmetric distribution of the mean flow and turbulence structure in the near wake.

In an experimental investigation conducted by Ozbay *et al*. (2016), on wake characteristics and aeromechanics of Dual-Rotor Wind Turbines, the vortex structures were found to move outward with the expansion of the wake flow as they moved downstream, and finally merged with the tip vortex structures and eventually dissipated further downstream. In an experimental study on the evolution of unsteady wake vortex structures in turbine wake flows, Tian *et al*. (2014), Hu *et al*. (2012), and Whale *et al.* (2000) also observed related vortex structures at approximately 50-60% span of the rotor blades. In this study, wind flow trajectories, wind field regime and characteristics were modelled at various wind speeds, and their effects on horizontal axis wind turbine performance were examined.

Materials and Method

The flow around a rotor blade is modelled by using blade element/momentum theory and employing sectional airfoil data (Sørensen, 2011). The airfoil data have been found to depend heavily on unsteady flow (Devinant *et al*., 2002). The airfoil data is practically obtained from a wind tunnel experiments but can also be obtained through conventional methods such as computational fluid dynamics or aerodynamic design methods. In this study, the flow around a rotor blade was modelled using blade element/momentum theory embedded in QBlade software. A generator for turbulent windfields and module to generate a simplified structural model is integrated in QBlade v0.8 which was used to setup a FAST unsteady aeroelastic simulation reported in this study. Turbulent Windfield Generator which is a submodule of QBlade uses the Sandia Method to create turbulent windfield. The QBlade simulation interface is presented in Figure 1.

Figure 1. QBlade simulation interface

The windfield objects generated were further used in a FAST simulation. From inside the FAST module, aeroelastic FAST simulation was set up, simulated and post processed from QBlades internal database. To setup a FAST simulation for the windfield, details of the rotor, simulation parameters, windfield parameters and the blade structure were specified in the Parameter tab as shown in Table 1. This enabled the visualization of different time steps using the slider inside the toolbar.

Table 1. Flow parameters employed in the wind field simulation

Wind field Parameter	Simulation Parameter	Wind Field Properties	Environment
Time: 60s	Hub Height: 15 m	2 m/s	Gravity: 9.81 m/s^2
Time steps: 100	Measurement Height: 15 m	4 m/s	Air Dens: 1.225 k/m^3
Points per direction: 40	Turbulence Intensity: 5%	6 m/s	Kin Visc: 1.4661e-05 m/s
No of blades: 3	Include Shear Layer: True	8 m/s	
Nacelle Yaw: 0 Deg.	Roughness Length: 1e-02 m		

The degrees of freedom of the structural model (FlapDOF 1&2, EdgeDOF) was enabled in order to effectively observe the simulation iterations through visual process. The simulation was initiated by pressing the start simulation button from the dock. When the simulation was completed, the FAST results were automatically loaded inside QBlades database for observation. The theory and mathematical formulations upon which the simulation in this study is based are already embedded in the software, and can be expressed in the following Equations:

Reynolds number which is considered as the inertial forces divided by viscous forces is given by Equation 1.

$$Re = \frac{U_\infty D}{v_w} \quad (1)$$

where U_∞ is the free stream velocity, D is the turbine diameter and ν is the wind viscosity. The chord Reynolds number Re_c is the same as Equation 1, with the blade chord length c being the characteristic length scale:

The kinetic energy of an air mass m moving at a velocity U can be expressed as:

$$E = \frac{1}{2}mU^2 \quad (2)$$

The mass flow rate of air with density p, passing through the rotor cross-sectional area A is given by Equation 3 while the power available in the air stream is expressed in Equation 4.

$$\dot{m} = \rho UA \quad (3)$$

$$P = \frac{1}{2}\rho U^3 A \quad (4)$$

The lift and drag coefficients, based on the lift L and drag D per unit length are given by Equation 5 and 6.

$$C_L = \frac{L}{\frac{1}{2}\rho U_{rel}^2 c} \quad (5)$$

$$C_D = \frac{D}{\frac{1}{2}\rho U_{rel}^2 c} \quad (6)$$

where U_{rel} and c denotes the chord length. The relative wind velocity U_{rel} expressed in Equation 7, is the relative velocity between the axial velocity U and the rotational velocity $r\Omega$ at the local intermediate radius r. The solidity σ of a turbine at a radial position r is given by Equation 8.

$$U_{rel}^2 = U^2 + (r\Omega)^2 \quad (7)$$

$$\sigma(r) = \frac{c(r)B}{2\pi r} \quad (8)$$

where B is the number of blades. The total solidity can then be found by integrating Equation 8 along the blade radius. According to Fukumoto & Okulov (2005), Wind turbine wakes are modelled as helical vortices which represents the region where the flow is spinning about an axis. Figure 2 shows the cross sectional view of a helical vortex around a wind turbine rotor.

In a cylindrical coordinate system, the velocity field is described (Zheng & Wu, 2018) as follows:

$$u_\rho = \frac{\Gamma}{2\pi\rho l}\sqrt[4]{(l^2+\rho^2)(l^2+a^2)}\,Im\left\{\frac{e^{ix}}{e^{\pm\xi}-e^{ix}} \pm \frac{l}{24}\left[\frac{2l^2+9a^2}{(l^2+a^2)^{3/2}} - \frac{2l^2+9\rho^2}{(l^2+\rho^2)^{3/2}}\right] log\left(1-e^{\pm\xi+ix}\right)\right\}, \quad (9a)$$

$$u_z = \frac{\Gamma}{2\pi l}\begin{Bmatrix}1\\0\end{Bmatrix} + \frac{\Gamma}{2\pi l}\frac{\sqrt[4]{(l^2+a^2)}}{\sqrt[4]{(l^2+\rho^2)}}\,Re\left\{\frac{\pm e^{ix}}{e^{\pm\xi}-e^{ix}} + \frac{l}{24}\left[\frac{3\rho^2+2l^2}{(l^2+\rho^2)^{3/2}} + \frac{2l^2+9a^2}{(l^2+a^2)^{3/2}}\right] log\left(1-e^{\xi+ix}\right)\right\}, \quad (9b)$$

$$u_\phi = \frac{\Gamma}{2\pi l} - \frac{l u_z}{\rho} \quad (9c)$$

where u_ρ, u_z and u_ϕ are the velocities in *p, z* and ϕ coordinates in Figure 2, Γ is the circulation of the vortex filament and α is the radius of the helical vortex. To avoid singularity at the mid-section of the helical vortex filament which may result in overestimated velocity values in the airflow close to the vortex centre, flow velocity around the helix is modelled as the rotation core axis (Fukumoto & Okulov, 2005, Mulinazzi & Zheng, 2014).

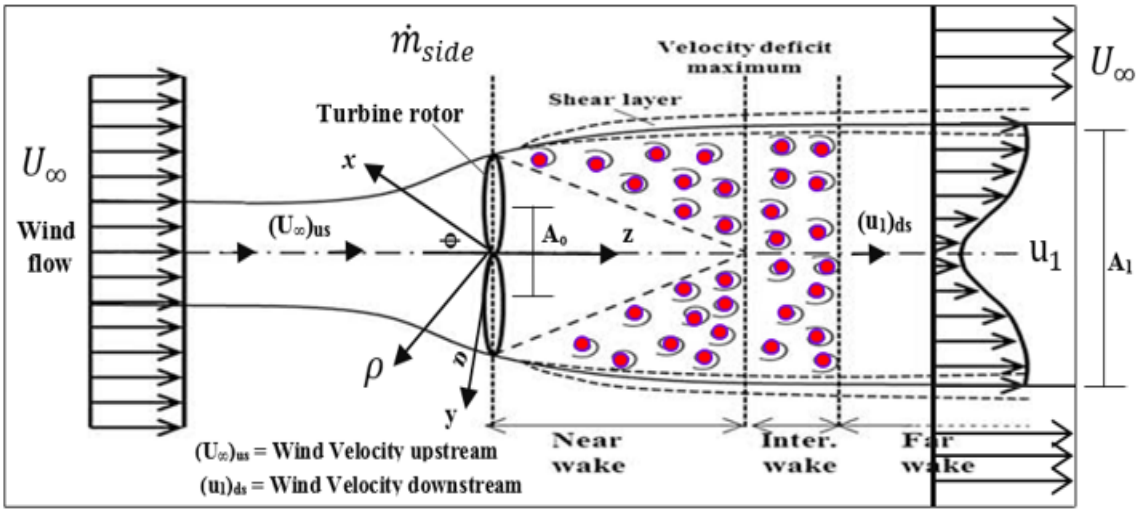

Figure 2. Cross sectional view of a helical vortex around a wind turbine rotor

$$v = \frac{\Gamma}{2\pi\sigma^2}\alpha \quad (10)$$

Where σ is the core size of the helical vortex. Conservation of momentum and mass for the helical control volume with a cross section shown in Figure 2 are given by Equation 11 and 12 (Odemark, 2012).

$$\rho u_1^2 + \rho u_\infty^2(A_0 - A_1) + \dot{m}_{side}U_\infty - \rho U_\infty^2 A_0 = -T \quad (11)$$

and

$$\rho u_1 A_1 + \rho U_\infty(A_0 - A_1) + \dot{m}_{side} = \rho U_\infty A_0 \Rightarrow \dot{m}_{side} = \rho A_1(U_\infty - u_1) \quad (12)$$

Mass conservation is also expressed as:

$$\dot{m} = \rho u A = \rho u_1 A_1 \quad (13)$$

Combining Equation 11-13 yields:

$$T = \rho u A(U_\infty - u_1) = m(U_\infty - u_1) \quad (14)$$

where U_∞ is the free stream velocity (upstream), u_1 is the wind velocity downstream, T is the thrust force, A is the rotor area, ρ is the air density, $\dot{m}_{side}$ and m are the total mass flow out of the surface area. The wind velocity at the rotor plane is the mean between the velocity far upstream and downstream, and can be expressed as:

$$u = \frac{1}{2}(U_\infty - u_1) \quad (15)$$

By defining a control volume following the streamlines and applying the conservation of energy, the following relationship for the power P is found (Odemark, 2012).

$$P = \dot{m}\left(\frac{1}{2}U_\infty^2 + \frac{\rho_\infty}{\rho} - \frac{1}{2}u_1^2 - \frac{\rho_\infty}{\rho}\right) \Rightarrow P = \frac{1}{2}\rho U A\,(U_\infty^2 - u_1^2) \quad (16)$$

where ρ_∞ is the free stream static pressure. By introducing the axial induction factor a and applying Equation 15, the power and the thrust forces can be expressed as:

$$P = 2\rho U_\infty^3 a(1-a)^2 A \quad (17)$$

and

$$T = 2\rho U_\infty^2 a(1-a)\,A \quad (18)$$

where the axial induction factor a is given by Equation 19 while the angular induction factor a' is defined by Equation 20.

$$a = \frac{U_\infty - u_1}{U_\infty} \quad (19)$$

$$a' = \frac{\omega}{2\Omega} \quad (20)$$

where Ω denotes the angular velocity of the wind turbine rotor, and ω is the angular velocity imparted to the flow stream. The dimensionless power and thrust coefficients thus become:

$$C_P = \frac{P}{\frac{1}{2}\rho U_\infty^3 A} = 4a\,(1-a)^2 \quad (21)$$

and

$$C_T = \frac{T}{\frac{1}{2}\rho U_\infty^2 A} = 4a\,(1-a) \quad (22)$$

The tip speed ratio (TSR) λ is the ratio between the rotational velocity at the tip of the blade and the free stream velocity U_∞, expressed in Equation 23:

$$\lambda = \frac{\Omega R}{U_\infty} \quad (23)$$

Using the energy equation on a control volume that moves with the blade, the pressure difference across the blade can be expressed as (Manwell et al., 2009):

$$p_2 - p_3 = \rho\left(\Omega + \frac{1}{2}\omega\right)\omega r^2 \quad (24)$$

where ω is the angular velocity and R is the rotor radius. Applying Equation 20, 23 and 24, the thrust on an annular element can be expressed in Equation 25.

$$dT = 4a'(1+a')\frac{1}{2}\rho\Omega^2 r^2 2\pi r dr = 4a(1-a)\frac{1}{2}\rho U^2 2\pi r dr \quad (25)$$

The torque Q, exerted on the blade, is equal to the change of angular momentum of the wake. Therefore, the torque for an incremental annular area element, is given by Equation 26.

$$dQ = d\dot{m}(wr)r = 4a'(1-a)\frac{1}{2}\rho U\Omega r^2 2\pi r dr \quad (26)$$

The instantaneous wind speed in the three dimensions u, v and *w* can be defined as,

$$u_1 = U_\infty + u_1' = \bar{u}_1 + u_1' \quad (27a)$$

$$v = V + v' = \bar{v} + v' \quad (27b)$$

$$w = W + w' = \bar{w} + w' \quad (27c)$$

The characterization of turbulence may be by a relatively constant short-term mean, with fluctuations about the mean, and the probability density function that best describes the type of behaviour for turbulence is the Gaussian distribution expressed as:

$$f(u_1) = \frac{1}{\sigma_u\sqrt{2\pi}} exp\left[-\frac{(u_1 - U_\infty)^2}{2\sigma^2_{u_1}}\right] \quad (28)$$

Turbulence intensity in the streamwise direction is given by Equation 29.

$$T_u = \frac{\sigma_u}{U} \quad (29)$$

where σ_u is the standard deviation of wind speed variations about the mean wind speed U.

Using the mean turbulent normal stresses $\bar{u}_1'$, kinematic viscosity v' and the rotational speed of wake w', the turbulent kinetic energy can be quantified as:

$$k = \frac{1}{2}(\bar{u}_1'\,\bar{u}_1') + (\overline{v'}\,\overline{v'} + \overline{w'}\,\overline{w'}) \quad (30)$$

The equation for the evolution of turbulent kinetic energy is expressed as:

$$\frac{Dk}{Dt} + \nabla.T' = P - \epsilon \quad (31)$$

where $\nabla.T'$ is the turbulent transport or turbulent diffusion, P is the production of turbulent kinetic energy (the source) and ϵ is the dissipation of turbulent kinetic energy.

Windfield Plots

Modelling of wind field is an important aspect of wind turbine blade related studies, as it provides images as well as animated visuals of how the wind velocity impacts forces on the rotor blade to cause its rotation. To understand the interplay between the rotor blade and its driving mechanism, wind field must be modelled to effectively represent the wind speed range in the domain intended for the rotor blade to perform. The flow field around a wind turbine may be characterized by two major mechanisms including convection and turbulent diffusion (Vermeer et al., 2003). In this study, the wind field plots as shown in Figure 3a-d represents the distribution of surface plot of the wind perpendicular to the turbine axis. All wind heights are taken at 15m and a constant turbulence of 5%. A wind shear of 0.001m is assumed for all wind fields. The simulation was run for 60s and results are shown at a time step of 100. The wind measurement height was at 15m from sea level.

Cold air which is denser, sinks to the ground because the air molecules are too heavy to soar higher in the atmosphere while hot air which is less dense rises and in the process circulates across the atmosphere. The air circulation process may be referred to as "Wind" because it is characterized by a current of air flowing in various directions across the earth's surface.

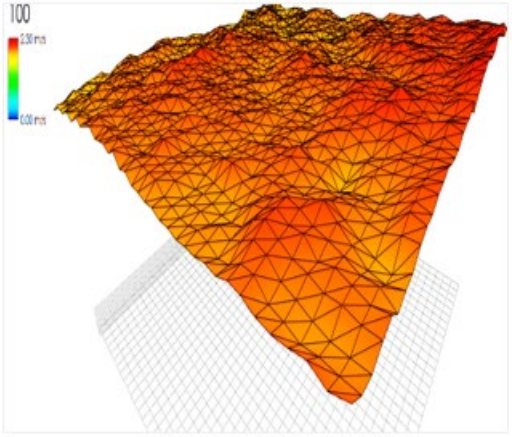

Figure 3a. Winfield plot at mean wind speed of 2 m/s

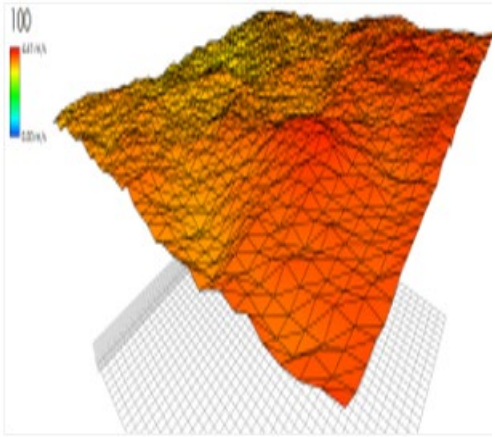

Figure 3b. Winfield plot at mean wind speed of 4 m/s

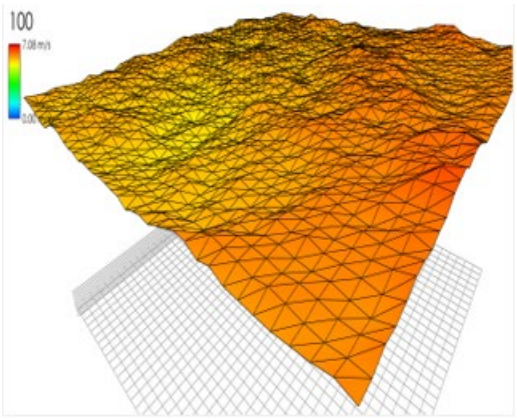

Figure 3c. Winfield plot at mean wind speed of 6 m/s

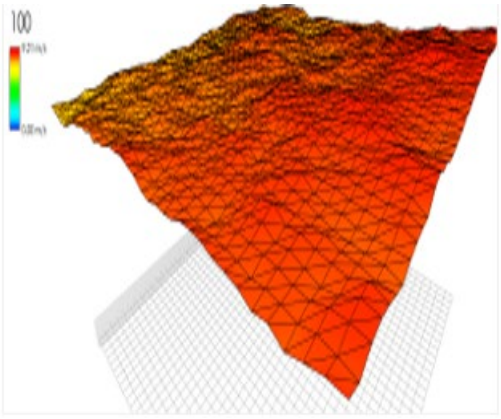

Figure 3d: Winfield plot at mean wind speed of 8 m/s

Generally, wind direction which is usually parallel to isobars due to earth's rotation may also be horizontally transverse such that it either flows sideward from the direction it originates towards an angle ranging from 0º- 360º and across the windfield as shown in Figure 4a-b, or may occur in the vertically transvers direction as shown in Figure 4c-d. It should be noted that the rotational speed of a given turbine blade is highly dependent on not only the wind speed but also on the wind direction. Therefore, if the maximum wind flow is not towards a direction suitable enough to cause the wind turbine rotor blade to attain its optimum speed, the wind turbine may perform below the expected capacity. Hence, it is necessary for the wind direction in a particular region to be studied extensively before mounting the wind turbine as well as its blades, as this can provide useful information on the angle of attack or angle of incidence and the direction to which high velocity magnitude gradient/maximum wind speed is expected.

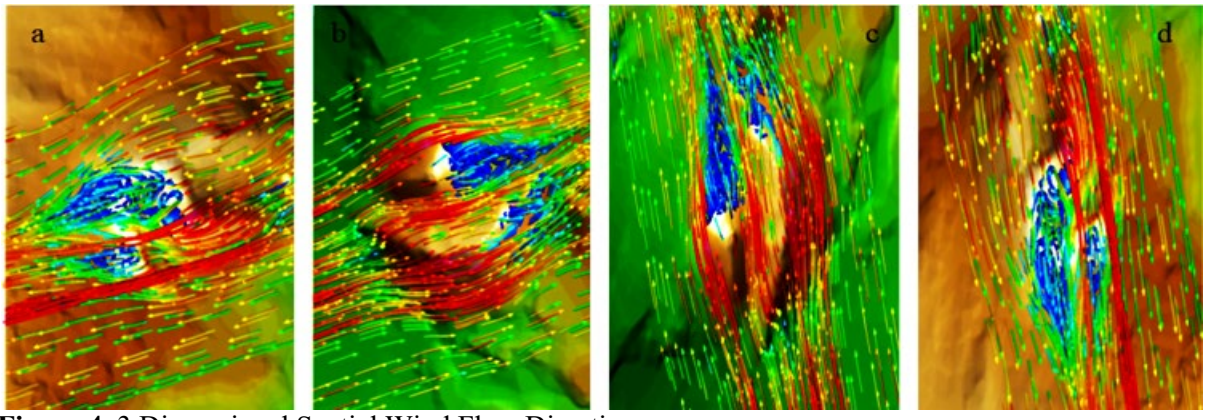

Figure 4. 3 Dimensional Spatial Wind Flow Directions

The wind flow regime as observed in Figure 4a-d, shows a network of wind current that is distributed across a given flow path. This is independent on the wind speed and dependent on the flow direction which usually produce an aerodynamic wake region downstream from the rotor blade. There are two major occurrences that take place during the operation of a wind turbine and rotation of its blade along the axis. First, the turbine extracts energy from the windfield and in the process reduces the wind speed. Second, turbulence is created in the air passing through the rotor blades which is then carried downwind. In other words, the region at which wind flow recirculates downstream or immediately behind the rotating blades which may be accompanied by flow separation and turbulence is known as wake. The wake region is generally associated with some aerodynamic characteristics such as velocity deficit, pressure differential, flow expansion, rotation of the wake field and increased turbulence. (Mckay et al., 2012). The theory of wind turbine wakes is classified into two categories namely: near wake and far wake. The near wake region deals with the extraction of energy from the wind by a single turbine, whereas, the far wake is more particular about the effects on the downstream turbines (Marmidis et al, 2008). Zhang et al. (2012) observed that, while the wind turbine extracts momentum from the flow and induces rotation, the stream-wise velocity decreases significantly and the lateral and vertical velocities increase immediately behind the rotor. In addition, the wake grows with increasing downwind distance from the rotor, as the stream-wise velocity increases and the other velocity components decrease. As the wind flow proceeds downstream the wake spreads in a non-uniform pattern as shown in Figure 5 but recovers towards free stream condition. The aerodynamic force driving the rotors result in an opposing force on the air stream causing the air column to rotate. The low pressure column of rotating air expands as it flows downstream of the turbine blades and consequently dissipates as the surrounding airflow reaches equilibrium (McKay et al., 2011, Burton et al., 2001). In event of a single wind turbine unit, the aforementioned wake does not have any effect on the wind turbine. However, in the event of a windfarm which consists of multiple stands of wind turbine, wake may have a cascading effects on a number of wind turbines in the farm. The wake effect becomes the aggregated influence on the energy produced from a wind farm due to the variations in wind speed as a result of the turbine impact on one another. In this case, each turbine unit extracting energy from the wind domain causes a reduction in the wind speed flowing to the next unit, increases vibration due to turbulence, increases wear around contacting members and increases maintenance cost. The radius of wake effect region downwind the rotors *x*, can be expressed as (Li et al., 2017):

$$R_w = \left(\frac{35}{2\pi}\right)^{\frac{1}{5}} (3c_1^2)^{\frac{1}{5}} (C_T Ax)^{\frac{1}{3}} \tag{32}$$

$$c_1 = l(C_T Ax)^{-\frac{1}{3}} \tag{33}$$

The wind speed reduction ΔU is described as:

$$\Delta U = -\frac{U_{WT}}{9} (C_T Ax^{-2})^{\frac{1}{3}} \left[R_w^{\frac{3}{2}} (3c_1^2 C_T Ax)^{-\frac{1}{2}} - \left(\left(\frac{35}{2\pi}\right)^{\frac{3}{10}} (3c_1^2)^{-\frac{1}{3}} \right) \right]^2 \tag{34}$$

where A is the swept area, T_C is the thrust coefficient, c_1 is constant, U_{WT} is the average wind speed on the wind turbines' hub height. Turbulent flow patterns in the incoming wind are rotationally sampled by the rotor blade. The turbulence in each section of the rotor blade is modelled on the basis of a spectrum (Kaimal et al., 1972), in combination with inverse Fourier transforms (Veers, 1984) or an approach based on rapid distortion theory (Mann, 1998).

As mentioned earlier, turbulence is created in the air flowing through the rotor blades as it rotates along its axis. Turbulent flow is a set of seemingly random and continuously changing wind motions that are superimposed on the wind's average motion. As shown in Figure 6, it is characterized by irregular swirls or fluctuations in the wind flowing towards and across the wind rotors, and is quantified with a metric known as turbulence intensity. An increase in downstream turbulence is caused by wake rotation, disruption of the air flow across the rotor blades and the vortices formed at the blade tips. This results in variation in wind speed and increased displacement in wind direction, causing less power being available for the downstream turbines (Mckay *et al*., 2012). The incoming turbulent flow causes the flow field in the boundary layer around the blades to transform rapidly into a turbulent boundary layer. This increases the boundary layer thickness as indicated by the red regions in Figure 6 and hence, the drag also. Effect of increased turbulence may result in increase in the power present in the wind while drag forces may act negatively against it. This correlates with the findings of Mikkelsen (2013)

who reported that turbulence increases the relative velocity of the wind which in turn increasing the power extraction. However, at extremely high turbulence, wind direction may be displaced, leading to decrease in the velocity of wind flowing towards the turbine rotors which consequently result in the reduction of power output.

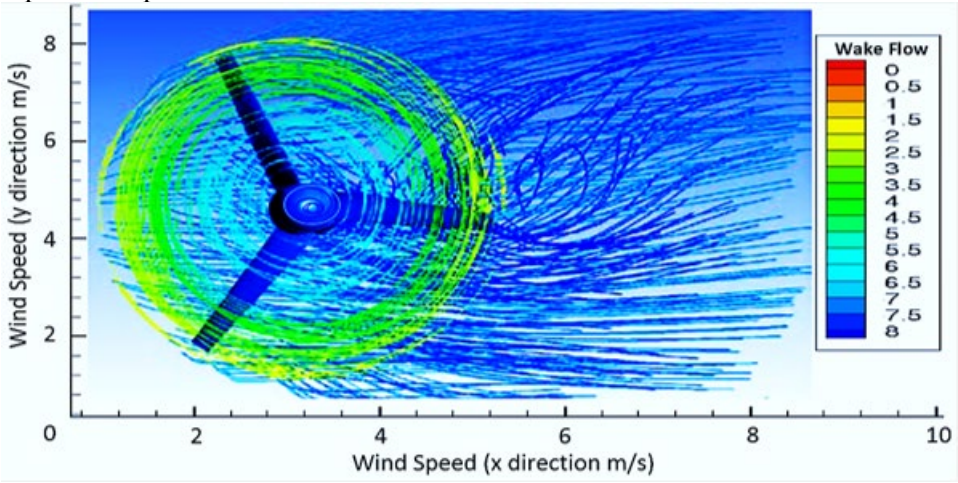

Figure 5. Wake distribution patterns behind the rotors

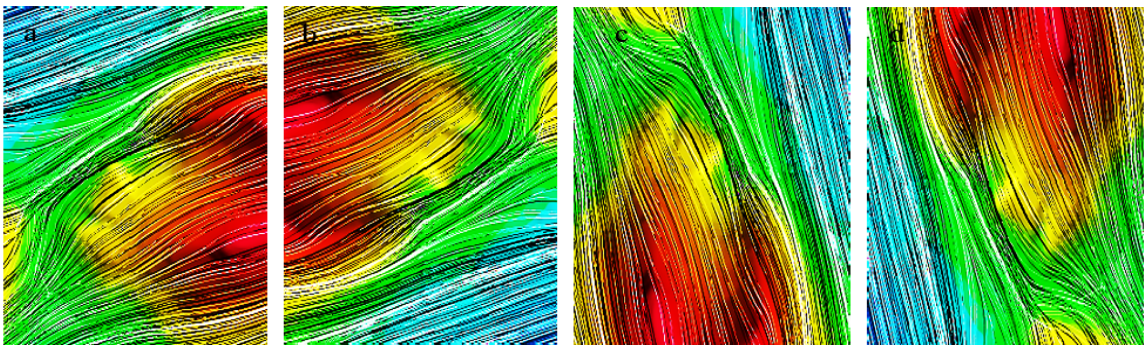

Figure 6. 3 Dimensional Spatial Turbulent Wind Distribution Patterns

The mathematical equation for the relative velocity of a uniform non-turbulent flow field is given by Equation 35, whereas, relative velocity of the incoming turbulent flow field is expressed in Equation 36.

$$U_{rel}^2 = U_{ref}^2 + \Omega r^2 = U_{ref}^2(1 + \lambda^2) \quad (35)$$

$$U_{rel}^2 = \left(U_{ref} + u'\right)^2 + (\Omega r + v')^2 \simeq U_{ref}^2 + u'^2 + (\Omega r)^2 + v'^2 \quad (36)$$

Brand et al. (2011) reported that the wind flowing towards a wind turbine is already turbulent, and in the process of extracting energy from the turbulent wind creates additional turbulence. Atmospheric turbulence impact wind energy through power performance, impacts on turbine loads, fatigue and wake effects as well as noise propagation. Therefore, Understanding and considering turbulence before and behind a wind turbine is believed to be vital in turbine applications (Mücke et al., 2010). The aerodynamic power is a function of the rotor shaft torque and the rotor speed upon which turbulence evolve. Atmospheric turbulence therefore gives rise to variations in the energy derived, power and consequently the electricity produced. In addition, turbulence is believed to be very instrumental in assessing energy yield in wind turbine applications (Gottschall & Peinke, 2008).

Results and Discussion

Vortex and Velocity Cut Plots

The following diagrams (Figure 7-10a-b) show the vortex flow and the velocity cut plots simulated at different wind speeds, while power and wake properties are examined. The simulation data from the turbine LLT simulation coupled with the different wind fields previously simulated are applied. A rotor overhang length of 0.6m and a hub height of 15m was used. The upwind type simulation was selected; the rotor shaft tilt was set at 5 deg in the downward direction. A TSR of 5 was selected for all scenarios and the simulation was run for 10s time steps. The results were read after 6s. From Fiure 7a, It can be

observed that as the flow progressed the velocity of wind along the axis of the turbine decreased steadily. As shown in Figure 7b, It can also be seen that wake shedding began to occur at about halfway across the cut plane at 4s. At 6s, it can be observed that the wind flow became more developed. The power was found to reduce by 0.1% per every 2s. The coefficient of power was 0.560359 and the power obtained was 0.041903Kw as shown in Figure 7b.

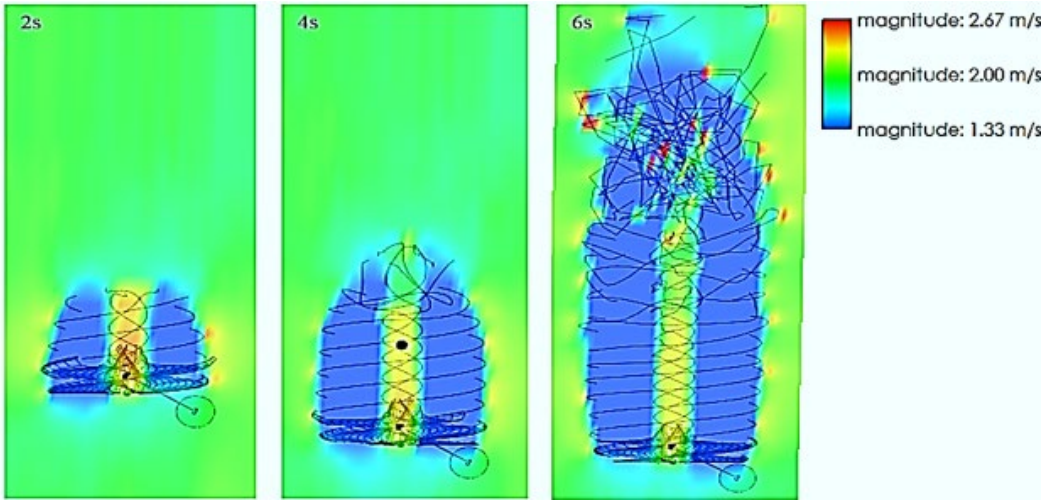

Figure 7a. Velocity cut plots at 2m/s after 2s, 4s and 6s

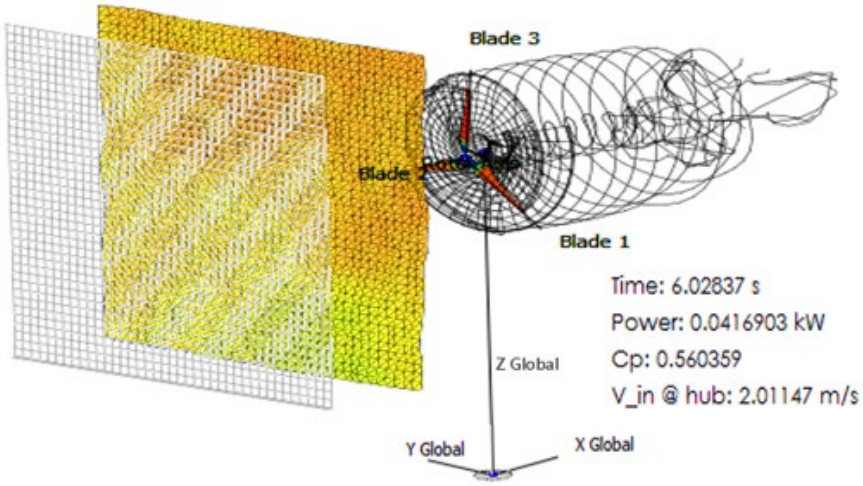

Figure 7b. Simulated profile of wake vortex trajectories at 2m/s.

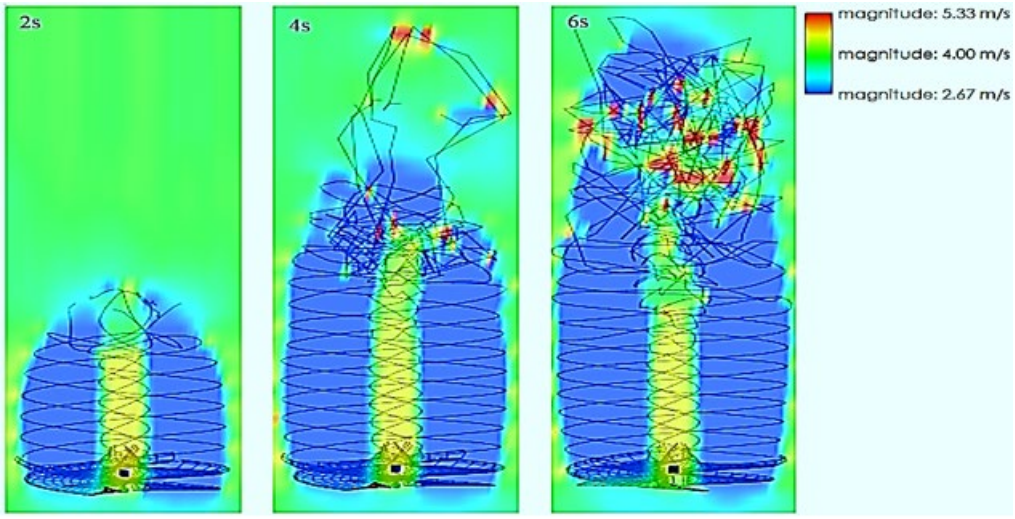

Figure 8a. Velocity Magnitude cut plots at 4m/s after 2s, 4s and 6s

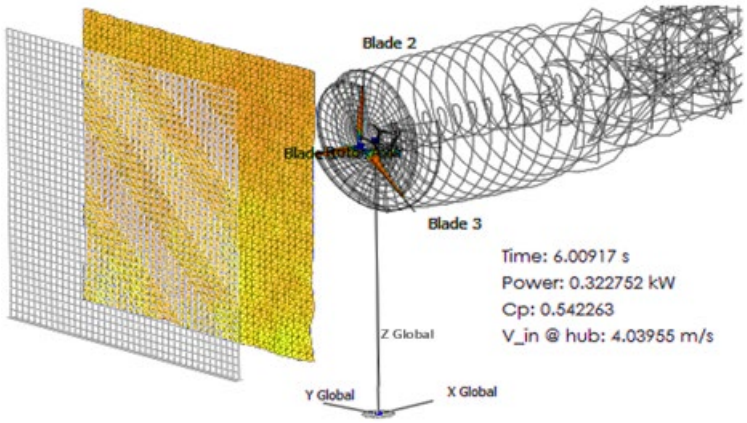

Figure 8b. Simulated profile of wake vortex trajectories at 4 m/s

From Figure 8a, It can be seen that the flow is uniform at 4s just as shear begins. The reduction in power is noticed in the third plot as it can be seen that the flow uniform length have reduced. The V_{in} and V_{out} is observed to increase due to an increase in the windspeed compared with the velocity plot at 2m/s. The power output is found to increase to 0.3228KW as shown in Figure 8b. The drop in power extracted from the wind to 0.54226 can be attributed to increased shedding and higher turbulence causing an overall decrease in turbine thrust. From Figure 9a, the cut plots show greater wake shedding and turbulence at 4s compared to the velocity plots at 4m/s. The velocity magnitude in Figure 9a is observed to reduce uniformly in the flow as well as the coefficient of power when compared to previous plots. The coefficient of power is 0.48407 and the power is found to be 0.96503Kw as presented in Figure 9b.

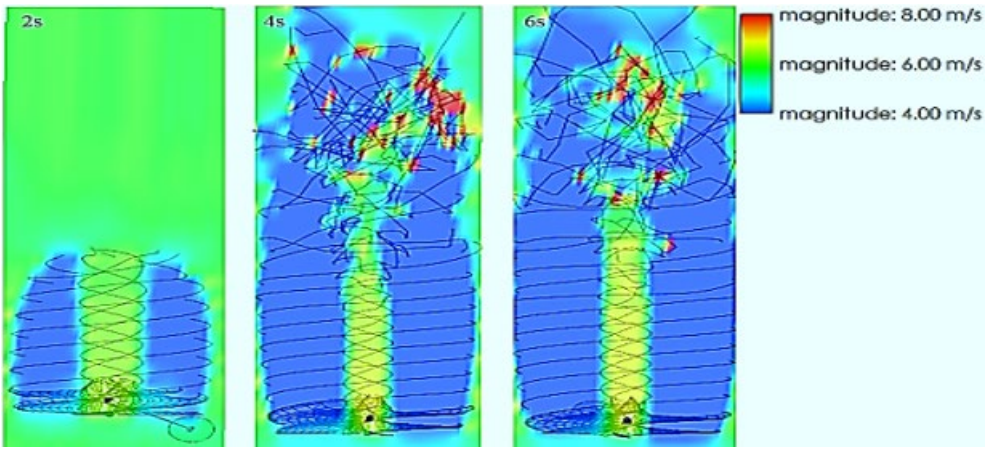

Figure 9b. Velocity Magnitude cut plots at 6m/s after 2s, 4s and 6s

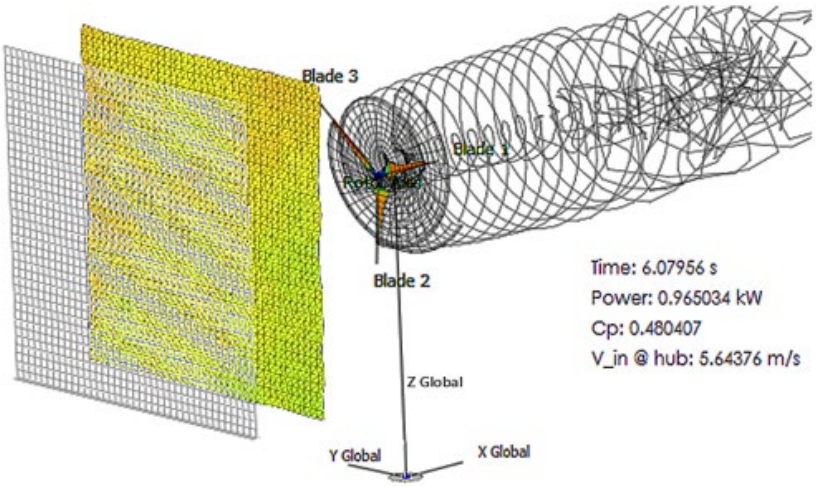

Figure 9a. Simulated profile of wake vortex trajectories at 6m/s

From Figure 10a, the wind turbulence at this wind speed (8m/s) is highly increased, but it can be noticed that the uniform flow length is greater than previous plots. This results in the increase in C_p to 0.5279 and power output to 2.514Kw as shown in Figure 10b. Figure 11 represents a plot of power coefficient and power output against wind speed. It can be observed from the plot that the power coefficient is not coherent with the wind speed possibly as a result deviation in the direction of wind by extreme effect of turbulence, whereas, the power output is coherent with the wind speed.

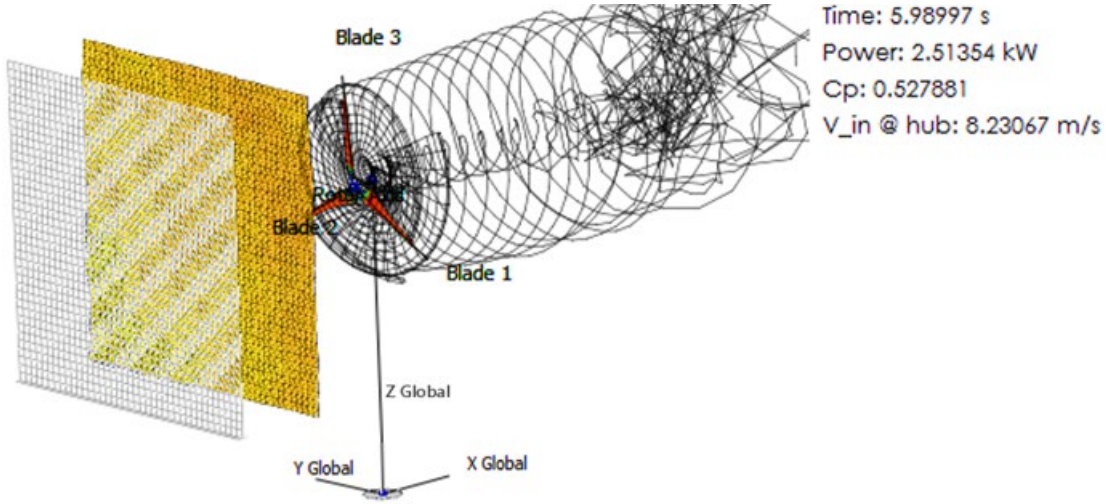

Figure 10a. Simulated profile of wake vortex trajectories at 8m/s

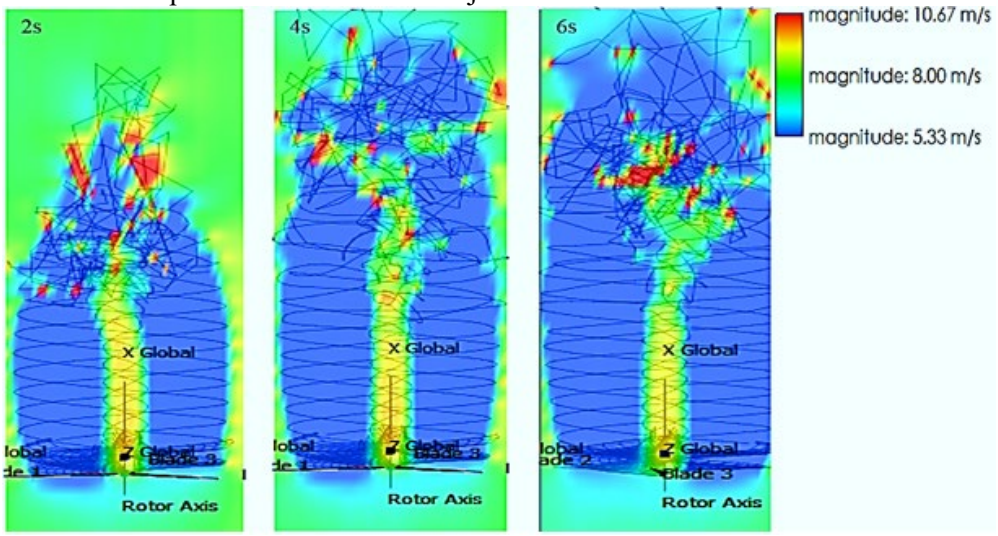

Figure 10b. Velocity Magnitude cut plots at 8m/s after 2s, 4s and 6s

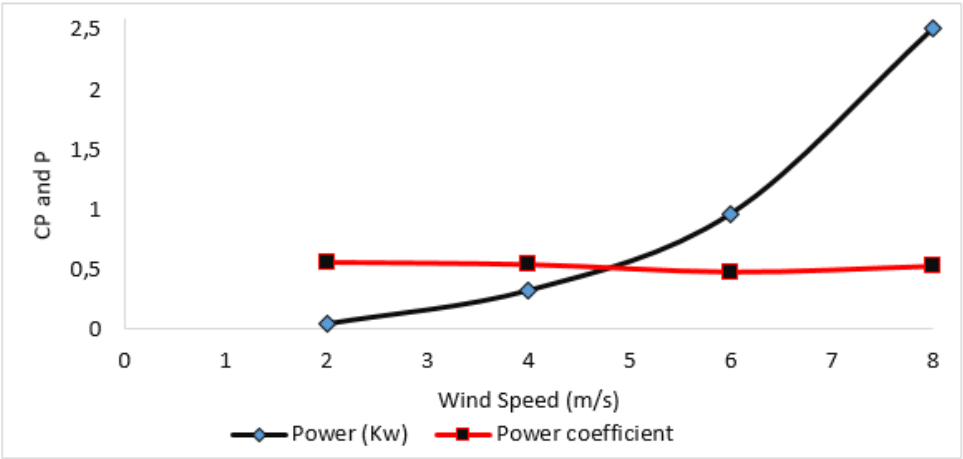

Figure 11. Plot of CP and P Vs wind speed

Conclusion

Increasing the number of points or time steps in the simulation resulted in much larger computational times and less computational errors. Furthermore, computational domain of atmospheric wind flow is very large and complex, thus, requires very large number of computational meshes. The results of the simulation revealed an increasing trend in power output (0.0416903, 0.322752, 0.965034 and 2.51354 kw) at increasing wind speeds (2, 4, 6 and 8 m/s) and varying trend in power coefficient (0.560359, 0.542263, 0.480407and 0.527881) at the same increasing wind speeds. The velocity magnitude cut plots simulated for the same range of wind speeds and time steps (2, 4 and 6 s) indicate that, failure of the wind velocity to attain optimum magnitude can affect the power coefficient as well as the energy available in the wind for extraction. In other words, if the wind flow, aerodynamic and turbine conditions are appropriate, the wind velocity can increase from few seconds or minutes, up to optimum magnitude suitable to impact on the rotors and cause rotation. The 3 dimensional spatial turbulent wind distribution patterns presented in this study shows that, turbulence in wind flow is characterised by wave patterns in all degrees of rotation of the turbine blade, and at extreme condition can distort the direction of wind flowing towards the rotors.

References

Kim D, Kim B, (2012) Development and validation of Computational Wind Field Model (Wind scape). Proceedings of 4th Asian Joint Workshop on Thermophysics and Fluid Science, October, 14-17, Busan, Korea.

Brand AJ, Peinke J, Mann, J, (2011) Turbulence and Wind Turbines. 13th European Turbulence Conference, Journal of Physics: Conference Series, 318(072005).

Satoh M, (2004) *Atmospheric circulation dynamics and general circulation models*. Springer. ISBN 3-540-42638-8.

Mikkelsen K, (2013) Effect of free stream turbulence on wind turbine performance. Norwegian University of Science and Technology, EPT-M-2013-84.

Li L, Liu Y, Yuan Z, Gao Y, (2018) Wind field effect on the power generation and aerodynamic performance of offshore floating wind turbines. Department of Naval Architecture, Ocean and Marine Engineering, University of Strathclyde, UK.

Ainslie J, (1988) Calculating the flowfield in the wake of wind turbines. *Journal of Wind Engineering and Industrial Aerodynamics,* **27**(1), 213-224.

Jimenez A, Crespo A, Migoya E, Garcia J (2007) Advances in large-eddy simulation of a wind turbine wake. Journal of Physics: Conference Series, 75, 012041, August, 28-31, Denmark.

Troldborg N, Sørensen JN, Mikkelsen R, (2010) Numerical simulations of wake characteristics of a wind turbine in uniform inflow. *Wind Energy* 13(1), 86-99.

Troldborg N, Larsen GC, Madsen HA, Hansen KS, Sørensen JN, Mikkelsen R, (2011) Numerical simulations of wake interaction between two wind turbines at various inflow conditions. *Wind Energy* **14**(7), 859-876.

Sanderse B, (2000) Aerodynamics of Wind Turbine Wakes. Technical Report ECN-E-09-016, Energy research centre of the Netherlands, Netherlands.

Wußow S, Sitzki L, Hahm T, (2007) 3D-simulation of the turbulent wake behind a wind turbine. Journal of Physics: Conference Series, 75, 012033, August, 28-31, Denmark.

Zhang W, Markfort CD, Porte-Agel F, (2012) Near-wake flow structure downwind of a wind turbine in a turbulent boundary layer. Springer, *Experiments in Fluids*, 52, 1219-1235.

Ozbay A, Tian W, Hu H, (2016) Experimental Investigation on the Wake Characteristics and Aeromechanics of Dual-Rotor Wind Turbines. *Journal of Engineering for Gas Turbines & Power,* **138**(042602), 1-15.

Tian W, Ozbay A, Hu H, (2014) Effects of Incoming Surface Wind Conditions on the Wake Characteristics and Dynamic Wind Loads Acting on a Wind Turbine Model. *Physics of Fluids,* **26**(12), 5108.

Hu H, Yang Z, Sarkar P, (2012) Dynamic Wind Loads and Wake Characteristics of a Wind Turbine Model in an Atmospheric Boundary Layer Wind. *Experiments in Fluids,* **52**(5), 1277-1294.

Whale J, Anderson CG, Bareiss R, Wagner S, (2000) An Experimental and Numerical Study of the Vortex Structure in the Wake of a Wind Turbine. *Journal of Wind Engineering and Industrial Aerodynamics,* **84**(1), 1-21.

Sørensen JN (2011) Aerodynamic aspects of wind energy conversion. *Annual Review of Fluid Mechanics,* 43, 427-448.

Devinant PH, Laverne T, Hureau J, (2002) Experimental study of wind turbine airfoil aerodynamics in high turbulence. *Journal of Wind Engineering and Industrial Aerodynamics,* **90**(6), 689-707.

Fukumoto Y, Okulov VL (2005) The velocity field induced by a helical vortex tube. *Physics of Fluids,* **17**(10), 107101.

Zheng ZC, Wu H, (2018) Classification of Wind Farm Turbulence and Its Effects on General Aviation Aircraft and Airports. University of Kansas, Report No. K-TRAN: KU-16-3.

Mulinazzi TE, Zheng ZC, (2014) Wind farm turbulence impacts on general aviation airports in Kansas (K-TRAN: KU-13-6). Topeka, KS: University of Kansas.

Odemark Y (2012) Wakes behind wind turbines-Studies on tip vortex evolution and stability. Royal Institute of Technology, SE-100 44 Stockholm, Sweden.

Manwell JF, McGowan JG, Rogers AL, (2009) *Wind Energy explained*, 2nd Edition, Wiley.

Vermeer L, Sorensen J, Crespo A, (2003) Wind Turbine Wake Aerodynamics. *Progress in Aerospace Sciences*, **39**, 467-510.

Mckay P, Carriveau R, Ting D, Newson T, (2012) Turbine Wake Dynamics, Advances in Wind Power. IntechOpen Limited, London, EC3R 6AF, United Kingdom.

Marmidis G, Lazarou S, Pyrgioti E, (2008) Optimal placement of wind turbines in a wind park using Monte Carlo simulation. *Renewable Energy,* **33**, 1455-1460.

McKay P, Carriveau R, Ting DS, (2011) Farm Wide Dynamics: The Next Critical Wind Energy Frontier. *Wind Engineering,* 35(4), 397-418.

Burton T, Sharpe D, Jenkins N, Bossanyi E, (2001) *Wind Energy Handbook.* John Wiley & Sons Ltd, Chichester.

Li L, Wang Y, Liu Y, (2017) Impact of wake effect on wind power prediction. State Key Laboratory of Alternate Electrical Power System with Renewable Energy Sources, North China Electric Power University, Beijing, 102206, China.

Kaimal JC, Wyngaard JC, Izumi Y, Coté OR, (1972) Spectral characteristics of surface layer turbulence. *Quarterly J. Royal Meteorological Society,* **98**(417), 563-589.

Veers PS, (1984) Three-dimensional wind simulation. Technical report SAND88-0152, Sandia National Laboratories.

Mann J, (1998) Wind field simulation. *Probabilistic Engineering Mechanics,* **13**(4), 269-282.

Mücke T, Kleinhans D, Peinke J, (2010) Atmospheric turbulence and its influence on the alternating loads on wind turbines. *Wind Energy,* 14(2), 301-316.

Gottschall J, Peinke J, (2008) How to improve the estimation of power curves for wind turbines. *Environmental Research Letters,* **3**(1), 015005, 1-7.

J. Int. Environmental Application & Science, Vol. 15(2): 81-90 (2020)

Research Paper

Early Cretaceous Benthic Foraminifera from Guri I Pellumbit Section, Klosi Region, Albania

Andreea Uta[1, *], Eleni Gjani[2]

[1]*nstitute of Geosciences, Energy, Water and Environment, Rruga Don Bosko 60, Tirana, Albania;* [2]*Polytechnic University of Tirana, Faculty of Geology&Mining, Elbasani street, Tirana, Albania*

Received April 11, 2019; Accepted June 13, 2020

Abstract: This paper presents the preliminary results of a micropaleontological study performed on Guri e Pellumbit stratigraphic section, in Klos region (Mirdita area). Benthic foraminifera together with "microproblematica", calcareous algae and calpionellids are the main components of Lower Cretaceous reefs and carbonate platforms and have proved to be extremely helpful in the zonation of platform carbonates. The mixture of typical elements of shallow water environments (foraminifera, calcareous algae and microproblemica) with elements of deep environments (calpionellids) and the specific microfacies shortly described in this study are typical for an allodapic limestones (turbidites). Based on the micropaleontological associations with biostratigraphical importance, the age of these deposits is Upper Beriassian-Lower Valanginian.

Keywords*: Early Cretaceous, benthic foraminifera, Mirdita zone, biostratigraphy, Beriassian-Valanginian.*

Introduction

The geological zone of Mirdita has wide spread in Albania, where the ophiolites which are the major components, represent parts of the ocean basin expanded from Middle Triassic to Middle Jurassic between the Adriatic plate and the Korab-Pelagonian continental microblock. The closure of Mirdita ocean basin has occurred throughout Middle Jurassic until the beginning of Late Jurassic. (Xhomo 2002, 2005).

The Middle-Upper Jurassic and Jurassic-Cretaceous deposits covering the ophiolites and the surrounding continental formations have been largely treated by many authors (Shehu et al. 1990, Meço&Aliaj. 2000, Xhomo. 2002, Marku D. 1999, 2000, 2001).

This paper is focused on the micropaleontological and biostratigraphical study from a stratigraphic section within the Jurassic-Cretaceous deposits, Guri i Pellumbit, in Klos (Mirdita area) represented by carbonate deposits interpreted as slope sediments (Figures1 & 2).

Materials and Methods

Our study is based on the investigation of a number of 105 samples collected from a stratigraphic section on the Beriassian-Valanginian carbonate deposits belonging to Mirdita geological zone, followed by a detailed investigation of microfacies types and micropaleontological content under a Zeiss Axioplan 2 imaging microscope.

The geological background of the section

In the studied section are present the ophiolitic formations and their covering deposits (Fig. 1, 2), where the ophiolitic formations are represented by an oceanic crust sequence with gabbros at the bottom and andesites with dacite-rhyolitic dykes on the top, while the deposits covering the ophiolites are represented by:

- limited strips of "blocks in matrix" mélange covering the volcanic rocks. The age of these deposits is given as Upper Callovian - Lower Oxfordian (Xhomo et al. 2002, Aliaj, Kodra 2016).

- "Firza" flysch deposits above the andesites with dacite-rhyolitic dykes where the next horizons have been detailed:

* *Corresponding: E-Mail; andreauta@gmail.com; Tel: +355688333026; Fax: +35542259540*

• Sandy-clayey-marly horizons of Beriassian age

• A thin horizon of Beriassian plately limestones.

• A shallow water carbonate horizon and slope deposits of Guri i Pellumbit section of Upper Beriassian-Lower Valanginian age.

• Conglomerates and clayey-sandy-marly flysch deposits of Valanginian-? Hauterivian age.

Melo 1971 and Meço 1975 by studying the ammonites and calpionellides have assigned the Beriassian age for the horizons below Guri i Pellumbit section. Regarding the above mendioned studies, we think that the andesite with dacite-rhyolitic dykes stretching between the two lower flysch horizons does not represent Beriassian volcanic activity or olistoliths in flysh and we interpret these volcanites as the basement of Beriasian flysch deposits, repeated in the section as consequence of the Beriassian synsedimentary tectonics.

These deposits are in a form of a horizon of several kilometers long and with an average thickness of 50-70 m. In the northeastern part, these deposits are settled above the volcanic and "blocks in matrix" melange, while in the southwestern part are stratigraphically placed above the flysch horizon and the Beriassian plately limestone. In the ceiling of Guri i Pellumbit carbonate deposits, in the northern part, are lying conglomerate deposits, while in the southern part, these conglomerates are facially passing into clayey-sandy-marly flysch deposits.

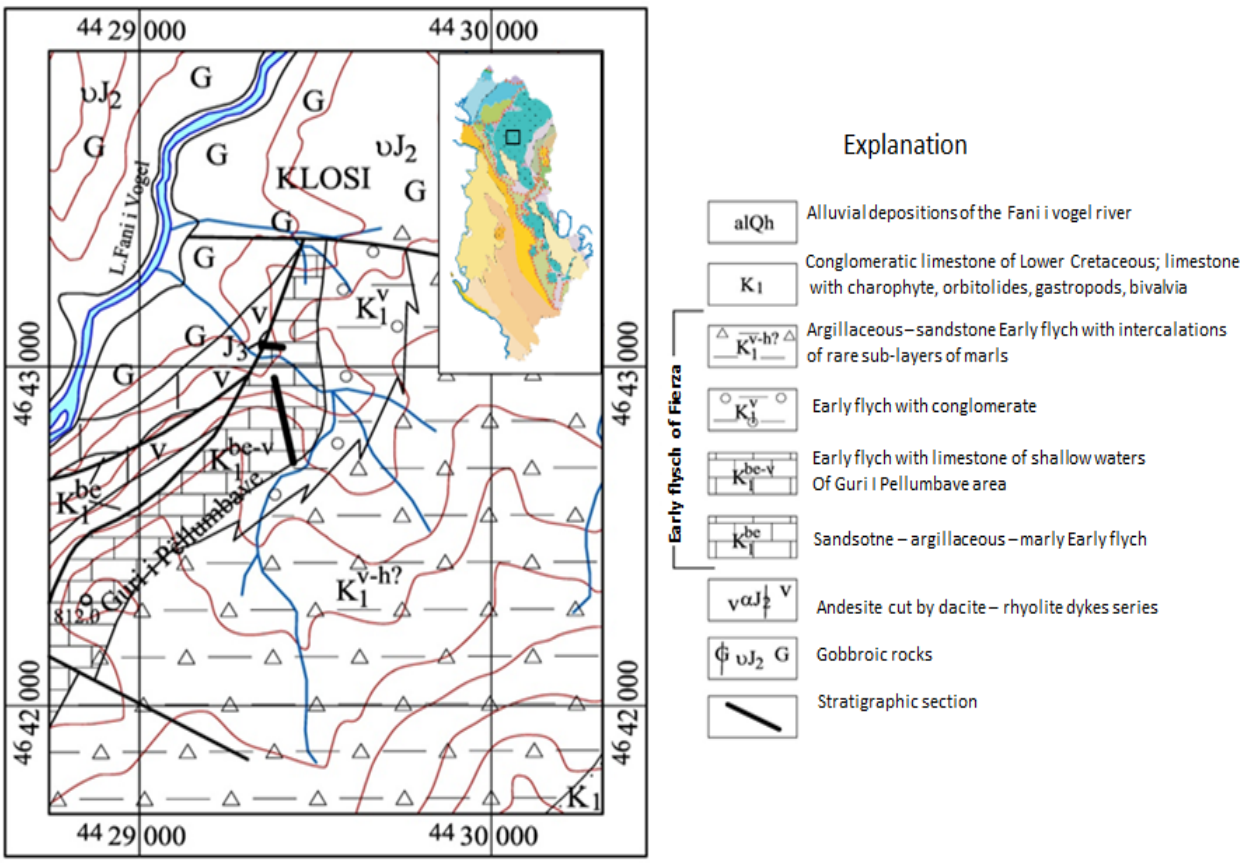

Figure 1.The geology of Guri i Pellumbit section, 1: 25 000 scale

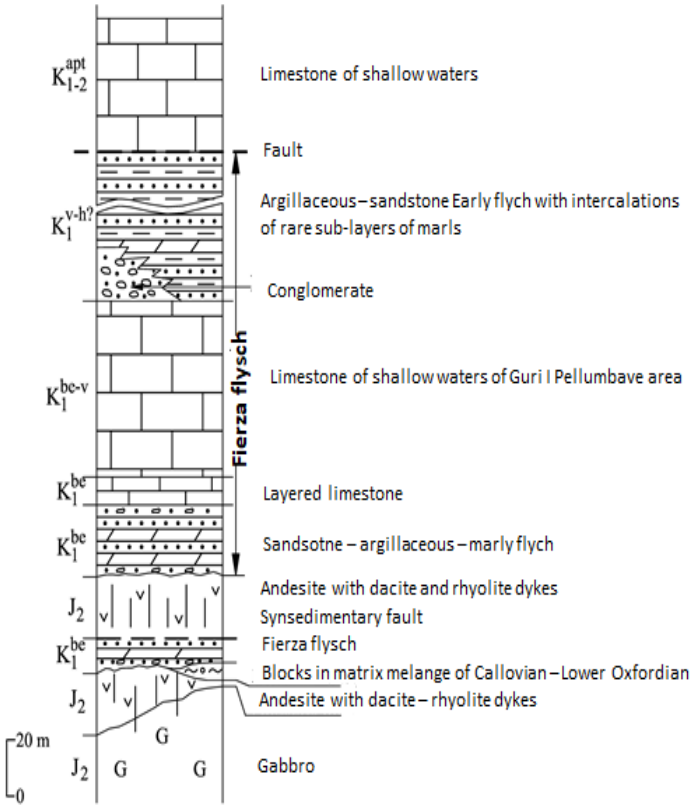

Figure 2. Stratigraphic column of Guri i Pellumbit section

Results

The next dominant microfacies types with their micropaleontological associations each of them pointing to a specific depositional environment were identified in a number of 105 samples systematically collected along the studied section.

Bioclastic peloidal packstone-grainstone

This microfacies is characterized by an abundant presence of bioclasts and peloids as allochems in the micrite dominated matrix, where the larger allochems are represented by corals, sclerospongiaires, echinoderms and bivalves, while the microfauna mainly consists of microbial structures, dasycladacean algae, calpionellids and benthic foraminifera as: ?*Reophax* sp, *Nodophtalmidium* sp, *Ammobaculites* sp, ?*Rectocyclammina* sp, ?*Schythiolina/Histerolina*, *Protopeneroplis cf. banatica*, *Protopeneroplis ultragranulata, Neotrocholina* sp.

Packstone/rudstone

This microfacies contains large fragments of corals, sclerospongiaires, bivales and a microfauna mainly consisting of microbial structures, dasycladacean algae, rare calpionellids and benthic foraminifera as: *Protopeneroplis ultragranulata, Mohlerina basiliensis, Lenticulina* sp, *Neotrocholina* sp, *Ammobaculites, Nodophtalmidium* sp

Bioclastic grainstone

This microfacies is characterized by abundant bioclasts and calcitic cement where the larger allochems are generally represented by corals or sclerospongiaires fragments. The microfauna is represented by microbial structures, dasycladacean algae and benthic foraminifera as: *Protopeneroplis ultragranulata, Coscinophragma* sp, *Scythiolina cf laurentii, Coscinoconus* sp and dasycladacean algae: *Salpingoporella pygmaea*, *Suppiluliumaella polyreme*,? *Suppiluliumaella sp*.

Peloidal bioclastic grainstone
This microfacies is characterized by an abundant presence of peloids as allochems in the micrite dominated matrix where most of these peloids are probably related with microbial activity [microbial peloids as defined in Flügel (2004)]. The microfauna is represented by microbial organisms, dasycladacean algae, calpionellids and benthic foraminifera: *Coscinoconus cf. alpinus, Coscinoconus alpinus, Haplophragmoides jourkovsky, Mohlerina basiliensis*, Protopeneroplis *ultragranulata*, *Coscinoconus cf. alpinus*, *Haplophragmoides jourkovsky*, Neotrocholina sp, *Lenticulina* sp;

Peloidal bioclastic packstone-grainstone
This microfacies consists of abundant peloids, bioclasts and sparry calcitic cement (if the texture is dominantly grainstone) or micritic matrix (if the texture is dominantly packstone) as background material. It consists of microbial structures, dasycladacean algae, calpionellids and benthic foraminifera: *Montsalevia salevensis*, *Haplophragmoides jourkovsky*, *Protopeneroplis ultragranulata*, *Mohlerina basiliensis, Neotrocholina* sp, *Lenticulina* sp, *Coscinoconus* sp. Most of these peloids are probably related with microbial activity [microbial peloids as defined in Flügel (2004)].

Bioclastic rudstone, **packstone rudstone and rudstone/boundstone**
This microfacies contains fragments of corals, sclerospongiaires, bryozoans, bivalves, gastropods and a microfauna represented my microbial structures, dasycladacean algae, calpionellids and benthic foraminifera: *Protopeneroplis ultragranulata*, *Pseudocyclammina lituus, Everticyclammina* sp, *Neotrocholina* sp, *Coscinoconus aff. delphinensis*, *Conscinoconus cherchiae, Coscinoconus* sp, *Gaudryna ectypa*, *Mohlerina basiliensis, Charentia* sp.

Bindstone
This microfacies is rich on *Bacinella irregularis,* bacinelloid and microbial structures, rudists and sponigiaires fragments, algae and benthic foraminifera: *Lithocodium aggregatum*/*Troglotella incrustans, Troglotella incrustans* and *Mohlerina basiliensis, Protopeneroplis ultragranulata*, *Coscinoconus delphinenis* and miliolids.

Boundstones
Corals and sponges play a major role in the construction of the boundstones as well as the microbial organisms that play a secondary role. The cavities and the spaces between the pores are filled with different allochems, with a micrite or sparitic matrix, the calcite being the dominant cement. In most cases the corals are recrystallized. Together with the corals and the sclerospongiaires, the others organisms as *Radiomura cautica, Crescentiella morronensis, Koskinobulina socialis, Terebella lapilloides, Protopeneroplis ultragranulata,* shows that these boundstones are formed in the marginal reefal setting on the platform.

Microbialites
This microfacies fragments of corals, sclerospongiaires, echinoderms and bivalves and a microfauna mainly represented by microbial stuctures, rare sections of calpionellids and benthic foraminifera as *Neotrocholina* sp, *Neotrocholina valdensis, Mohlerina basiliensis* and *Everticyclammina* sp.
The above described microfacies are typical for an allodapic limestone - in fact, the whole sampled section shows a mixture of elements of typical of shallow water and calpionellids, typical elements of deep water - can be interpreted as slope sediments.

Discussions

Based on the above identified micropaleontological assemblages, the studied deposits were assigned to the Upper Berriasian- Lower Valanginian (? Hauterivian) by taking into consideration the next associations with biostratigraphical significance:

Benthic foraminifera as *Pseudocyclammina lituus*, *Protopeneroplis ultragranulata*, *Mohlerina basiliensis*, *Coscinoconus alpinus*, *Coscinoconus elongates* are typical forms for Upper Jurassic but they are also often found in the lower part of the Lower Cretaceous.

Gaudryina ectypa is widely spread within the Lower Cretaceous (Beriasian-Albian) deposits but the most typical species are *Haplophragmoides joukowskyi*, *Montsalevia salevensis*, *Coscinoconus cherchiae*, *Coscinoconus delphinensis*, *Neotrocholina valdensis* and *Protopeneroplis banatica* which are exclusively Beriassian-Valanginian species.

Haplophragmoides joukowskyi was firstly described from the deposits assigned to Valanginian (Charollais et al., 1966), then from Berriasian-Valanginian deposits by Darsac (1983), Bucur et al. (1995), Ivanova (2000) but also from the Hauterivian deposits (more exactely Lower Hauterivian) (Bucur, 1988; Altiner, 1991; Sokač, 1983; Boisseau, 1987; Chiocchini et al., 1988; Velić, 1988; Altiner, 1991; Bucur et al., 1995; Ivanova, 2000; Husinec & Sokač, 2006).

Coscinoconus cherchiae (Arnaud-Vanneau, Boisseau & Darsac, 1988) and *Coscinoconus delphinensis* (Arnaud- Vanneau, Boisseau & Darsac, 1988) are exclusively described from the Beriasian-Valanginian deposits (Boisseau, 1987, Arnaud-Vanneau et al, 1988; Altiner, 1991; Chiocchini et al, 1994; Bucur et al, 1995; Mancinelli & Coccia, 1999); Only *Coscinoconus delphinensis* was described from the Upper Tithonian deposits (Gorbachik & Mohamad 1997).

Montsalevia salevensis was firstly described from the Valangian deposits (Charollais et al., 1966) and then from the Upper Beriassian (Salvini, Bonnard et al, 1984; Zaninetti et al, 1987; Chiocchini et al, 1994) or Hauterivian (Lower Hauterivian (Masse, 1976, Peybernès, 1976; Bucur, 1988), but almost all references of this species are from the Valanginian deposits (Azema et al, 1977;. Vila, 1980, Darsac, 1983; Velić& Sokač, 1983, Boisseau, 1987; Chiocchini et al, 1988; Velić, 1988; Altiner 1991; Bucur et al, 1995; Ivanova 2000, Husinec & Sokač 2006, Schlagintweit & Gawlick, 2006; Granier & Bucur, 2011; Bonin et al, 2012).

-*Neotrocholina valdensis* Reichel, 1955 which is was initially described as typical for the Valanginian deposits (Reichel, 1955) as *type species* for Neotrocholina is very often described as typical species for the deposits **exclusively assigned to Beriassian-Valanginian** (Vila, 1980, Darsac, 1983, Boisseau, 1987, Granier, 1987, Bucur, 1988, Chiocchin et al, 1988, Altiner, 1991, Luperto Sinni & Masse, 1994; Bucur et al., 1995; Neagu, 1995; Clark & Boudagher-Fadel, 2001.

-*Neotrocholina valdensis* Reichel, 1955 was described as Valanginian species (Reichel, 1955) but now is mentioned as exclusively Beriasian-Valanginian species (Vila, 1980, Darsac, 1983, Boisseau, 1987, Granier, 1987, Bucur, 1988, Chiocchin et al, 1988, Altiner, 1991, Luperto Sinni & Masse, 1994; Bucur et al., 1995; Neagu, 1995; Clark & Boudagher-Fadel, 2001.

-*Protopeneroplis banatica* Bucur, 1993. *P. banatica* which was firstly described (si *Protopeneroplis aff. trochronulata*) as hauterivian species (Bucur, 1988); then assigned to Late Valanginian-Early Hauterivian (Bucur, 1991), also identified in southeastern France, (Blanc et al., 1992), in Serbia within the Valanginian deposits (Bucur et al., 1995) and in Slovenia from the Valanginian and Aptian deposits (Bucur, 1997).

A special regard is accorded to *Protopeneroplis ultragranulata* (Gorbachik, 1971) firstly described from the Lower Cretaceous deposits from Crimea (Gorbachik,1971) and considered for a long time as a marker for the Beriassian-Valanginian, but later was also described from the Middle Tithonian (Heinz & Isenschmidt, 1988) or from the Barremian deposits (Bucur, 1993, 1997; Arnaud-Vanneau & Sliter, 1995, nën *Protopeneroplis* sp.) but in the literature is very often described from the Beriassian-Lower Valanginian (Azema et al., 1977; Azema et al., 1979; Salvini-Bonnard et al., 1984; Boisseau, 1987; Granier, 1987; Zaninetti et al., 1988 , Bucur, 1988, Chiocchini et al., 1988; Velić, 1988; Chiocchini et al., 1994; Bucur et al., 1995). Bucur (1993, 1997).

Spiraloconulus suprajurasicus Schlagintweit, 2011 also has a special significance, this foraminifer being described in the Upper Jurassic -? Beriasian deposits from the Northern Calcareous Alps (Schlagintweit, 2011), then mentioned and described from the Tithonian- Upper Beriasian deposits in the Hăghimaş area (Eastern Carpathians, Romania) by Bucur et al. (2011) and Dragastan (2011).

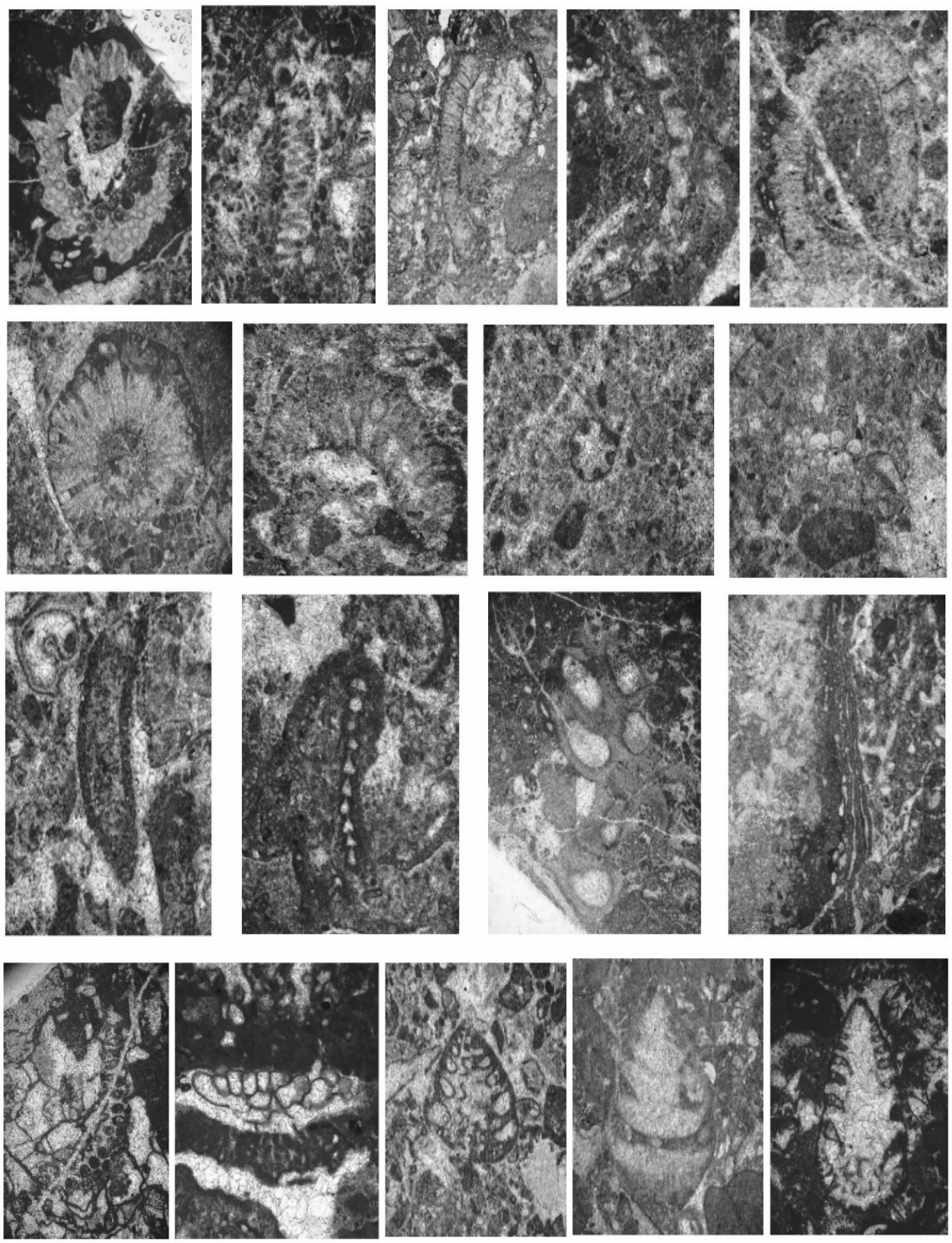

Figure 3. ***1.*** *Zujovicella polonini,* ***2.*** *Neomeris sp.,* ***3***. *Steinmanniporella sp.,* ***4.*** *Griphoporella sp,* ***5.*** *Arabicodium sp.,* ***6.*** *Salpingoporella praturloni,* ***7.*** *Suppiluliumaella polyreme,* ***8.*** *Terquemella sp.,* ***9***. *Koskinobulina socialis?* ***10.*** *Terebella lapilloides sp.,* ***11***. *Crescentiella morronensis,* ***12.*** *Radiomura cautica,* ***13***. *Rodhpletzella sp.,* ***14***. *Bacinella irregularis sp.,* ***15***. *Lithocodium-Troglotella incrustans****16***. *Conscinoconus cherchiae,* ***17.*** *Coscinoconus campanellus,* ***18***. *Coscinoconus alpinus*

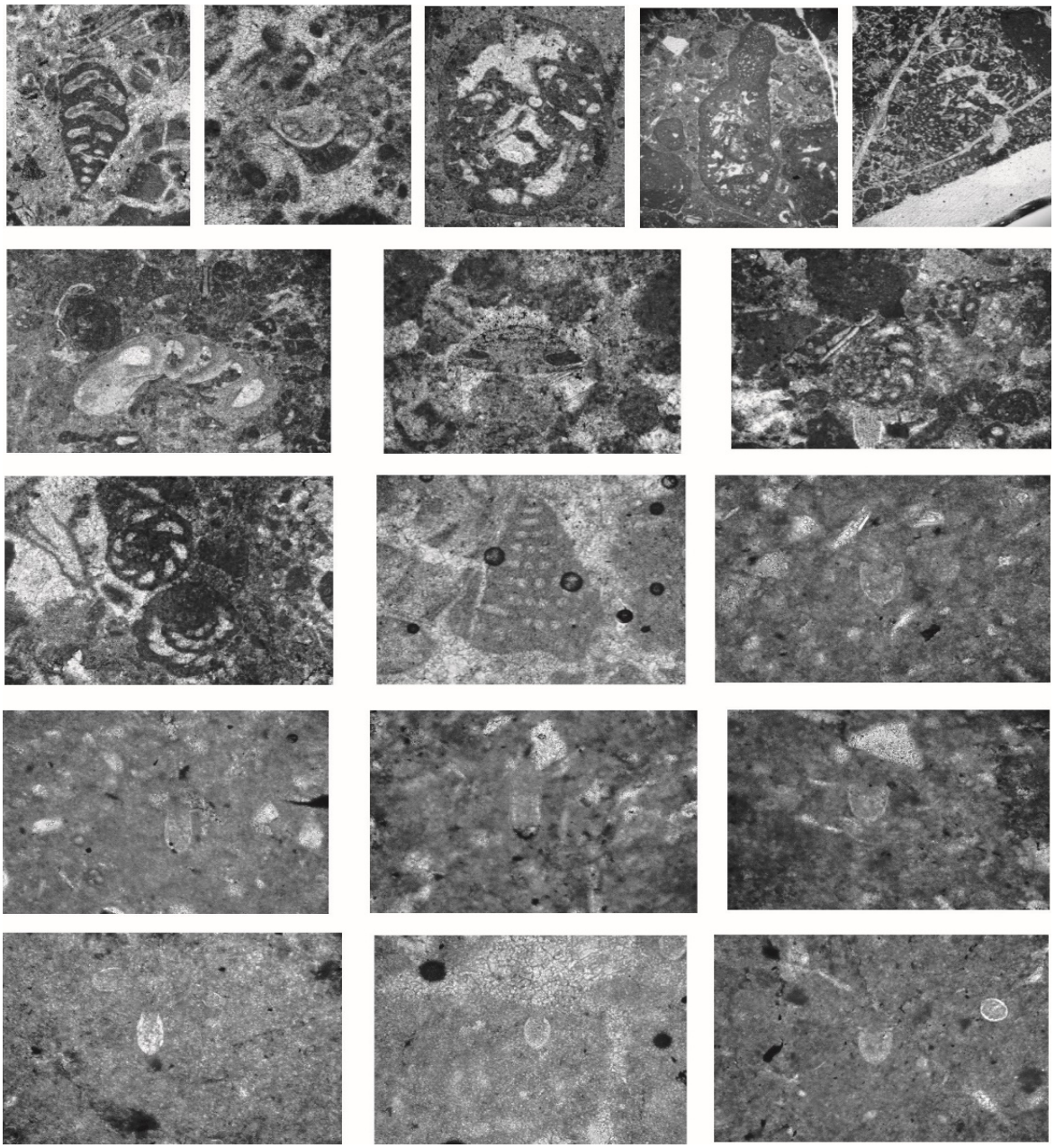

Figure 4. **1**.*Gaudryna ectypa* sp., **2**. *Mohlerina basiliensis*, **3.** *Everticyclammina sps.*, **4**. *Spiraloconus suprajurassicus, **5**. Pseudocyclammina lituus* **6**. *Protopeneroplis ultragranulata* **7.** *Neotrocholina valdensis, **8**. Ammobaculites sp.**, 9**. Charentia* sp., **10**. *Scythiolina cf laurentii,* **11.** *Calpionellites darderi* **12.** *Tintinopsella. carpathica*,. **13.** *Tintinopsella longa,* **14.** *Calpionellopsis,* **15.** *Calpionella elliptica, **16**. Calpionella alpina,* **17.** *Remaniella cadischiana*

Conclusions

Numerous studies throughout the years have proved that in the regional context during Jurassic-Cretaceous time the existence of a deep basin where “Firza" flysch (Xhomo 2002) was deposited.

In the central part of Mirdita zone and rarely in its eastern part, there have been existed sectors that during Beriassian and Valanginian have been occupied by shallow water carbonate deposits (Meço 1975, Peza 1983, Schlagintweit 2006).

As in the Guri i Pellumbit section, also in Kreje Lura region, the calpionelides have been signaled within the shallow water carbonate limestone deposits as Calpionellopsis biozone of Beriassian age and Calpionellites darderi of Lower Valanginian age (Peza et al. 1983).

The next microfacies were identified: peloidal bioclastic packstone-grainstone, packstone-rudstone, bioclastic grainstone, bioclastic peloidal packstone-grainstone, rudstone, packstone-rudstone,

bioclastic rudstone-boundstone, bindstone and microbialites which together with their microfaunistic associations allow us to interpret the whole succession as slope deposits.

Taking into consideration all the microfacies and microfaunistic associations described above along with the geological context, Guri i Pellumbit section can be interpreted as an isolated "haut fond" type platform where bioclasts with shallow water origin have been transported and resettled by turbidic currents and are mixed with typical deep water biota represented by calpionellides.

The age of this section on the basis of foraminifera and calpionellides is Upper Beriassian-Lower Valanginian.

References

Aliaj Sh, Kodra A, (2016) The Albanides setting in the Dinaric-Albanian-Hellenic belt and their main geological features. *JNTS*. **XXI**, 31-73,.

Altiner D, (1991) Microfossil biostratigraphy (mainly foraminifers) on the Jurassic-Lower Cretaceous carbonate successions in north-western Anatolia (Turkey). *Geologica Romana*, **27**, 167-213.

Arnaud-Vanneau A, Boisseau T, Darsac C, (1988) Le genre Trocholina Paalzow 1922 et ses principales espèces au Crétacé. *Revue de Paléobiologie*, **2** (86), 353-377.

Arnaud-Vanneau A, Sliter WV, (1995) Early Cretaceous shallow-water benthic foraminifera and fecal-pellets from Leg-143 compared with coeval faunas from the Pacific basin, Central America and Tethys. In: Winterer (eds.) *Proceedings of the Ocean Drilling Program, Scientific Results*, **143**, 537-564.

Azema J, Chabrier G, Fourcade E, Jaffrezo M, (1977) Nouvelles données micropaléontologiques, stratigraphiques et paléogéographiques sur le Portlandien et le Néocomien de Sardaigne. *Revue de Micropaléontologie,* **20**(3), 125-139.

Azema J, Chabrier G, Chauve P, Fourcade E, (1979) Nouvelles données stratigraphiques sur le Jurassique et le Crétacé du Nord-Ouest d'Ibiza (Baleares, Espagnes*). Geologica Romana*, **18**, 1-21.

Boisseau T, (1987) La plate-forme jurassienne et sa bordure subalpine au Berriasien-Valanginien (Chartreuse-Vercors). Analyse et corrélation avec les séries de bassin. *Thèse Univ. Grenoble*, 413 pp.

Bonin A, Vennin E, Pucéat E., Guirand, M, Arnaud- Vanneau, A, Adatte, T, Pittet, B, Mattioli, E, (2012) Community replacement of neritic carbonate organisms during the late Valanginian platform demise: A new record from Provence platform. *Palaeogeography, Palaeoclimatology, Palaeoecology***, 365-366**, 57-80.

Bucur II, (1988) Les foraminifères du Crétacé inférieur (Berriasien-Hauterivien) de la zone de Reşiţa-Moldova Nouă (Carpathes Méridionales, Roumanie). Remarques biostratigraphiques. *Revue de Paléobiologie*, **2** (Benthos '86), 379-389.

Bucur II, (1991) The study of Jurassic and Cretaceous from some areas with perspective for Liassic coals between Miniş and Nera valley (central part of the Reşiţa zone, Banat*). PhD Thesis,* Babeş-Bolyai University, 203 pp (in Romanian).

Bucur II, (1993) Les représentants du genre Protopeneroplis Weynschenk dans les dépôts du Crétacé inférieur de la zone de Reşiţa-Moldova Nouă (Carpathes Méridionales, Roumanie). *Revue de Micropaléontologie*, **36** (3), 213-223.

Bucur II, Conrad MA, Radoičić R, (1995) Foraminifers and calcareous algae from the Valanginian limestones in the Jerma River Canyon, Eastern Serbia. Revue de Paléobiologie, **14** (2), 349-377.

Bucur II, (1997) Representatives of the genus Protopeneroplis (Foraminifera) in the Jurassic and Lower Cretaceous deposits in Romania. Comparisons with other regions of the Tethyan area. *Acta Palaeontologica Romaniae*, **1**, 65-71.

Bucur II, Dragastan ON, Lazăr I, Săsăran E, Popa M, (2011) Mesozoic algae-bearing deposits from Hăghimaş Mountains (Bicaz Valley area). In: Bucur, I.I. & Săsăran, E. (eds.) – *Calcareous algae from Romanian Carpathians. Field Trip Guidebook*, 10th International Symposium on Fossil Algae, Cluj- Napoca, 12-18 September 2011, pp: 7-16.

Bulot L.G, Thieuloy J-P, (1994) Les biohorizons du Valanginien du Sud-Est de la France: un outil fondamental pour les corrélations au sein de la Téthys occidentale*. Géologie Alpine,* Mémoire H.S., **20**, 15-41.

Charollais J, Brönnimann P, Zaninetti L, (1966) Troisième note sur les foraminifères du Crétacé inférieur de la région genovoise. Remarques stratigraphiques et description de *Pseudotextulariella salevensis*, n. sp.; *Haplophragmoides joukowskyi*, n.sp.; Citaella? favrei n. sp. *Archives des Sciences S.P.H.N. Genève*, **19** (1), 23-48.

Chiocchini M, Mancinelli A, Marcucci C, (1988) Distribution of benthic foraminfera and algae in the Lazium-Abruzzi carbonate platform facies (Central Italy) during Upper Malm-Neocomian. *Revue de Paléobiologie*, **2** (Benthos '86), 219-227.

Chiocchini M, Farinacci A, Mancinelli A, Molinari V, Potetti M, (1994) Biostratigrafia a foraminiferi, dasicladali e calpionelle delle successioni carbonatiche mesozoiche dell'Appennino centrale (Italia). *Studi Geologici Camerti, Vol. Spec. "Biostratigrafia dell'Italia centrale*", pp: 9-128.

Clark N, Boudagher-Fadel M, (2001) The larger benthic foraminifera and stratigraphy of the Upper Jurassic/Lower Cretaceous of Central Lebanon. *Revue de Micropaléontologie*, **44** (3), 215-232.

Darsac, C., 1983. La plate-forme berriaso-valanginienne du Jura méridional aux massifs subalpins (Ain, Savoie). Sédimentologie, minéralogie, stratigraphie, paléogéographie, micropaléontologie. *Thèse, 3e cycle, Université Grenoble*, 319 pp.

Dodona E, Meço S, Xhomo A, (1975) Kufiri Jurasik - Kretak ne Shqiperi. *Permbledhje Studimesh,* **3**, 39-52.

Dodona E, (1982) Stratigrafia, mikrofaciet dhe mikrofauna e zones Mirdita. *Disertacion.*

Dragastan, O. N., 2010. Platforma Carbonatică Getică. Stratigrafia Jurasicului şi Cretacicului inferior, reconstituiri paleogeografice, provincii şi biodiversitate. Editura Universităţii Bucureşti, 621 pp.

Dragastan O, (2011) Early Cretaceous Foraminifera, Algal Nodules and Calpionellids from the Lapoş Valley, Bicaz Gorges (Eastern Carpathians, Romania*). Analele Ştiinţifice ale Universităţii "Al. I. Cuza" din Iasi, Seria Geologie*, **57** (1), 91–113.

Gorbachik TN, (1971) On Early Cretaceous foraminifera of the Crimea. *Akademia Nauk, Voprosy Micropaleontologii*,**14**, 125-139. (in Russian).

Gorbachik TN, Mohamad GK, (1997) New species of Lituolida (Foraminifera) from the Tithonian and Berriasian of the Crimea. *Paleontological J.,* **31** (4): 345-351 (Translated from Paleontologicheskii Zhurnal, **4**, 3-9.)

Granier B, (1987) Le Crétacé inférieur de la Costa Blanca entre Busot et Altea (Alicante, Espagne): biostratigraphie, sédimentologie, évolution tectono- sédimentaire. *Thèse Univ. P. et M. Curie*, 281 pp.

Heinz RA, Isenschmid CH, (1988) Microfazielle und stratigraphische Untersuchungen im Massivkalk (Malm) der Préalpes médians. *Eclogae Geologicae Helvetiae*, **81** (1), 1-62.

Husinec A, Sokač B, (2006) Early Cretaceous benthic associations (foraminifera and calcareous algae) of a shallow tropical-water platform environment (Milet Island, southern Croatia*). Cretaceous Research*, **27**, 418-441.

Ivanova D, (2000) Middle Callovian to Valanginian microfossil biostratigraphy in the West Balkan Mountain, Bulgaria (SE Europe*). Acta Palaeontologica Romaniae,* **2**, 231-236.

Luperto Sinni E, Masse J-P, (1994) Precisazioni micropaleontologiche sulle formazioni di piattaforma carbonatica del Giurasico superiore e del Cretacico basale del massicio del Gargano (Italia Meridionale) e implicazioni stratigrafiche. *Palaeopelagos*, **4**, 243-266.

Mancinelli A, Coccia B, (1999) Le Trocholine dei sedimenti mesozoici di piattaforma carbonatica dell'Appennino centro-meridionale (Abruzzo e Lazio). *Revue de Paléobiologie,* **18** (1), 147-171.

Marku D, (1999) Kretaku i Munelles. *Disertacion*. I.S.P.GJ.

Marku D, (2000) Mbi transgresionin e Baremianit ne rajonin e Munelles (zona Mirdita qendrore) dhe ndryshimin e skemes stratigrafike. *Kongresi i 8-te shqiptar i Gjeoshkencave*. F. 104.

Marku D, (2001) Kretaku i rajonit Zepe - Guri i Nuses *I.K.GJ*.

Masse, J.P., 1976. Les calcaires urgoniens de la Provence. Valanginien-Aptien. Stratigraphie, paléontologie, les paléoenvironments et leur évolution. *Thèse, Univ. D'Aix-Marseille* II, 511 pp.

Meço S, Dodona E, Melo V, (1975) Perpjekje per ndarjen zonale te depozitimeve Berriasiane te Krahines se Fanit. (Zona Tektonike e Mirdites) ne baze te amoniteve e tintinideve. *Permb. Stud*. **1**, 7-15.

Meco S, Aliaj S, (2000) Geology of Albania. *Beiträge zur Regionalen Geologie der Erde*, Bd. 28, Borntraeger. 246 p.

Melo V, Kote Dh, Dodona E, (1971) Mbi transgresionin e Beriasianit ne rajonin e Xhuxhes. *B.U.T. ser. Shkenc. Nat*. Nr.1, Tirane.

Neagu Th, (1995) Early Cretaceous Trocholina group and some related genera from Romania. Part I. *Revista Espanola de Micropaleontologia*, **26** (3): 117-143.

Pop G, 1994a.) Systematic revision and hiochronology 01' some Berriasian-Valanginian Calpionellids Genus Remaniella. *Geol. Carp.,* **45** (6), 323-331.

Pop G, (1994b) Calpionellid evolutive events und their use in hiostratigraphy. R Olli. 1. *Stratigraphy*, **76**, 7-24.

Pop G, (1996) Trois nouvelles especees du genre Remaniella (Calpionellidaa BO NET. 1956). *C R. Acad. Sci. Paris, t.* **322**, 17-323.

Peza LH, Pirdeni A, Toska Z, (1983) Depozitimet kretake ne rajonin Kurbnesh - Krej Lur dhe te dhenat per zhvillimin paleogjeografik te zones se Mirdites gjate Jurasikut te siperm dhe Kretakut*. Buletini i Shkencave Gjeologjike,* **4**, 71-95.

Peza HL, Arkaxhiu F, (1988) Aspekte te Kretakut te Zones se Mirdites. *Buletini i Shkencave Gjeologjike*.**1**, 95 – 104.

Reichel M,., 1955. Sur une trocholine du Valanginien d'Arzier. *Eclogae Geologicae Helvetiae.,* 48 (2): 396-408.

Salvini-Bonnard G, Zaninetti L, Charollais J, (1984) Les foraminifèrs dans le Crétacé inférieur (Berriasien moyen-Valanginien inférieur) de la région de la Corraterie, Grand-Salève (Haute Savoie, France) : inventaire préliminaire et remarques stratigraphiques. *Revue de Paléobiologie,* **3** (2). 175-184.

Schlagintweit F, Gawlick HJ, Missoni S, Lein R, Hoxha L, (2006) Late Jurassic to Early Cretaceous dasycladales and benthonic foraminifera from the Munella carbonate platform s.l. of the Mirdita Zone. *XIII-th Congress of Carpatian-Balcan Geological Association*. p. 527 – 530.

Schlagintweit, F, (2011) Spiraloconulus suprajurasicus n. sp. – a new benthic foraminifer from the Late Jurassic of the Northern Calcareous Alps of Austria*. Jahrbuc der Geologischen Bundesanstalt*, **151**(3-4), 397-406.

Shehu R, (1990) Gjeologjia e Shqiperise. *SH.GJ.SH.* 306 faqe

Velić I, Sokač B, (1983) Stratigraphy of the Lower Cretaceous index fossils in the Karst Dinarids (Yougoslavia). *Zitteliana,* **10**: 485-491.

Velić I, (1988) Lower Cretaceous benthic foraminiferal biostratigraphy of the shallow-water carbonates of the Dinarids. *Revue de Paléobiologie*, **2** (Benthos'86), 467-475.

Vila J.M,., 1980. La chaine alpine d'Algérie orientale et des confins algéro-tunisien*s*. *Thèse, Univ. P. et M. Curie*, 665 pp.

Zaninetti L, Salvini-Bonnard, G, Decrouez, D, (1987) Montsalevia, n. gen. (Montsaleviidae, n. fam., Foraminifère), dans le Crétacé inférieur (Berriasien moyen-Valanginien) du Mont Salève et du Jura Méridional (Haute-Savoie, France). Note préliminaire. *Revue de Paléobiologie*, **6** (1), 165-168.

Zaninetti L, Charollais, J, Clavel B, Decrouez D, Salvinni-Bonnard G, Steinhauser N, (1988) Quelques remarques sur les fossiles du Salève (Haute- Savoie, France). *Archives des Sciences Genève*, **41** (1), 43-63.

Xhomo A, (2002) Gjeologjia e Shqiperise. 404 faqe.

Xhomo A, Harta Gjeologjike e Shqiperise ne shkallen 1 : 200 000. *SH.GJ.SH*., Tirane

J. Int. Environmental Application & Science, Vol. 15(2): 91-103 (2020)

Research Paper

A Planning Studio Experience in Landscape Architecture Education: Gökçeada Example

Çiğdem KAPTAN AYHAN*

Department of Landscape Architecture, Faculty of Architecture and Design, Çanakkale Onsekiz Mart University, Çanakkale, Turkey

Received April 03, 2020; Accepted June 12, 2020

Abstract: The European Landscape Convention describes landscape planning as strong future actions for the development, improvement and creation of landscapes. In parallel to this, it also highlights the necessity to train landscape-related experts and to provide planning education in various educational institutions while stressing the importance of the sustainable planning of landscapes under various headings. Landscape architecture departments, which gave their first graduates in our country in 1973, have since had a landscape planning infrastructure. This infrastructure constitutes an important place in the landscape architecture education process. Almost all landscape architecture departments in Turkey have landscape planning division. Landscape planning is also considered to be a necessary process for the protection and sustainable use of landscapes on a local, regional, territorial, and even global scale. Gökçeada, the largest island in Turkey, is one of the settlements which need sustainable land use decisions with its different natural and cultural landscape features. The island, which is in the process of declaring an organic agricultural center through the support of the Ministry of Agriculture and Forestry and related provincial agencies while also trying to meet high tourism demands, is under the influence of different sectors in terms of future land use decisions. Thus, Gökçeada was selected as a field of study for the Project V (Planning Studio) course which was carried out during the fall semester of the 2016-2017 academic year by the Department of Landscape Architecture in the Faculty of Architecture and Design of Çanakkale Onsekiz Mart University. In the operation of the studio, students experienced a planning process with all the steps, starting with the description of the subject and problem. In this study, as a result of the functioning of the Gökçeada landscape planning studio mentioned above as well as its gains and limitations for students and their research, spatial decisions for the future of the island have been put forward. In addition, the operational problems of landscape planning studios and their solutions have been expressed through the Gökçeada studio.

Keywords: *Landscape Planning Studio, Island Landscape, Gökçeada, Çanakkale*

Introduction

Landscape planning in the European Landscape Convention (ELC) is defined as strong prudential actions on development, improvement, and creation of landscapes (Official Gazette, 2003). Ahern (2002) mentions that landscape planning aims to protect rare, scarce, and unique resources with controlled usage, prevent potential threats and pre-identify areas suitable for development (Kaptan Ayhan and Hepcan, 2009).

With landscape planning, ecological principles are included in spatial planning. What makes the landscape plan different from other physical plans is that this plan is the result of an ecologically based planning (Ortaçeşme, 2007; Cetinkaya & Uzun, 2014). The ELC, which Turkey signed in 2000, states that the landscape should be put into practice for all country policies on various scales. Besides, each country that signed this agreement is committed to creating and implementing landscape policies for the protection, management, and planning of the landscape. Further, the ELC considers the awareness of civil society, the public and private sectors under the heading "Special Measures" on the value of landscaping and the effects of changes in landscapes. The subheading "Training and Education" under the same title includes articles about the training of landscape-related experts, the creation of multidisciplinary education programs, and the provision of courses covering the preservation,

*Corresponding: E-Mail: ckaptanayhan@comu.edu.tr, Tel: +90 286 218 00 18-3086

development, management, and planning of landscapes in universities and other educational institutions (Official Gazette, 2003).

The Landscape Architecture Education in Turkey began in 1968 on a departmental basis and gave its first graduates in 1973. Since then, there has been a landscape planning infrastructure in landscape architecture departments; however, it has not reached the expected/desired level (Uzun *et al*. 2019). Although there has not been an agreement on the practice of landscape planning education (course time, number of semesters, class content, *etc*.) in the departments, landscape planning studios and related courses hold an extremely important place in the education of students.

In this study, the Project V (Planning Studio) course, conducted in the fall semester of the 2016-2017 academic year in the Department of Landscape Architecture in the Faculty of Architecture and Design of Çanakkale Onsekiz Mart University, has been evaluated. Thus, it is aimed to discuss the achievements and limitations of the planning studio operation in landscape architecture education for the students. Within the scope of this course, 31 students were shared between 2 faculty members responsible for the course. The content of this study was based on the plans and reports of two different groups selected from Group A (consisting of 15 students).

As the study area, Gökçeada district of Çanakkale Province, which is an important settlement in terms of its historical, ethnic, agricultural and touristic aspects and contains different landscaping and field use samples, was selected.

This decision was made in relation to the fact that students would come across many different forms of land use and that the island has special examples of urban, rural and coastal landscapes. In addition, the study area faced unplanned and uncontrolled tourism movements, especially in recent years. Therefore, it is obvious that Gökçeada's future should be constructed with approaches based on sustainable use of resources.

Material and Method

The main material of the study consists of the Gökçeada district and the reports and maps put forward by the students during the studio process. Written and visual information and documents related to the field were used in the preparation of these reports and plans. In addition, information was obtained through oral interviews with various institutions. All of these are other research materials.

Study Area: Gökçeada District

Gökçeada district of Çanakkale province is in the northeast of the Aegean Sea (Figure 1). The area is 289km^2 and the shore length is 95 km. (Gökçeada Kentsel Tasarım Rehberi, 2016). The population of the island was 8769 in 2017, and 9440 according to the data of 2019 (Turkish Statistical Institute, 2020). There are 9 villages in the district. Tepeköy, Dereköy, Kaleköy, Bademli and Zeytinli villages are ancient Greek villages. Eşelek, Şirinköy, Uğurlu and Yeni Bademli are state-owned settlement villages. In terms of historical development, it is estimated that the first settlement on the island was between 3000 and 2000 B.C. (Kahraman, 2006). The Pelasgians (Achaeans) were the first tribe to settle on Gökçeada (Özbek, 2008), and the island had been dominated by many different realms (Rome, Latin, Venice and Genoese and finally Ottoman) throughout its history (Gökçeada Urban Design Guide, 2016). Lastly, on September 22, 1923, the island joined the territory of the Republic of Turkey under the Treaty of Lausanne (Çapa, 2017). A great part of the Greek population, which was dominant until 1946, emigrated to Greece after 1960. The previous name of the island, Imbros, was changed to Gökçeada on this date. The Greeks who have left with migration keep their bonds with Gökçeada and visit the island on various special and religious days. Some of them resettled in the island after their retirement (South Marmara Development Agency, 2012).

The service sector and agricultural activities in Gökçeada are the two most important branches of the economic structure. Avcı (2008) indicates that olive and grains are the most significant agricultural products of the island. The Imbros sheep, which is unique to the island, also has an important role in animal production (Konyalı *et al*., 2004). Beekeeping activities are also developing due to organic agricultural projects (Şahin, 2015). Avcı (2008) says that viticulture is decreasing compared to the periods when the Greek population was dense. In addition, efforts to declare Gökçeada as an organic farming island continues with the cooperation and support of central and local administrations and related institutions. The fact that the natural landscape is not polluted with any industrial activities

makes the agricultural activities in Gökçeada unique and important. However, the fact that the area is an island also causes it to be more ecologically fragile.

Figure 1. Gökçeada's Geographic Location (ESRI, 2016, Cengiz et al., 2009)

In addition to its agricultural potential, Gökçeada also has a rich cultural landscape with important traces of Aegean islands' settlement culture and traditional living habits. Additionally, due to the limited access to the mainland (although significant improvement has been achieved compared to past years), the people living on the island have learned to meet their own needs and turned this into a way of life. Today, this culture, which is part of the past and was born of limitations, is an important cultural value of the island. In addition, this cultural value is a rural development tool of the island (island-specific products in national markets) in terms of gastronomy. Gökçeada was joined International Slow City Network (Cittaslow) in 2011 with a project that began with this movement. The island remains the first and only island in the world to achieve this status (Özdemir and Kaptan Ayhan, 2019).

With its natural and cultural values, especially in recent years, the island faces an increasing tourism demand. The relative increase in transportation opportunities, advertisements through written and visual press and social media has made the island an important destination. However, these economy-focused tourism activities, which are far from any planning, pose a threat to Gökçeada.

Considering all these assessments, this course is looking for an answer to the following question: "On which areas and sectors should the future of Gökçeada be built?"

The method of this study is based on the operation of the planning studio, which is carried out in the fall semester of the 2016-2017 academic year. Within the framework of the studio, the current state of the natural and cultural landscapes of Gökçeada was analyzed and planning studies based on sustainable use were revealed in line with this analysis. Within the scope of the course, firstly, data for

the natural and cultural landscape of Gökçeada were obtained for analysis studies. Then, for the purpose of on-site survey and observation, a technical trip to Gökçeada was held between 13-14 October 2016 with 2 faculty members, 2 research assistants, and 31 students. During the technical trip, a meeting with the Mayor of Gökçeada took place in addition to field survey, and information about the current state of the island, its problems and future projects planned by the authorities was obtained. In addition, the students conducted interviews with local people, obtaining various information about the island, both from the past and present.

After the data collection phase, the students analyzed land-use suitability in Gökçeada. AutoCAD and Photoshop software were used in these analyses. Consequently, the students came up with suggestions about which sector and identity could help Gökçeada reach a sustainable future. The limited use of geographic information systems software is mentioned in the "Results and Discussion" section.

Results and Discussion

Revealing the Current Situation

After deciding on the study area, the students were expected to collect data on Gökçeada's natural and cultural landscape. They, then, conducted on-site observations and inspections during the technical trip. Notes, photographs and information obtained from the mayor's office and local public interviews during this stage also helped establish the current state of the area. All the data collected from the study area are shown in Table 1. Revealing the current situation was very important to effectively continue the planning process, and the students, therefore, understood the importance of written resource diversity and personally took over the process of acquiring information and documents from institutions and organizations in person. They also experienced the necessity to allocate information as necessary/unnecessary in the process of reporting these spatial planning and plan decisions. In addition, during the technical trip, they followed the footsteps of traditional life and the traces of the Greek-Turkish culture's common features, while trying to get to know Gökçeada with all its landscape features. They submitted a "Current Situation Report" according to all information, documents and maps provided and prepared "the Current Situation maps" (Natural Landscape/ Cultural Landscape) (Figure 2-3).

Table 1. Current status data of the Study Area

Natural Structure	Topographic Structure
	Flora
	Fauna
	Climate
	Soil Properties
	Geology
	Hydrology
Spatial Features	Urban Infrastructure
	Urban Conservation Areas
	Rural Conservation Areas
Economic Structure	Vegetable Production
	Animal Production
	Tourism
Sociocultural Structure	Demographic Data
	Health Care
	Education Services
	Transportation Services
	Traditional Living Habits
Historical and Administrative Structure	Historical Development
	Archaeology
	Location Properties
	Historical/Traditional Villages - Settlement Villages
	Zoning Plans
	Investment-Incentive Areas

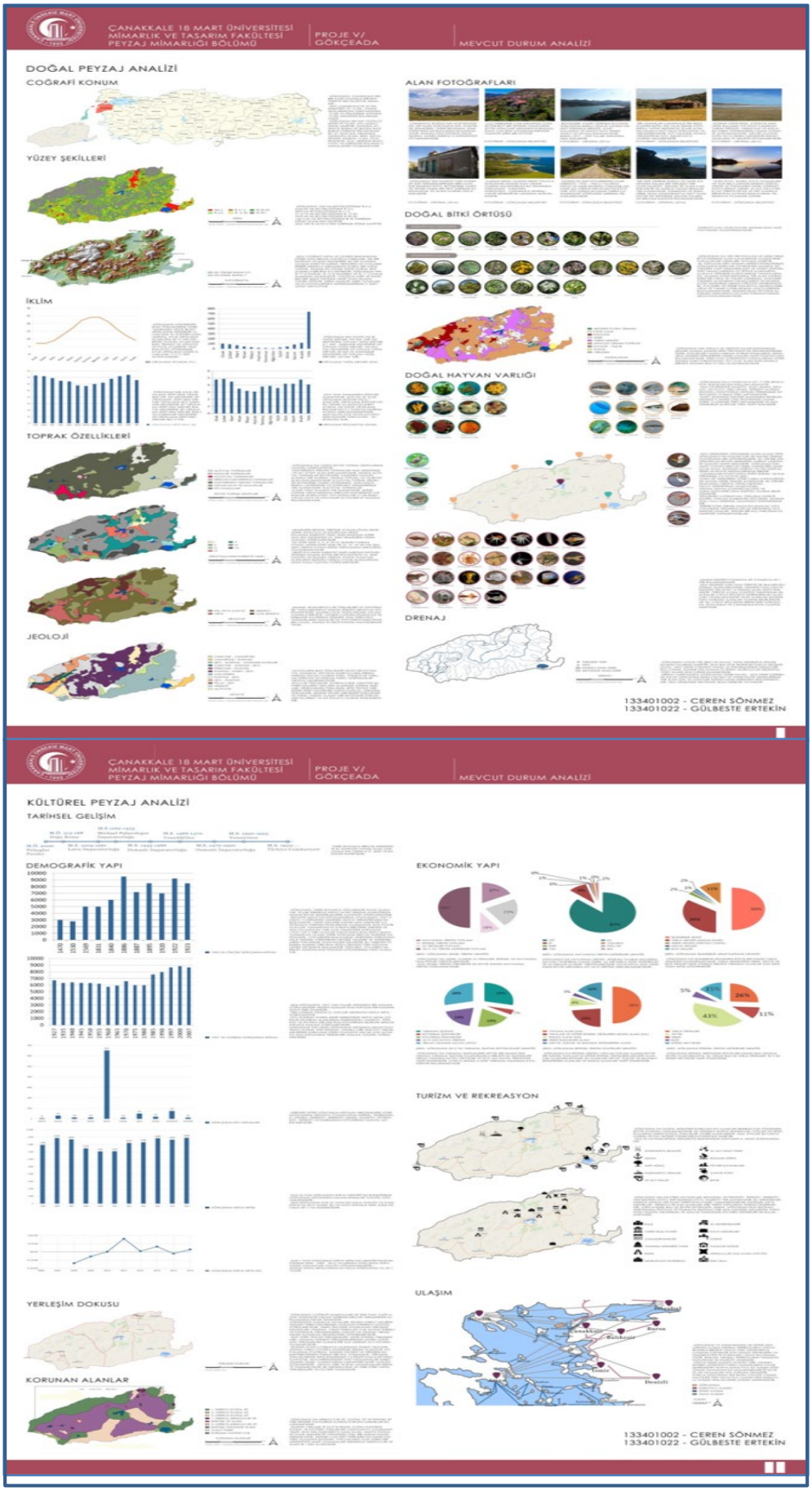

Figure 2. (Cultural/Natural) Current Situation Maps (Group 1: Ceren Sönmez, Gülbeste Ertekin)

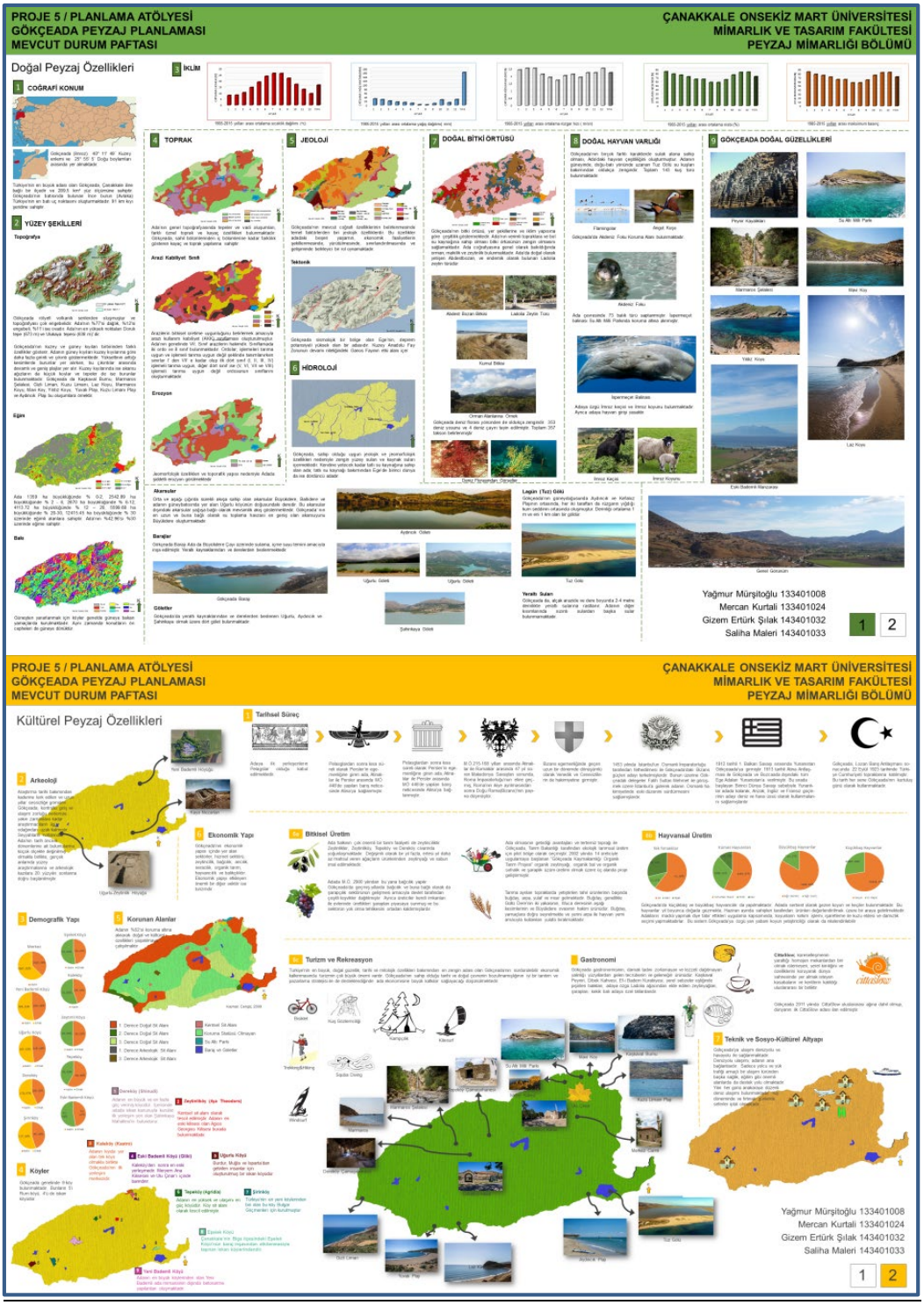

Figure3. (Cultural/Natural) Current Situation Maps (Group 2: Yağmur Mürşitoğlu, Mercan Kurtali, Gizem Ertürk Şılak, Saliha Maleri)

Land Use Suitability Analysis

The students overlaid thematic maps according to the data obtained and spatialized at the previous stage. Then, they carried out suitability analyses for Gökçeada's current and future land use. As a result, they attempted to determine the optimal areas for forests, agriculture/pasture and tourism/recreation uses (Figure 4-5). In addition, they developed several recommendations for these identified uses.

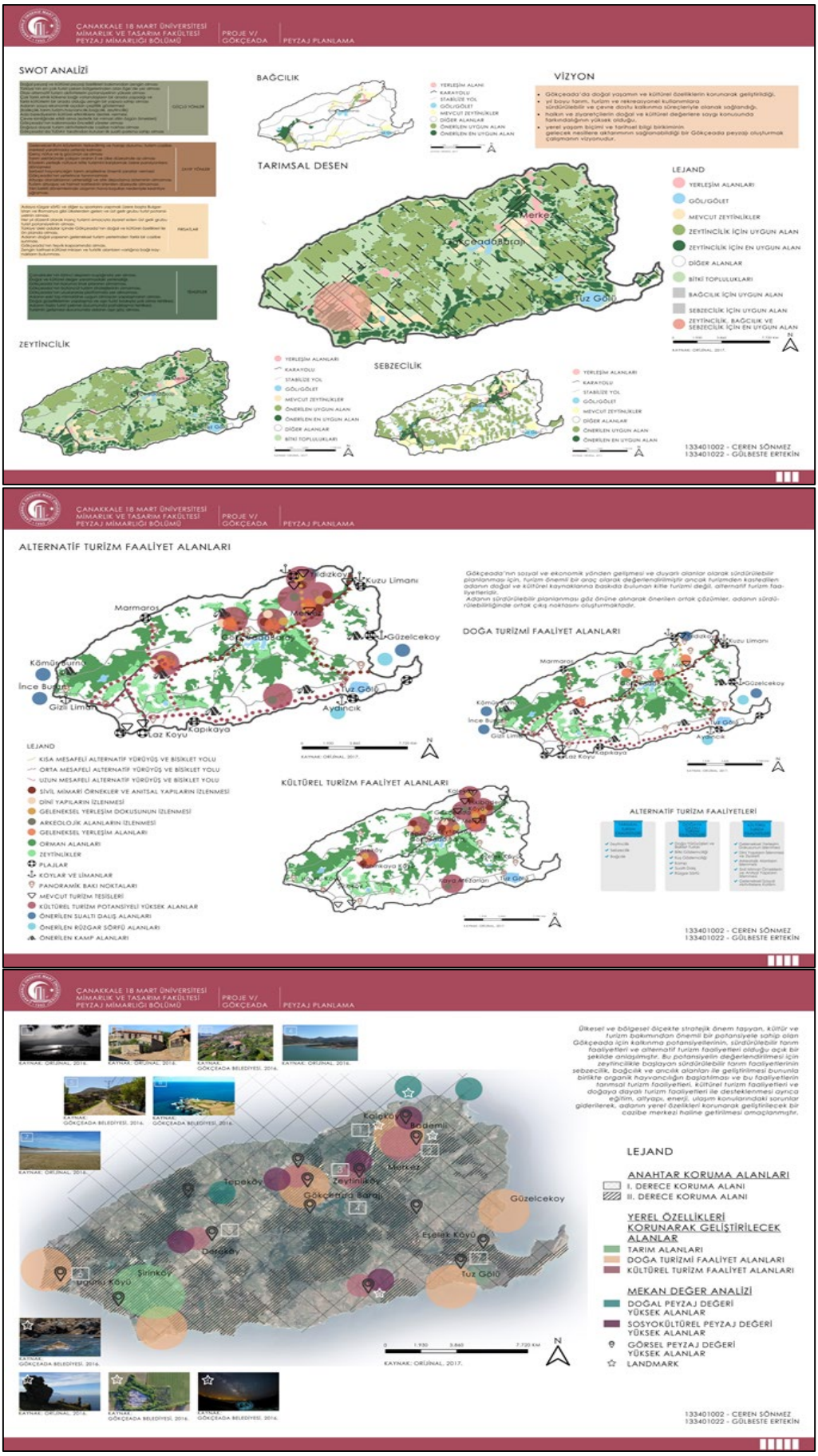

Figure 4. Land use Suitability Maps (Group 1)

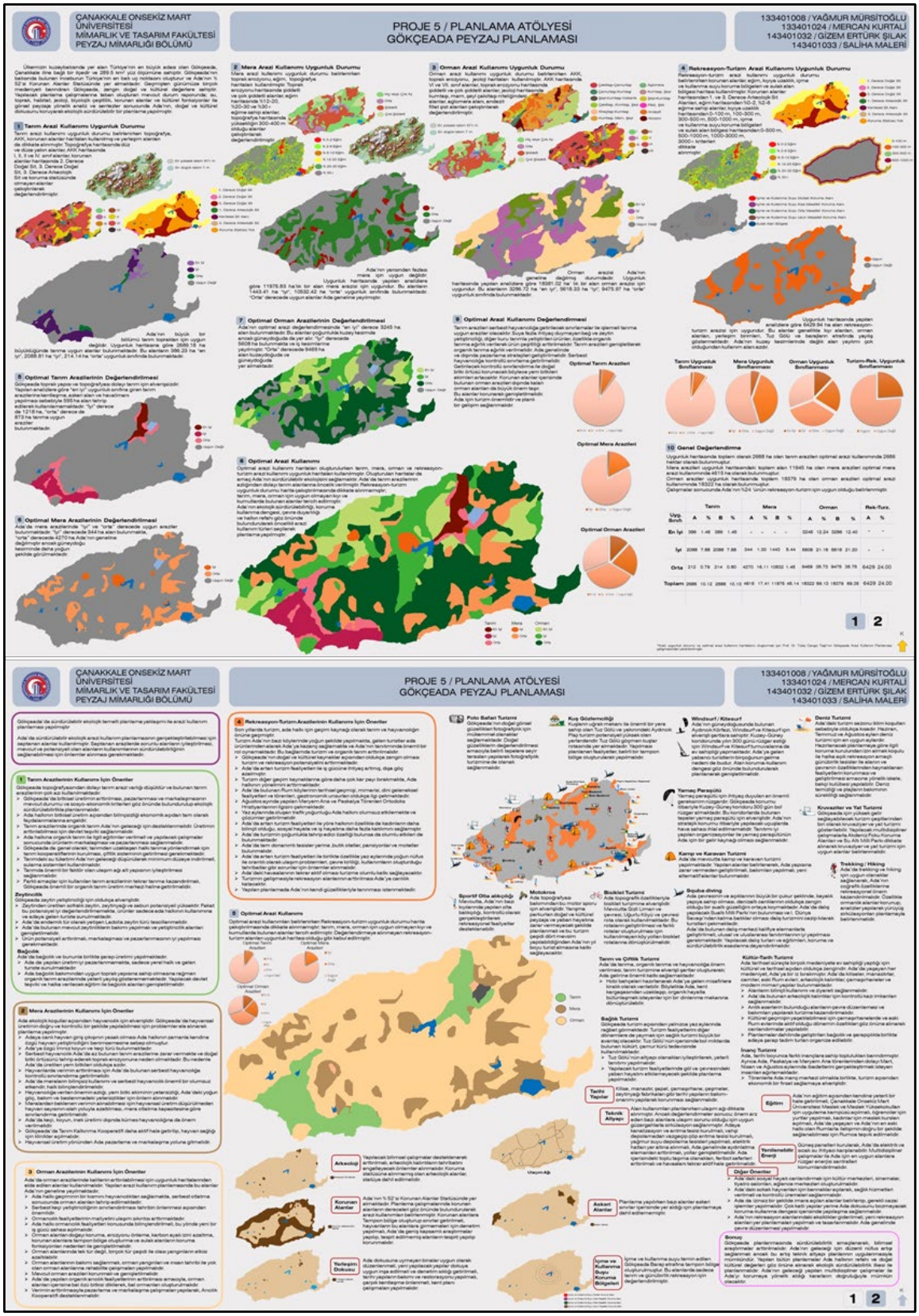

Figure 5. Land use suitability maps (Group 2)

In the process of deciding on the sustainable future of Gökçeada, both student groups accepted the consideration of protection-use balance, staying within the limits of ecological thresholds, and the persistence of conservation decisions as their main principles. In this context, the main uses which

both groups recommended for the island are organic agriculture and tourism according to the island's ecology and cultural texture. The plan decisions created for this is generally as follows:

1.Agricultural activities are particularly important on islands. The fact that access to the mainland is not always possible is forcing the island people to meet their own nutritional needs. Therefore, agricultural production is an indispensable life culture for the island. That is why it is necessary to continue the traditional and modern agricultural methods by combining them. In addition; the efforts to declare Bozcaada and Gökçeada as "organic agriculture island" with the cooperation of both central and local administrations and related institutions are extremely important for rural development. The continuity of agricultural activities is an issue that should be emphasized in terms of not allowing the whole economic structure of the island to depend on tourism activities and preventing misuse of agricultural land.

2. Olive cultivation has an important potential which should be considered in terms of island agriculture. A variety of olive named Ladolia is especially important, since it grows only in Gökçeada in Turkey and has a unique smell and taste properties.

3. Viticulture and winemaking is a very old culture of Gökçeada. According to Avcı (2008), the discovery of carbonized grape seeds from the 2900s BC indicates that viticulture activities have been carried out on the island since ancient times. The production of homemade wine, a tradition from past, must be supported by complying the process with the laws and regulations.

4. In terms of animal production, Imbros Sheep is especially important. This species, which is cultivated on the island in conditions that can be considered "wild" (Konyalı *at al*, 2004), is under protection as a genetic resource. Studies focused on Imroz sheep production should be increased. In addition, Gökçeada has the potential to develop in terms of beekeeping activities.

5. The continuity of agricultural activities in Gökçeada should be ensured by the cooperation of the state and relevant institutions and organizations. Furthermore, the quality of island agriculture will improve, and the market share of the products will increase by providing related training to farmers.

6. Tourism is a sector that both groups of students recommend for Gökçeada's future. However, the inability to achieve economic satisfaction from agricultural activities leads local people to tourism. The island is suitable for coastal tourism for only 2-3 months due to its climatic properties. The lack of planning to spread tourism throughout the year causes intense visitor pressure in this period. This situation results in insufficient accommodation capacity. For this reason, the public ignores the necessity of protection decisions and approaches positively to various zoning decisions made especially for marginal lands. Awareness of the local people towards the protection of the island's natural and cultural values should be increased through various educational activities. With various educational studies, local awareness on the protection of the island's natural and cultural values should be increased.

7. Tourism activities to be carried out in Gökçeada should be planned carefully to prevent a mass tourism effect. Tourism construction should prioritize protection and should be conducted in harmony with the traditional architectural texture and the living culture of the island.

8. In coastal tourism activities, the human impact is felt most intensely. The balance between protection and usage must be contained in coastal planning.

9. The sustainable future of Gökçeada will be possible through the planning of agricultural and tourism activities together and in relation to each other. Starting from here, agricultural tourism has been given a wide coverage for planning. Maintaining the stages of agricultural activities, spanning the whole year (pruning, harvesting, etc.) in parallel with tourism, and making Gökçeada a destination for individuals adopting this tourism concept were suggested.

10. The understanding of sea-sun-sand oriented tourism in the past is now replaced with a highly aware thinking structure that respects nature, culture and traditional life and would like to experience it. The Slow City status is an important approach, especially for foreign and local tourists who embrace this type of tourism. The Slow City approach, which includes many criteria, such as the protection of the original rural and urban character and the survival of traditional handicrafts, is an opportunity to carefully evaluate Gökçeada's sustainability. At this point, previous studies aiming to raise the awareness level of the local people regarding the concept of a slow city – such as giving nutrition and taste training in primary schools with the collaboration of Slow Food Gökçeada Convivium and the Department of Gastronomy in the Gökçeada School of Applied Sciences of Çanakkale Onsekiz Mart University; determining traditional professions and related handicrafts in

relation to Traditional Professions: A Study of Oral History in Gökçeada in 2006 conducted through the support of the same cooperation; the introduction of an oral history documenting work on Gökçeada Cuisine and its publication as a book entitled "Slow Food and Gökçeada: A Managerial Approach"; and the publication of another book entitled “Slow Movement” in 2010 and its distribution to the local public (Özdemir & Kaptan Ayhan, 2019) – should be repeated. It would also be an important step for the local authorities to own the title of Slow City and focus on projects towards the criteria that must be met in order to preserve this title.

In accordance with the planning studio which is the subject of this study, student groups examined the existing natural and cultural landscape values through an example area and brought various plan proposals focused on the sustainability of Gökçeada's cultural identity. However, another purpose of this study is to reveal the achievements and limitations of planning studios in landscape architecture education. In the context of this project and the Gökçeada planning studio example, student gains and problems encountered can be sorted as follows, according to Uzun *et al*. (2019):

Planning Studio Achievements

The students, who experienced the whole process of landscape planning from the beginning, grasp the evaluation of many different disciplines via planning. With this studio, the students experienced the necessity of multidisciplinary work in order to achieve the resulting product while planning in an area with both natural and cultural resources, such as Gökçeada.

They gained experience in achieving results by performing the exact process described theoretically in the landscape planning course. They also gained experience on the importance of teamwork and how they could turn individual differences into an advantage. In this course, the students were free for choosing their groups. The number of students in the groups changed between 2 and 5 times. At this point, the students learned task sharing, fulfilling their responsibilities promptly and developing an awareness of taking joint action.

They clearly experienced the importance of the concept of geographic information systems and using the software. The use of GIS software provides great convenience in planning efforts within today's technology. However, the students experienced several difficulties during the data processing and planning due to their GIS usage limitations. In addition, the lack of Photoshop software and similar programs used for overlays as well as the program’s lack of details needed to achieve the desired result also increased their awareness and desire to learn about GIS software.

They also gained experience in the data collection phase during the planning project. They understood the importance of digital data along with which information and documents they needed to access and from which institutions they could obtain information and documents. They experienced the necessity of a systematic data collection process while working in an area such as Gökçeada where access to the island was relatively limited.

In terms of sustainability, they learned about the necessity and importance of defining and classifying landscapes and they gain the ability to carry out these basic steps. Gökçeada, the largest one among a few islands of Turkey, contains many different landscapes. With this study, they understood the importance of identifying and classifying landscapes, thus ensuring sustainable use, with the example of Gökçeada. In addition, they carried out very basic studies on the identification and classification of landscapes. As a result, their awareness about the importance of the determination of landscape characters on the local, regional and national scale increased and they gained experience in the preparation process of landscape atlases.

With the contribution of all other courses associated with the planning studio, the students who completed this studio gained the competence to recognize and analyze different landscapes and to plan these landscapes without ignoring the social needs and characteristics, with a perspective on sustainability. The obvious effect of the Greek culture in Gökçeada is still perceived in many parts of life. There are also settlement villages on the island built for individuals from different regions of Turkey. This has created a wide variety for the island's living culture. As a consequence of this study, the students stepped up to gain the planning ability to satisfy different spatial desires and habits of different cultures. While finding solutions for different sectors (agriculture, tourism, etc.), they also gained the ability to produce plans that would correlate with the ecological basis.

Problems and Limitations Faced During Planning Studio Courses

Difficulties were faced in the supply of printed/digital map data on natural and cultural landscape elements required in planning studies. The faculty members were obligated to choose from the available data. This issue leads to repetition.

Departmental quota determined by the Council of Higher Education (YÖK) is increasing with each passing year. The average number of classroom size is 70, leading to both spatial inefficiencies and a considerable increase in the number of students per each faculty member. Even the presence of 31 students during the planning studio, which is the subject of this study, led to limitations in terms of both accommodation and in-area transportation. Similarly, crowded classes make it difficult to allocate vehicles to transport students to the field.

The insufficient knowledge and experience of the students in GIS programs negatively affected the planning process, especially during the data analysis phase. The students tried to come to a solution using AutoCAD and Photoshop programs in this studio for similar reasons.

There were also problems with area selection for the planning studio. At least a two-day travel program with accommodation was needed in order to have enough time required for necessary inspections and observations in the area, local interviews and surveys with residents and related public institutions and organizations. However, the desired land trip planning could not be made due to the conflicts in the weekly curriculum of the students and faculty members, along with the economic inadequacies of the students and the university.

If daytrips are preferred, the study area repetition issue occurs. In this context, the selection of Gökçeada as a study field ensured that the students had a different experience in terms of land travel, but economic limitations were handled only through the contributions of the university and Gökçeada Municipality. Considering that the classroom sizes are more than 2 times higher today unlike the period when the project started, it was difficult to provide similar economic supports.

The students were unable to establish the connection between the design and planning scale at the expected speed and had difficulties in developing a holistic perspective and reaching conclusions. They also had a difficulty in connecting the studio with the courses they previously took to form a basis for the planning studio.

Conclusion

In planning-design education, studios are the most accurate courses that shape students in the process from theory to practice. As it is also stated in various studies in departments which focus on design and planning education and in which the studio outputs and results are discussed (Dikmen, 2011, Yaşar and Düzgüneş, 2013, Alpak et al., 2018, Acar and Bekar, 2017, Ter and Derman, 2018, Erdoğan, 2018, Altanlar, 2018), it is possible for students to gain professionally necessary abilities such as developing concrete and abstract concepts, solution-oriented approaches and ecology-based solutions in these studios. Planning and design studios must have sufficient equipment, including physical facilities and technological infrastructure, in order to educate students from object design to spatial planning and to give students the ability to work as a team.

The high efficiency processing of these classes will allow the student to begin to work as a graduate with the best potential. In this context, it is necessary to ensure the urgent reduction of departmental quotas, to support departments in terms of hardware and software to ensure the necessary development in GIS, to program the term schedule to allow GIS and planning classes to support each other in class schedules, and to provide necessary facilities for at least two-day land trips which are the absolute requirements for planning studios. The legal and administrative inclusion of landscape planning in spatial planning processes (Aşur & Alphan, 2018; Yilmaz Kaya & Uzun, 2019) will encourage students to be more interested and productive in landscape planning studios. Inter-departmental studio collaborations are also important for students to learn different perspectives. A stronger connection should be established between courses and planning studios that can build support in landscape planning studios, and students should get prepared for this process. In theoretical courses, day trips or shorter field trips will help students adapt to planning processes.

This study, which aims to reveal the process of the operation of the course within the planning studio, the achievements and limitations of students in the course, and the results of students' outcomes despite restrictions, is supportive in the process of the proper construction of planning

studios, especially in the landscape architecture departments that have not yet started their educational activities.

Defining and classifying landscapes is a commitment of Turkey, as well as all countries that have signed the ELC, as stated in the agreement. In addition, integrating landscape plans with our country's spatial planning system is necessary for this process to go appropriately. Planning studies in both urban and rural areas are crucial to the sustainable future of the country. Accurate analysis of natural and cultural data will only be possible with educated individuals equipped both theoretically and in terms of land studies. For this purpose, it will be the most appropriate step to improve the quality of education in the departments of landscape architecture, to establish relevant standards, and to build consensus as much as possible for landscape planning and planning studio courses.

References

Acar H, Bekar M, (2017) A studio work in landscape architecture education: waterfront landscape design project (in Turkish). *MEGARON* **12**(2), 329-342.

Alpak EM, Özkan DG, Düzenli T, (2018) Systems approach in landscape design: a studio work. *Int J Technol Des Educ*. **28,** 593–611.

Altanlar A, (2018) The basic design education in the context of the human-space relationship:"the city of Sofular neighbourhood an example of urban abstraction workshop" (in Turkish). *JOSSE*, **1**(1),1-25

Aşur F, Alphan H, (2018) Visual Landscape Quality Assessment and the Impacts on Land Use Planning (in Turkish), *Van Yüzüncü Yıl University Journal of Agricultural Sciences,* **28**(1), 117-125

Avcı N, (2008) Gökçeada'da organik tarım ve organik ada. In Proceedings of Gökçeada Değerleri Sempozyumu pp. 85-88, Gökçeada, Çanakkale.

Cengiz T, Özcan H, Baytekin H, Altınoluk Ü, Kelkit A, Özkök F, Akbulak C, Kaptan Ayhan Ç, (2009) Gökçeada Arazi Kullanım Planlaması, TÜBİTAK Proje Sonuç Raporu Proje No: 107Y337

Çapa M, (2017) Restoring the Turkish sovereignity in Imbros and Tenedos after the Treaty of Lausanne (1923-1928): A report on the islands. (in Turkish) *The Journal of Black Sea Studies*, **11**(22), 91-108.

Çetinkaya G, Uzun O, (2014) Peyzaj Planlama, Birsen Yayınevi, Ankara.

Dikmen B. Ç, (2011) Importance of the studio courses in architectural education: basic design studios. (in Turkish) *Engineering Sciences,* **6** (4), 1509-1520.

Erdoğan G, (2018) Studio experiences in planning education: Muğla (Menteşe) studio (in Turkish) *MEGARON* **13**(4), 651-664

ESRI, (2016). ArcGIS 10.5 Software, Environmental Systems Research Institute, CA.

Gökçeada Urban Design Guide (Gökçeada Kentsel Tasarım Rehberi), (2016). Atelye 70 Planners & Architects (in Turkish)

Kahraman SÖ, (2006) Effects of factors on disperse of settlement in Gökçeada (Imbros) from past today. (in Turkish) *Coğrafya Dergisi,* **14**, 25-42.

Kaptan Ayhan Ç, Hepcan Ş, (2009) Developing a landscape planning approach for the areas having unique landscape characteristics: the case of Bozcaada (in Turkish), *Journal of Tekirdag Agricultural Faculty,* **6** (1), 93-105.

Konyalı A, Daş G, Savaş T, Yurtman İ.Y, (2004) Imbros sheep raising in Gökçeada: A potential for organic animal production. (in Turkish) In Proceedings of 21st International Congress on Organic Animal Production and Food Safety, Kuşadası, Turkey.

Official Gazette (2003) Law on the Approval of the Ratification of the European Landscape Convention. Retrieved June 24, 2019 from http://www.resmigazete.gov.tr/eskiler/2003/06/20030617.htm#6 (in Turkish).

Ortaçeşme V, (2007) Landscape Planning within the Context of the European Landscape Convention (in Turkish) In Proceedings of Avrupa Peyzaj Sözleşmesi'nin uygulanması Yolunda Türkiye Uluslararası Katılımlı Toplantı pp81-86, Ankara.

Özbek Ç, (2008) Antik çağda Gökçeada. In: Proceedings of Gökçeada Değerleri Sempozyumu pp. 59-68, Gökçeada, Çanakkale.

Özdemir E, Kaptan Ayhan Ç, (2019) The importance of the slow city movement for the conservation of cultural landscape in Gökçeada sample. (in Turkish) *The Journal of Social Sciences Institute*, Winter (Special Issue) 291-310.

South Marmara Develeopment Agency (Güney Marmara Kalkınma Ajansı), (2012) Çanakkale: Bozcaada & Gökçeada Değerlendirme Raporu 2012.

Şahin Ç, (2015) AB Bölgesel Politikası Adalar ve Gökçeada. Beta Press, İstanbul.

Ter Ü, Derman S, (2018) Şehir planlama eğitiminde temel tasarım öğretisi: planlama stüdyosu 1 dersi deneyimi. *Online J. Art & Design* **6** (2) 132-147.

Turkish Statistical Institute, Pupulation Registration System, Retrieved March 1, 2020 from https://biruni.tuik.gov.tr/medas/?kn=95&locale=tr (in Turkish).

Uzun O, Gültekin P, Karadağ A, Müderrisoğlu H, Uzun S, Kaplan A, Mansuroğlu S, Alphan H, Açıksöz S, Ayhan Ç, (2019) Türkiye'de peyzaj planlama dersi ve peyzaj planlama stüdyosu deneyimleri, In: 50. Yılında Peyzaj Mimarlığı Eğitimi ve Öğretimi (Eds. O. Uzun, P. Köylü, S. Özdede Bacı, P. Gültekin and H. Müderrrisoğlu) pp 144-154. Düzce Üniversitesi Yayınları No:9, Orman Fakültesi Eğitim Dizisi: 1, Pelin Ofset, Ankara.

Yaşar Y, Düzgüneş E, (2013) Integration of sustainability concept to landscape design: a studio work. (in Turkish). *İnönü Un. J. Art & Design* **3** (7) 31-43.

Yılmaz Kaya M, Uzun O, (2019) Evaluation of the relationship between ecosystem services and spatial planning in landscape planning framework (in Turkish) *Düzce Üni. Bilim ve Teknoloji Dergisi*, **7**, 2166- 2193.

J. Int. Environmental Application & Science, Vol. 15(2): 104-108 (2020)

Research Paper

Investigation of some Yield Characteristics of Hemp (*Cannabis sativa* L.) in Tokat Ecology

Levent YAZICI[1, *], Gungor YILMAZ[2], Talip KOCER[3], Hazal SAKAR[3]

[1]Directorate of Middle Black Sea Transition Zone Agricultural Research Institute, Tokat, Turkey; 2Faculty of Agriculture, Yozgat Bozok University, Yozgat, Turkey; [3]Tokat Gaziosmanpasa University Graduate School of Natural Sciences, Tokat, Turkey

Received March 26, 2020; Accepted May 28, 2020

Abstract: The hemp plant has two important products in terms of use, one is the stems and fibers obtained from them, the other is the seeds and oil. In this study was aimed to determine some yield characteristics of hemp varieties and populations in Tokat ecological conditions. In the experiment, five local hemp populations and two industrial type hemp cultivars were used as materials. The trial was carried out in 2019 with three replications according to the Randomized Block Trial Design. According to the research results; plant height values ranged from 50.40 cm to 363.35 cm, stem thickness from 4.32 to 16.77 mm, technical stem length from 5.10 cm to 246.60 cm, dry stem yield from 82.54 kg da^{-1} and 3143.75 kg da^{-1}, fiber yield from 29.64 kg da^{-1} and 638.76 kg da^{-1}, seed yield from 72.98 kg da^{-1} and 474.87 kg da^{-1}. According to the average findings, the populations Narlısaray were identified as the best in a result of investigated all traits.

Keywords: *Cannabis sativa L., hemp, population, variety, stem yield, fiber yield*

Introduction

The hemp is a one-year industrial plant of *Cannabis sativa* L. species and *Cannabis* genus belonging to the *Cannabinaceae* family. Hemp can be grown as a fiber, seed, or dual-purpose crop. Hemp, whose homeland is Central Asia, is widely found in nature (Warf, 2014). Fiber is obtained from the stems of the plant and oil from the seed. It is one of the oldest fiber plants used by humans since ancient times in various parts of the world. The hemp has a tap root. Tap roots can reach a depth of 3-4 m under suitable moisture and soil conditions. Cannabis stems have a structure that is 4-25 mm thick and its length can vary up to 0.5-6 meters depending on the climate and variety characteristics. Female plants have thicker stems, longer plants and higher fiber yields than male plants. The highest quality fibers in hemp are obtained from the part called technical handle length. Hemp leaves are composed of 3-11 narrow leaflets joining together on a stalk at the bottom and the same point with their shorter lengths, the longest in the middle. The edges of the leaves are toothed. Leaflets are the most in the middle of the stem. Hemp is a dioecious plant. So male and female flowers are found in separate plants. However, it also exists in monoecious forms. In male flowers, there are 3 outer (protective) leaves, 5 male organs (stamens) in them. Female flowers are located on short stalks from the leaf seats at the top of the stem in female plants. Foreign fertilization is observed in the cannabis plant. Cannabis seeds can be 3-6 mm long, 2-4 mm wide, grayish-brown, blackish-brown, greenish-brown, and have a very thin skin. Hemp has a grain weight of 9-27 g and contains 20-30% oil in its seed. (Ronde, 2013; NASEM, 2017; Baldini *et al*., 2018; ORAN, 2019; Gizlenci *et al*., 2019; Anonymous, 2020). In the study conducted in 2015 to determine the adaptation and yield potentials of cannabis varieties in the South-western Colorado Research Centre, the biomass yield of 12 cannabis varieties is 3789 lb/acre, the seed yield is 25-519 lb/acre, the stem yield is 2415- 4848 lb/acre, stalk thickness is determined as 4.8-8.0 mm, plant height is 44-77 inches. (Berrada *et al*., 2019).

Hemp fibers are most often used in fabrics and textiles, making rope, tether, sack, yarns, paper, carpeting, home furnishings, construction and insulation materials, auto parts, and composites. Weaves with touristic value are knitted from finer hemp fibers. The leftovers after the fibers are removed can be used as fuel. Hemp seed and oil obtained from the seeds are used in a range of foods and beverages also in soap, cosmetics and dyeing. The pulp leftover from the seeds after the oil is taken is used in animal nutrition. Hemp is also used as biodiesel raw material. (Gurel *et al.,* 2000; CRS, 2017).

*Corresponding: E-Mail: leventyzc@gmail.com; Tel: 05337771188; Fax: 3562521253

Tetrahydrocannabinol (THC) and cannabidiol (CBD) are the two naturally occurring cannabinoids. In hemp produced for industrial purposes, the THC rate should be legally below 0.3% (Canada) and below 0.2% in the European Union. The use of THC and CBD in medicine has been used in the treatment of cancer pain, depression, anxiety disorders, sleep disorders, neurological disorders, childhood epilepsy, AIDS-related appetite-enhancing and intestinal diseases or relieving symptoms (EMCDDA, 2018; NASEM, 2017). This study was carried out to determine the some yield characteristics of hemp varieties and populations in Tokat ecological conditions.

Material and Method

Five local hemp populations of our country (Narlısaray, Kavacık, Kartal, Maltepe and Van) and two industrial type hemp cultivars (Fedora 17 and Finola) were used as materials in this experiment. The trial was carried out in the trial field of Gaziosmanpaşa University, Agricultural Application and Research Center under the conditions of Tokat in 2019 vegetation period. Soil preparation was done by the conventional method with plow and harrow. The trial was carried out in three replications according to the Randomized Block Trial Design with 5 meter length, 3 rows, 20 cm row spacing and approximately 150 plants per m2. Sowing was done manually to the rows opened with the marker. Fertilizer was applied in the amount of 10 kg da^{-1} of nitrogen (N) and 8 kg da^{-1} phosphorus fertilizer P_2O_5 (Ozdemir, 1993). Nitrogen was accomplished in two equal doses. At sowing half and the other half was given in the middle of May. The crop was irrigated 4 times with a drip system, the harvest was done by hand, at the stage of seed maturity. The data of the properties examined in the study were taken from male and female hemp plants during the plant seed maturity period. During the growing season of hemp (May to October), the sum of precipitation amounted to 149.7 mm in 2019. Air temperatures were mean 20.48 °C during the growing season (Table 1). In the sample the soil taken from the experiment area, organic matter is 0.97% (less), lime is 10.38% (medium-lime), phosphorus is low with 3.03 (kg da^{-1}), potassium is sufficient (Table 2). Analyses of variance were performed with the statistical program JMP. In the study, plant height, stem thickness, technical stem length, dry stem yield, fiber yield and seed yield values were determined.

Table 1. Climatic conditions during the growing season of hemp at Tokat in 2019*

Month	May	June	July	August	September	October	Mean	Total
Total rainfall (mm)	49.1	26.2	16.9	52.2	1.6	3.7	-	149.7
Minimum temperature (°C)	6.7	14.9	9.7	12.2	4.1	5.9	8.9	
Maximum temperature (°C)	34.8	33.5	38.7	38.0	30.9	31.3	34.5	
Mean temperature (°C)	19.1	23.1	21.9	22.4	19.0	17.4	20.4	

**Tokat Meteorology Directorate, (2019*)

Table 2. Physical and chemical properties of soil of the trial area*

Years	Soil depth (cm)	Total salt (%)	Lime (%)	Organic Matter (%)	Phosphorus P_2O_5 (kg/da)	Potassium K_2O (kg/da)	Structure	pH	EC
2019	0-30	0.02	15.38	0.97	3.03	50.11	Clayey	7.62	0.47

**The analyses were carried out in the soil analysis laboratory of the Directorate of Middle Black Sea Transition Zone Agricultural Research Institute*

Results and Discussion

The results of the variance analysis showed that plant height, stem thickness, technical stem length, dry stem yield, fiber yield and seed yield values were found to be significant at ($p \leq 0.01$ and 0.05) differences among hemp cultivars and populations. This indicated that there was a variation in varieties and populations (Table 3).

Plant height values ranged from 50.40 cm to 363.35 cm, with an average of 206.69 cm in hemp cultivars and populations. The average plant height was found as 118.80 cm in the varieties and 247.71 cm in the populations (Table 4). The highest plant height was found in population Narlısaray, while the lowest was in Finola varieties (Figure 1). Ceh (2018) reported that plant height was found to be 1.0-2.3 m in seed maturation period of USO 31 and 55-80 cm in the cultivar Finola. The highest were varieties of Carmagnola and KC Dora, which reached up to 3.4 m and 3.0 m, respectively. These results were similar to the data of our study. In a two-year study conducted in eight monoecious

cannabis varieties, the plant height average was 134-237 cm, the 1000 seed weight was 5.7-9.8 g, and the seed yield was 0.36-0.79 t / ha^{-1} (Baldini *et al*., 2018).

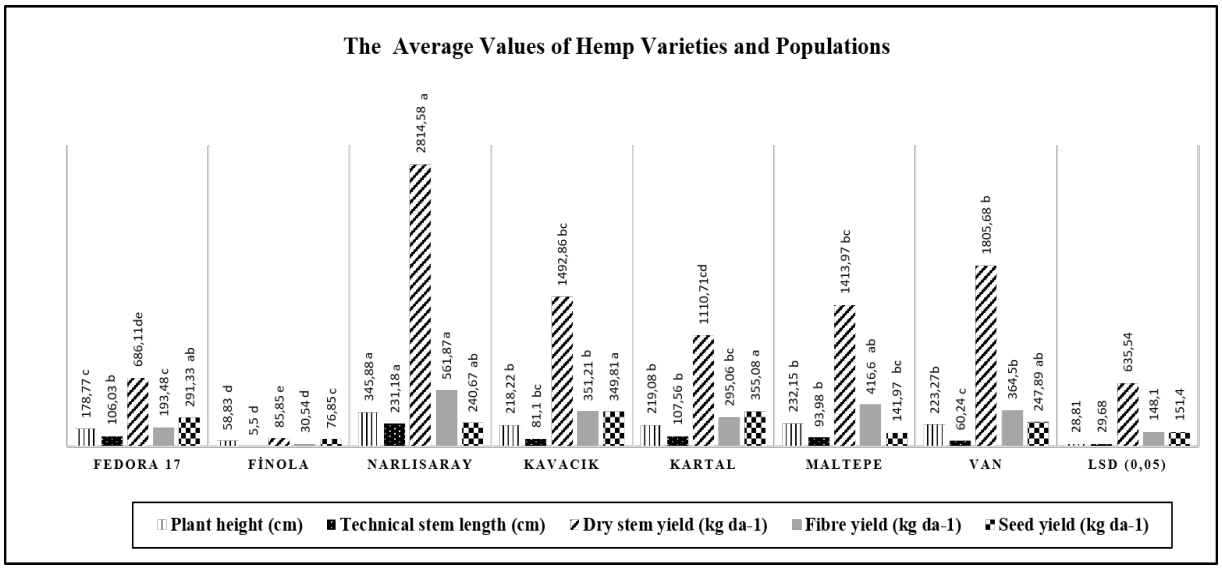

Figure 1. The average values of hemp varieties and populations

Table 3. Results of statistical analysis related to the mean squares and significance levels in hemp varieties and populations

Variation Sources	SD	Plant height (cm)	Stem thickness (mm)	Technical stem length (cm)	Dry stem yield (kg da^{-1})	Fiber yield (kg da^{-1})	Seed yield (kg da^{-1})
C. Total	20	6630.3	15.96	4414.1	764318.7	30364.8	14309.7
Var/Pop	6	21551.1**	50.20**	14088.7**	2236507.3**	85550**	32073.5*
Repeats	2	62.95	1.10	188.6	161627.5	5064.5	3062.5
Error	12	264.6	1.32	281.1	128673	6988.9	7302.2
CV(%)		7.71	9.53	17.11	26.68	26.43	35.11

Table 4. The mean values and groupings of hemp varieties and populations for each property

Varieties/ Populations	Plant height (cm)	Stem thickness (mm)	Technical stem length (cm)	Dry stem yield (kg da^{-1})	Fiber yield (kg da^{-1})	Seed yield (kg da^{-1})
			Means			
Fedora 17	178.77c	8.67c	106.03b	686.11de	193.48c	291.33ab
Finola	58.83d	4.41d	5.50d	85.85e	30.54d	76.85c
Narlısaray	345.88a	14.88a	231.18a	2814.58a	561.87a	240.67ab
Kavacık	218.22b	14.48a	81.10bc	1492.86bc	351.21b	349.81a
Kartal	219.08b	12.31b	107.56b	1110.71cd	295.06bc	355.08a
Maltepe	232.15b	13.97ab	93.98b	1413.97bc	416.60ab	141.97bc
Van	223.27b	15.66a	60.24c	1805.68b	364.50b	247.89ab
LSD (0.05)	28.81	2.01	29.68	635.54	148.10	151.40

In the study, stems thickness values ranged between 4.32-16.77 mm, and 14.25 mm on average. The average values of the populations were found higher than the varieties. Average stems thickness was found as 6.54 cm in the varieties and 11.80 mm cm in the populations (Table 4). The highest and the lowest stem thickness were found in population Van followed by Kavacık and variety Finola, respectively.

Technical stem length was found to range between 5.10 cm and 246.60 cm and the average was determined as 114.81 cm. The values of technical stem length in populations and varieties were determined as 96.02 and 55.76 cm, respectively. The highest technical stem length was found in population Narlısaray followed by Kartal, while the lowest was in Finola varieties (Figure 1).

Dry stem yield values ranged between 82.54 kg da^{-1} and 3143.75 kg da^{-1} with an average of 1727.56 kg da^{-1}. The stem yield in the varieties was found to vary between 82.54 kg da^{-1} and 718.75 kg da^{-1}. In populations ranged from 810.64 kg da^{-1} to 3143.75 kg da^{-1} (Table 4). The highest stem yield

was found in population Narlısaray followed by Van, while the lowest was in Finola varieties. Ceh (2018) determined the highest yield of Carmagnola as 18 t ha^{-1}, KC Dora as 14 t ha^{-1}, and Kompolti Hybrid TC as 11.5 t ha^{-1}. Flajman *et al*. (2016), identified the highest stem yield in Cannabis varieties (Fedora 17, Santhica 27, Futura 75, KC Dora, Finola, Kompolti hybrid TC and Monoica) as 3248 kg ha^{-1} (dry matter) and seed yield 1573 kg ha^{-1}. Kocjan Acko *et al*. (2002) reported that the effect of variety and seed amount on cannabis in hemp is important. Incekara (1971) determined the seed yield as 25-50 kg da^{-1} in fiber hemp and 80-100 kg da^{-1} in seed type hemp. Berrada *et al*. (2019) carried out to determine the adaptation and yield potentials of cannabis varieties, biomass yield of 13 cannabis varieties carried out in 2015 is between 4185-8283 lb/acre, stalk yield is 2577-5707 Ib/acre, seed yield is 240-1041 lb/acre, plant height is 44 -78 inch, handle thickness was determined as 5-9 mm.

Fiber yield ranged between 29.64 kg da^{-1} and 638.76 kg da-1, and 397.84 kg da^{-1} on average. Average fiber yield was found as 112.01 kg da^{-1} in the varieties and 306.89 kg da^{-1} in the populations. The highest fiber yield was found in population Narlısaray followed by Van, while the lowest was in Finola varieties (Figure 1).

Seed yield was determined between 72.98 kg da^{-1} and 474.87 kg da^{-1}, with an average of 267.08 kg da^{-1}. Average seed yield in populations and varieties was found to be 184.09 kg da^{-1} and 240.67 kg da^{-1} respectively. The highest seed yield was found in population Kavacık followed by Kartal, while the lowest was in Finola varieties. Deleuran and Flengmark (2005) reported that the total average dry matter yield of the cultivars Fedora, Fedrina, Felina, and Futura was approximately 13 t ha^{-1} and for Fasamo approximately 9 t ha^{-1}. The average fiber yields were 2.9 and 1.7 t ha^{-1}, respectively, the average seed yield over a period of 3 years was approximately 500 kg ha^{-1}.

Conclusion

In this study, were used two standard varieties and five local populations. The experiment was conducted in 2019. In this study were examined some yield characteristics of hemp varieties and populations and appropriate populations and varieties were determined according to some yield characteristics in Tokat ecological conditions. The research findings in this paper indicate that hemp has the potential to be grown in Tokat for both fiber and seeds. The performance of the populations was found to be higher than the varieties in all the characteristics studied. According to the average findings, the populations Narlısaray were identified as the best in a result of investigated all traits. Plant length, stem thickness, technical stem length, dry stem yield and fiber yield values of the Narlısaray population showed superior performance compared to others. The seed yield values of Kartal and Kavacık populations were higher. Therefore, they could be considered in cultivation and further breeding studies.

References

Anonymous, (2020) Fiber Plants, Ankara University Library and Documentation Department, Open Course Materials, Website: *https://acikders.ankara.edu.tr/*, 2020.

Baldini M, Ferfuia C, Piani B, Sepulcri A, Dorigo G, Zuliani F, Danuso F, Cattivello C, (2018) The Performance and Potentiality of Monoecious Hemp (*Cannabis sativa* L.) Cultivars as a Multipurpose Crop, Agronomy 2018, 8, 162; doi:10.3390/agronomy8090162.

Berrada AF, Berrada AY, McKay JK, Campbell B, (2019) Technical Report Colorado State University Agricultural Experiment Station Southwestern Colorado Research Center, 2014-2018.

Ceh B, (2018) Hemp in Slovenia, The Area Varieties and its Response to Some Agrotechnical Arrangements. *J. Int. Sc. Pub*., ISSN 1314-8591, **6**.

CRS, (2017) Hemp as an Agricultural Commodity, Congressional Research Service, *www.crs.gov*, March 10, 2017.

Deleuran LC, Flengmark PK, (2005) Yield Potential of Hemp (*Cannabis sativa* L.) Cultivars in Denmark, *J Indus. Hemp*, 10(2) Available online at *http://www.haworthpress.com/web/JIH, doi:10.1300/J237v10n02_03*.

EMCDDA, (2018) Medical use of cannabis and cannabinoids: Questions and answers for policymaking, Publications Office of the European Union, Luxembourg.

Flajsman M, Jakopic J, Kosmelj K, Kocjan Acko D, (2016) Morphological and technological characteristics of hemp (*Cannabis sativa* L.) varieties from field trials of Biotechnical faculty in 2016. *Hop Bulletin*, **23**, 88-104.

Gizlenci Ş, Acar M, Yiğen Ç, Aytaç S, (2019) Hemp Agriculture, Ministry of Agriculture and Forestry, General Directorate of Agricultural Research and Policies, Black Sea Agricultural Research Institute Directorate, Samsun, 2019.

Gurel, Akdemir H, Emiroglu SH, Kadoglu H, land, HB (2000) Turkey fiber crops, Cotton farming, overview, and other fiber crops Technology. Turkey Agricultural Engineering V. Technical Congress, 17-21 January, Ankara, 525- 566.

Incekara F, (1971) Industrial Plants and Breeding. Ege University Faculty of Agriculture Publications, No: 65.

Kocjan Acko D, Baricevic D, Rengeo D, Andresek S, (2002) Gospodarsko pomembne lastnosti petih sort konoplje (*Canabis sativa* L. var. sativa) iz poljskih poskusov Markišavcev pri Murski Soboti. In: Zbornik Biotehniške fakultete univerze v Ljubljani, Kmetijstvo, **79**(1), 237-252.

NASEM, (2017) The health effects of cannabis and cannabinoids: the current state of evidence and recommendations for research, National Academies Press for the National Academies of Sciences Engineering and Medicine, Washington, DC. The National Academies Press. *https://doi.org/10.17226/24625*.

ORAN, (2019) Hemp Breeding, Central Anatolian Development Agency, Kayseri.

Ozdemir O, (1993) Effect of nitrogen and plant frequency on the yield and some properties of cannabis. Ministry of Agriculture and Rural Affairs, Samsun Research Institute Directorate Publications. General Publication No: 78, Report Series No: 65. Samsun.

Ronde SM, (2013) Industrial Hemp in The Netherlands: The Effects of Changes in Policies and Subsidy Structure. A Thesis Presented to The Graduate School of the University of Florida in Partial Fulfilment of the Requirements for the Degree of Master of Scıence, University of Florida.

Warf B, (2014) High Points: An Historical Geography of Cannabis. *Geog. Review* **104**(4), 414–438.

J. Int. Environmental Application & Science, Vol. 15(2): 109-115 (2020)

Research Paper

Spread and Study of sp. *Castanea sativa* in the Albania

Ermal Lala, Mirela Lika (Çekani) *

Department of Biology, Faculty of Natural Sciences, University of Tirana, Bulevardi "Zogu I", Nr.25/1, 1001 Tirana, Albania

Received December 04, 2019; Accepted June 06, 2020

Abstract: Chestnut is one of the most remarkable trees in terms of greatness, hardness and endurance, as well as the most nutritious fruits in terms of nutritional value. It is not much known as industrial useful wood and therefore the use of this wood is scarce in the furniture and production of wood for construction. In patriarchal times, chestnuts have been used as wood for the production of beams in the construction of houses because it is distinguished for a high resistance to atmospheric and biological agents. Its fruits are used as nutrition not only delicious but also nourishing. Traditional culture has recognized chestnut as a tree of bread or as a means of exchange with other foods. Economic importance, even though it has been declining, chestnuts still occupy an important place in the agricultural economies of Albania, especially with the recent efforts of the Albanian government to turn the Albanian cultural identity as its representative, as in the highly urbanized foreign markets is especially demanding as a bio species. For livestock this species has emerged as valuable food for their fattening by farmers. Green dough and fruit are very nutritious and farmers use these for feeding small livestock as sheep of goat in the dry summer period and that of dense autumn rains. Green Fruit of Castanea sativa Mill carefully squeezed without damaging the embryo brought from the village of Gjoçaj with geographic coordinates 42°11'78"N 20°06'29". We have used cleavage methods, colloid methods, and biochemical protocols.

Keywords*: Chestnut, nutrition, Castanea sativa, colloid method.*

Introduction

Castanea Sativa Mill species has a total number of chromosomes 2n = 24 (Fedorov 1974). The origin of the European chestnut (Castanea sativa Mill), is from Asia Minor. Even today, many species of wild chestnuts are found on the southern coast of the Black Sea. Discovered fossils show the presence of European chestnut in the pre-glacial age, about 25 million years ago.

Chestnut foliage begins in late April, or beginning of May depending on altitude, terrain exposure and variety. Flowering begins in the first half and continues in the second half of June and at high altitude until the first decade of July.

Fruit ripening starts in late September and runs until October 25. There are varieties that mature even in early November. During flowering when the weather is hot and dry, it is difficult to pollinate the flowers. As a result, trees link fewer fruits, fewer cones, and the number of fruits per cones decreases since Alvisi (1979) has shown before. Intense rains and low temperatures at the time of flowering hinder flower pollination and consequently the shape of flowers. When the summer is humid, as occasional rains occasionally fall, the chestnut leaves fall prematurely. This usually occurs from the beginning of September as a result of being affected by *Mycosphaerella macuilflorum*. Chestnuts are very resistant to summer drought. Chestnut is very demanding on light, a characteristic that must necessarily be taken into consideration by its growers. It very hardly supports shading in the garden. This is agreement with results obtained from Brevigleri (1951).

Chestnut belongs to the Fagaceae family where oak trees are included. There are four main species known as European, Chinese, Japanese and American. Castanea sativa Mill or sweet chestnut as it is known in Europe is also known as Spanish chestnut or spanish chestnut which is the only species in America,

We mention some species: *C. almifolia. C. crenata* (Japanese Chestnut). *C. dentate* (American Chestnut). *C. henryyi. C. mollisima* (Chinese Chestnuts). *C. ozarkensis* or *C. chinkapin. C. pumila. C. seguini, etc*. since Rolando (2000) has shown before.

*Corresponding: E-Mail: mirela.lika@fshn.edu.al; Tel: +355 682055452; Fax: +355 42229590

Table 1. Scientific classification of *C. Sativa* Mill.

Type	Magnoliophyta
Class	Magnoliopsida
Order	Fagales
Family	Fagaceae
Genus	Castanea
Species	*Castanea sativa* Mill

Chestnut belongs to the genus Castanea, a genus of which 13 species of chestnut originate from the temperate zones of the boreal hemisphere. Chestnuts are widespread in the mountainous regions of the Caucasus, in the Southern Caspian Sea, in the Spanish Sub-Alpine Mountains, in France on the outskirts of Paris and particularly in the Normandy forests. It is found almost everywhere in Italy and Spain since Avolio (1985; 1987) and Baggio (1987) have shown before. In Central Europe, widespread in most favorable regions such as the Fohn valley (Switzerland), the Canton of Ticino, the Rhine area (Germany), especially in the Western Black Forest. Chestnuts are mainly found in Turkey, Syria, Algeria, Tunisia, Morocco, etc.

Materias and Methods

The Castanea Sativa Mill micro-pollination protocol comprises 4 stages:
• Start
• Breeding
• Rooting
• Plant acclimatization.
We will not dwell too much on the rooting and acclimatization phase because they are phases that are not needed for this paper.
When the initial explants are obtained from juvenile plants, the chestnut micro-pollination presents no problems. Conventionally obtained seeds should be grown in the greenhouse or preferably in a climatic chamber in order to lower the rate of explants contamination. This is agreement with results obtained from Zekaj (2013).
Green fruits of *Castanea sativa* Mill. carefully trimmed without damaging the embryo, brought from the village of Gjoçaj with geographical coordinates 42 ° 11'78 "N 20 ° 06'29" E.
We have used stereomicroscope, light microscope, Olympus microscope, digital camera, lama, lamella, toluidine blue, methylene blue, scotch, nail polish, distilled water, razors, scissors, cytometric ocular, cytometric lamina, hydrolytic enzymes, test methods, colloidal methods, working protocols etc. This is agreement with results obtained from Zekaj (2013).
Histological study techniques include: Macroscopic techniques; Stereomicroscope observation technique. Microscopic staining and colloidal techniques: Preparation of preparations for microscopic study This is agreement with results obtained from Zekaj (2013).
In conventional 40x light microscopy with colloidal technique such images of the mouths are obtained in the lower epidermis of the leaf (in situ). The pores are chaotic and often found on leaves.

Results and Discussion

The natural chestnut forests in Albania cover a total area of about 12 thousand hectares. In the Tropoja region (mainly in: Kolgecaj and Leke-Bibaj), they occupy the first place nationally with about 2,000 hectares. Chestnuts in the Tropoja area are distributed in several municipalities, as well as near "Bajram Curri" Municipality. Specifically, in the commune of Bujan there are about 600 ha of chestnut forests, about 500 ha in Mark-Gegaj, about 270 ha in Leke-Bibaj, about 15 ha in Pacite and about 100 ha in the Municipality of Bajram Curri since Elezi (1990) and Xhomara (2011) have shown before.

Their skin is polished as long as they are young (gray *C.sativa*). Over the years the skin becomes darker, thicker and deeper furrows become more visible. Wood, bark and leaves contain 6-14% tannin. The leaves are simple, oval or lance, obtuse and spaced at wide angles. Once the leaves appear, the chestnuts begin to bloom. The flowers are planted in flowers of both kinds, but always in the same

plant as the chestnuts are monoic plants. When roasted chestnut pollen emits a very strong aroma that causes the bee to be attracted for pollination and nectar intake, remember that chestnut honey is one of the most valuable and high quality honey.

Dried grains contain up to 14% sugar, 16-34% starch, 8% protein and 3% cellulose. Vitamin C is contained in 1500 mg / kg dry matter. Having cross pollination, lonely chestnuts over 300 m distance from companions will produce low yields and insects are the best pollinators especially bees and spring bulbs.

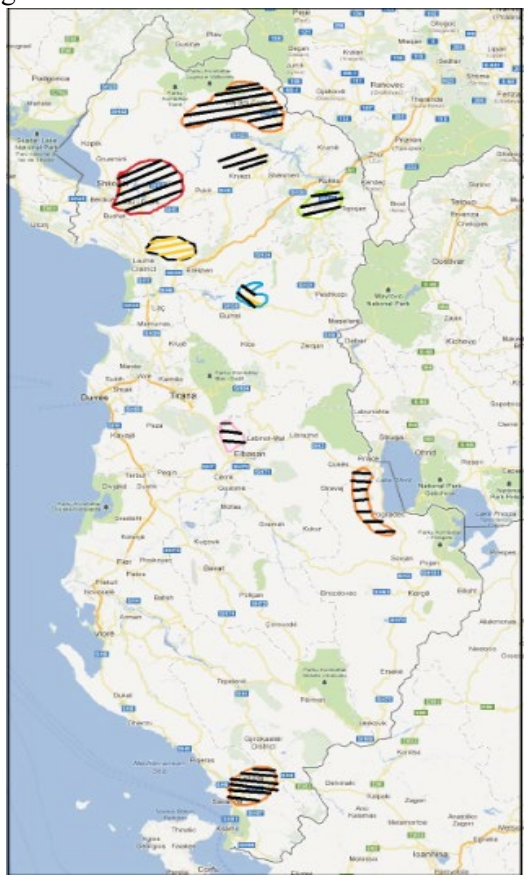

Figure 1. Map of distribution of *Castanea Sativa*

Figure 2. Chestnuts in flowering period (E. Lala)

Mill in Albania

Chestnuts are widespread in many countries around the world, and in Albania they meet in the form of forest massifs known as cashews or chestnuts. The largest massifs are found in Bajram Curri, Kolgecaj, Lekbibaj (Tropoja), Shimi (Kukes), Dukagjin, Mes, Shllak, Reç (Shkodra), Kashnjet (Lezha), Msuç, Gjoçaj, Macukull (Mat) Shupal (Tirana), Zrvaska (Pogradec), Gurakuq, Gracen and Shmil (Elbasan), Librazhd, Delvina, Saranda, Tepelena (Elezi 1990; Xhomara 2011).

Castanea sativa Mill has a monoic, deciduous trunk tree branching 2–3 m from the ground, with perennial bark and many wide and majestic cracks and crowns. The loops are singles. Leaves are long, apex with numerous and lustrous nerves.

The flowers are male and female in the same flower respectively at the top and bottom. Male flowers are 6-angled with 8-20 fringes, female flowers 5-8 teeth and 6-8 barrels. Ovary has 6-8 turns and 8-9 pillars. The fruits range from 1-3 grains depending on the successful egg bag pollination. What is worth noting is that chestnuts are treated more for fruit than for wood as chestnut wood is not very practical in the wood processing industry. Taste and nutritional values have been known since ancient times and many hill-and-mountain tribes have used chestnut as a food reserve in difficult times since Brevigleri (1951) has shown before.

Burrel chestnut tree has an altitude of 800-1100 m above sea level. Widespread in regions bordered by hills beaten by the wind and sun, it numbers over 3'500 individuals over 50, over 4'000 individuals over 25, and thousands of young mammals. The maximum trunk height reaches 25 m but the isolated chestnuts tend to extend the crown by remaining dwarf. Old chestnuts generally atrophy

the early top giving preference to lateral branch growth. The diameter of the trunk reaches up to 1.5-2m.

Figure 3. a) in its entirety; **b**) loops; **c**) chestnuts in winter; **d**) roots; **e**) fruits; **f**) leaves (E. Lala)

Figure 4. Male chestnut flowers

Figure 5. Female chestnut flowers

Figure 6. A chestnut bun with ripe fruit (E. Lala)

Chestnut begins to produce its leaves in early April as it finishes growing at the end of April and begins to bloom in early June yielding bloom shaped flower like 20-30 cm long sticks and hundreds of fringes, one single flower bud is able to give 5-12 parts. Characteristic of these parts is their very strong aroma that attracts bees due to the high amount of honey and pollen contained in parts but also being mono species, pollination by oats and winds is vital to chestnut. The parent flower has a fake part which usually serves as a pistil that cuts pollen grains and thus fertilizes the eggs in the ovary which will then give the next egg whilst the eggs will bear future fruit has Brevigleri (1951) has shown before.

Figure 7. Left: chestnut palm leaves; Right: flowering male flowers and some female flowers

At maturity the pupae turn yellow to light brown and begin to break through the wet cover after the September rains, and at the end of September the first drop of the first grains that are usually wormy or shrubby begins. The massive downturn begins on the first weekend of October, indicating that maturity has already taken place. Healthy squash on average contains 2-3 grains 1.2 cm high, 1

cm wide and 2-2.5 cm long and eggplant in glossy black. The grains weigh up to 10-13 grams and 1 kg = 75-100 grains has Zekaj (2013) has shown before.

The best time to collect the grains is the first 10-20 days of October because the maturity is already complete and a comprehensive action is needed before the leaf fall due to wintering makes it difficult to collect the grains through the leaves. The leaves in winter begin to fall when they have a "golden" yellow, at this point the chestnuts fall in winter and the first sign is the lymph circulating in the trunk.

Climate: Chestnut fits best in the continental climate of the Burrel area with minimum temperatures of 2 ° C-17 ° C and maximum average of 12 ° C-31 ° C. In sun-beaten hills, production is more abundant than in secluded and shady or sunny days.

Humidity: Average humidity ranges to 68% and amplitude humidity fluctuations are moderately extreme ranging from 60% in summer to 80% during winter months. Humidity plays a significant role in chestnut production because in its absence, grains are failing as in the case of 2012 which resulted in fatal low chestnut production. Also when the humidity is high and lasts for a period of time as in 2014, production will decline as it plays a role in the spread of pests, especially parasites and viruses, causing early death of embryos. A narrow amplitude steady humidity would be very efficient in productivity as it happened in 2013 where as a result of overproduction the price of the product in the market fell.

Soil: Chestnut prefers hilly, plain but drained soils. In deep and thick soils up to about 150-155 cm in the soil, the plants grow very well and produce fruit in satisfactory quality and quantity. Under these conditions, the surface of the land where the chestnuts are, occupies almost 100% of the area with chestnut plants. In such soils, trunk circumference, height, and productivity reach optimal limits, indicative of variations depending on species.

Generally chestnut augmentation is accomplished with seed-added material on which grafting is applied, or longer, the grafting season varies depending on the method of growth and the area in question. Speaking of hybridization, parent selection is required first; pollination is not difficult as being a mono-flowered plant separates the male flower from the parent.
Efforts have been made in Albania by many fruit and forestry scholars to describe chestnut cultivars, but there are no cultivars except ecotypes that come from cross pollination. In most cases, grafting has been used between different species and numerous species to rescue chestnut-related diseases.
The problem remains *Curculio elephas* (worm) which lays eggs in mature chestnuts since Elezi (1990) and Xhomara (2011) have shown before.

Table 2. Some general data on the geography of chestnut spreading in Albania

Districts	Area in acres	Altitude (m)
Dibër	172	400-900
Elbasan	168	400-855
Gjirokastër	199	750-1000
Korçë	151	800-1000
Krujë	147	480-816
Kukës	617	443-680
Lezhë	133	250-400
Librazhd	337	350-800
Mat	353	448-540
Mirditë	69	500-700
Pogradec	1728	800-1100
Pukë	185	500-790
Sarandë	220	700-1000
Shkodër	1604	250-505
Tiranë	318	350-800
Tropojë	1800	165-1100

Chestnut contains, although in small quantities, Vitamin A, Thiamine, Riboflavin, phosphorus, iron, sodium, potassium, etc. The calories contained in chestnuts are less than those of walnut and many other fruits of this group, they contain no cholesterol, they are low in fat and these are unsaturated (oily) fats, and have no gluten. The carbohydrate content is comparable to that of wheat and rice, with twice as many starches as potato. Contains about 8% of different sugars mainly sucrose, glucose, fructose etc. As long as the chestnut is immature, it has high water content that gradually disappears with its ripening, guaranteeing storage and at the same time hydrolyzing the starch into fructose and glucose. The other important feature is that the chestnut fruit contains all the non-synthesized or essential amino acids.

We do not get much data from the stereomicroscope. Mostly we observe the construction of the leaf nerves (in situ). Below are two pictures from the in situ leaf stereomicroscope:

Figure 8. View of the nerves of the lower epidermis. (Photo by E. Lala)

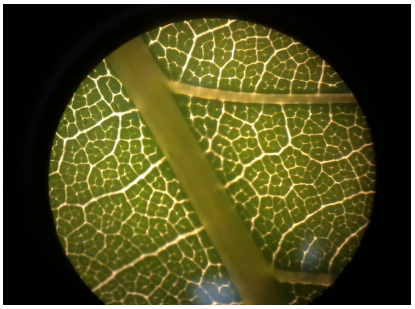

Figure 9. View of the nerves of the upper epidermis (Photo E. Lala)

In frequent observations and examinations looking for differences between in vitro and in situ environments, it was observed whether or not the presence of organs such as mouths, trichomes, parenchymal cells, woods, crystals, etc. were present or not there in two individuals of sp. *Castanea sativa* whether in vitro cultures or in-situ adult individuals.

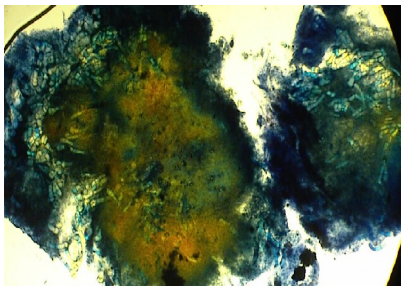

Figure 10. Callus colored with methylene blue where trichomes are clearly visible (photo E. Lala)

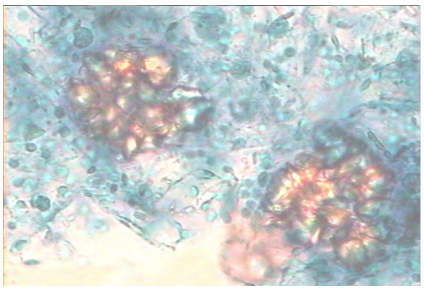

Figure 11. A view of the woods and crystalloids in the structure of the callus is also seen in the glandular and no trichomes (Zh. Zekaj)

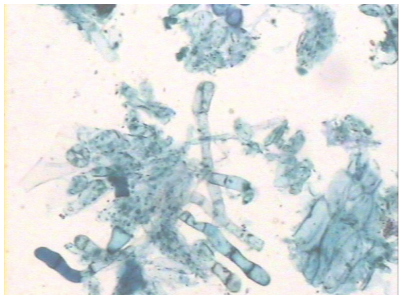

Figure 12. Callus of the bud treated with hydrolytic enzymes. The percussion bundles and peltate glandular trichomes appear

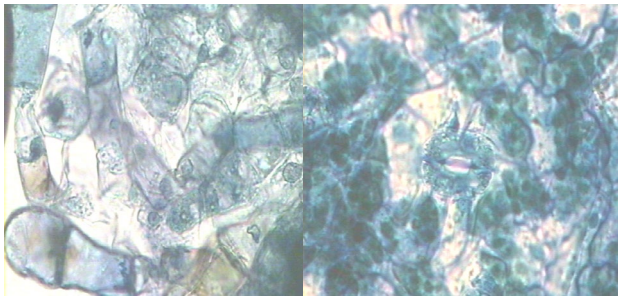

Figure 13. The first photo shows trichomes as cellular macrostructures, while the second photo shows a typical area of trichomes where the mouth is surrounded by chloroplasts dark blue with methylene blue. (Zh. Zekaj).

If we compare the statistical data of in vivo pores (5 leaves analyzed) and in vitro pores (one leaf analyzed due to limited material) we realize that the number of pores / microscopic field changes drastically, in ratio 2.5 with 1, that is, for each in vivo domain we have 2.5 times more pores than in vitro domain. This results from increased metabolism, aeration and transpiration of the substrate (which the plant needs to prepare itself in-vivo through complex photosynthetic processes) and moisture compared to the in-vitro plant that is in a transition state between heterotrophy and autotrophy since Zekaj (2013) has shown before.

The length and width of the mouths (pores) between the same species but in different environments (in vitro cultures and in-vivo natural environment) almost does not change except that in in vitro cultures the mouth (pores) appears to be assembled as a bean while being elongated elliptical in vivo leaves.

The stomatal index is roughly the same and oscillates at 35-50% and despite the fact that the oral / microscopic ratio is lower in the in vitro leaf, the epidermal cell count is also low and this is due to the size of the these in vitro epidermal cells that manifest with intense cell division and differentiation that is higher than in iv-in vivo cells.

Conclusions

Chestnut (*Castanea sativa* Mill) is a species of Sup-Mediterranean Atlantic. The area of its propagation is similar to the Bung (*Q. sessilflora*).

Chestnuts are widespread in many countries around the world, and in Albania they meet in the form of forest massifs known as cashews or chestnuts. The largest massifs are found throughout Albania.

What is worth noting is that chestnuts are treated more for fruit than for wood as chestnut wood is not very practical in the wood processing industry. Taste and nutritional values have been known since ancient times and many hill-and-mountain tribes have used chestnut as a food reserve in difficult times. The cultivation of cultivars requires a very strict selection method and these cultivars to be preserved and fixed by cloning (also applying in vitro methods and vegetative growth or grafting). Later on, after the establishment of the cultivars, their choice would depend on the climate, the terrain and the exposure to sun-struck areas.

References

Alvisi. F (1979) Sittuazione economico-comerciale del castango in Italia. *Agricoltura Bologna*, p.35-39.

Avolio. S. (1985) La castanicoltura in Calabria, p.61-68.

Avolio. S. (1987). Il castagno nell Italia meridionale, *p.114-120*.

Baggio. L (1987) Il castagno nel Lazio, *p.59-67*.

Brevigleri. N (1951) Ricerche sull biollogia fiorale e di frutificazione della castanea sativa e della *C.crenata,* p.234-241.

Elezi. C. (1990) Masivet me gështenja si pasuri e madhe kombëtare, p 12-16.

Rolando. V (2000*)* Arboricultura generale e speciale. *Edagricolo,* p.98-105.

Zekaj Zh. (2013) Leksionet e histoteknologjisë, FSHN, p. 132-151.

Xhomara. I. (2011) Gështenja, druri i bukës dhe i historisë, p. 5-28.

J. Int. Environmental Application & Science, Vol. 15(2): 116-121 (2020)

Research Paper

Soil Water Regime Spatial Heterogeneity Under Alfalfa Growing in The Forest-Steppe Zone of Ukraine

Inna S. Vlasenko*, Marina M. Ladyka, Vladimir M. Starodubtsev

Department of General Ecology and Life Safety, National University of Life and Environmental Sciences of Ukraine, Heroiv Oborony st., 13, Kyiv, 03041, Ukraine

Received April 28, 2020; Accepted June 02, 2020

Abstract. The article considers the issue of spatial heterogeneity of the soil water regime in agricultural fields in the forest-steppe zone of Ukraine. The studies were conducted under the conditions of growing perennial herbs, directly alfalfa varieties "Sinyukha". The redistribution of moisture over the microrelief elements in spring during snowmelt and the flooding of microdepressions with thawed water was shown, the duration of which was 10-15 days in the years of observation. The moisture reserves in the 0-100 cm layer amounted to 108-126% on the slopes compared to control, and increased on the bottoms (after filtration and evaporation of melt water) -to 137-148%. The harvest of green mass of alfalfa at the bottom was completely absent, and on their slopes it was 116-93% compared to control, depending on weather conditions. In the work, field and laboratory research methods and a system of UAV-ERS methods, as well as determination of vegetation indices, were used.

Keywords: *Soil, Spatial heterogeneity, Micro-depression, Water regime, Photosynthesis, Drones, alfalfa,*

Introduction

The phenomenon of mosaic soil cover is inherent in the Left Bank and Right Bank of Ukraine, with each region having its own characteristics depending on the historically established lithological processes of the territory. A common feature of the relief of playland territories is the presence of numerous micro-lowlands (micro-depressions). Their origin in the Right-Bank Forest-Steppe is most often associated with suffusion processes**.**

Investigations of the spatial heterogeneity of typical chernozem productivity on the right-bank Forest-Steppe because of the soils water regime features on flat plains with pronounced microrelief were carried out by us in 2008-2017, mainly under cereal crops, especially under winter wheat (Starodubtsev & Bogdanets, 2015; Starodubtsev *et al*., 2013; Starodubtsev *et al*., 2016; Starodubtsev & Bogdanets 2015; Starodubtsev *et al*., 2009; Starodubtsev *et al*., 2015; Starodubtsev 2017; Starodubtsev *et al*., 2018; Vlasenko & Starodubtsev 2020). The results of these studies showed that the redistribution of moisture of atmospheric precipitation over the soil surface during snowmelt in spring and, to a lesser extent, heavy rainfall in summer significantly affects the state and productivity of wheat, especially in years with a lot of snow and frozen soil before snowmelt. A detailed account of the winter wheat crop in 2017 on different morphological elements of microdepressions showed that crop losses at the bottom of microdepressions with a depth of up to 50-100 cm were 65-70%, and on the slopes of the depressions - 20-30% (Starodubtsev & Bogdanets, 2015; Starodubtsev *et al*., 2013; Starodubtsev *et al*., 2016; Starodubtsev & Bogdanets, 2015) On the whole, in the studied fields of the NULES of Ukraine at research farm in the Kiev region, the loss of winter wheat yields due to the peculiarities of the water regime of the soils of different elements of the microrelief amounted to approximately 15-25%.

Such significant crop losses made it relevant to assess the effect of the water regime of microdepressions on other crops, in particular on alfalfa, cultivated on the same field for several years and having a different resistance to flooding and over moistening of soils.

Objects and Methods

The basis of study is preliminary soil research work of Prof. V.M. Starodubtsev, which took place since 2008 in the Right-Bank Forest-Steppe soil province on typical chernozem. During 2016-2019, detailed studies are conducted on a field of 32.5 hectares, and review studies - on production fields of 400 hectares. Soil sections and drills up to 200 cm are dug on the plain, as well as on the bottom and

*Corresponding: E-Mail: innav_s@ukr.net; Tel: +380671390441; Fax: 280-57-05

slopes of microdepressions with various depths. For the first time in our studies, the heterogeneity of the soil cover is considered as an essential property which affects the soil cover water regime. The studies covered 3 crops: winter wheat of the «Merlena» cultivar (in the vegetation period 2016-2017), spring barley of the «Britney» cultivar (2018) and alfalfa of the «Sinyukha» cultivar (2017-2019).

Sowing alfalfa of the «Sinyukha» variety was completed in September 2017 with good soil moisture in October (Figure 1), therefore, good plant sprouts were obtained. Observations of the crops development were carried out systematically using Sentinel-2 satellite images, and soil moisture in the flat areas and in microdepressions was determined seasonally by soil sampling to a depth of 100 cm. The green mass of alfalfa was determined by mowing plots 1x1 m in 4 replicates at different relief elements, taking into account the timing of mowing plants on all field. It is important to note that the observation period was characterized by significant changes in weather conditions (Figure 1). Observation of the vegetation state under conditions of the soil spatial heterogeneity was carried out on key micro-depressions C-1 and C-5.

Results and Discussion

The structure of the soil covers at studied field of the research farm «Velikosnitinske» (Figure 1) indicates the dominance of meadow chernozem soils (26.69%) and typical chernozem (24.88%), and only 20,97% occupy titular modal chernozem shown on the standard soil map of this farm. As for the basic characteristics of the soils water regime of this field, in micro-depressions up to 1 m deep and in a large meso-depression in the southeastern part of the field with the same depth, the water regime is flushing, in which leaching of carbonates and other soil products to a depth of 4-5 m or more, that is, to a depth of groundwater, take place.

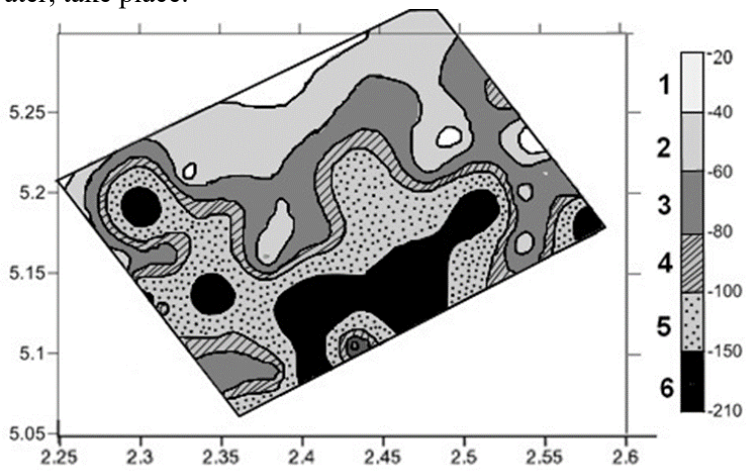

Figure 1. Part of the experimental field soil map: 1 – chernozem typical with high carbonate horizon - (20-40 cm); 2 – chernozem typical (modal or reference) - (40-60 cm); 3 – chernozem typical with more deep carbonate horizon - (60-80 cm); 4 – leached chernozem - (80-100 cm); 5 – meadow-chernozem soil - (100-200 cm); 6 – meadow-chernozem and chernozem-meadow soils on noncarbonate loess - (deeper than 200), **(**Starodubtsev & Bogdanets 2015)

In microdepressions with a depth of approximately 0.5 m, the water regime of the soils is periodic-leaching, carbonates are washed out of the soil profile to a depth of 1-2 m, sometimes even deeper. And only in micro-depressions of less than 0.3 m and in nano-depressions, that created by tillage, the water regime is unwashed out, except for wet years, when it becomes periodically flushing (Starodubtsev *et al*., 2013)

Depending on the weather characteristics of the transitional winter-spring period, the entire depressions in agro-industrial fields is filled with water, or waterlogged (depending on their depth), creating a network of cells with specific agroecological conditions. Visually, such areas are in the form of concentric circles, much darker in color compared to the background control areas. That is why the water regime is considered as the main process in studying soil cover heterogeneity, studies of its dynamics were carried out seasonally during the research period. The pictures clearly show the difference in the state of the experimental field in different wetting years (2018, 2019). The results of

the precipitation and temperature data analysis during the growing season made it possible to record periods of lack of moisture and temperature peaks and alfalfa productivity.

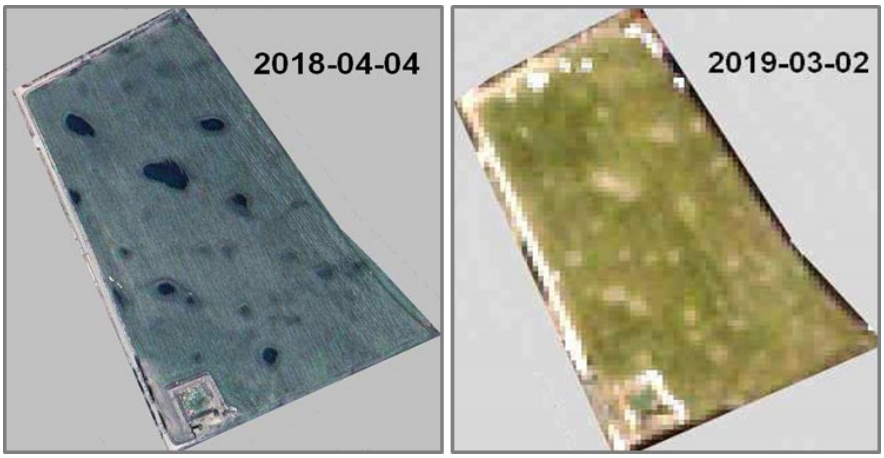

Figure 2. Flooding of microdepressions with alfalfa in the spring of 2018 (left) and the absence of flooding in spring 2019 (right) in Sentinel-2 satellite images.

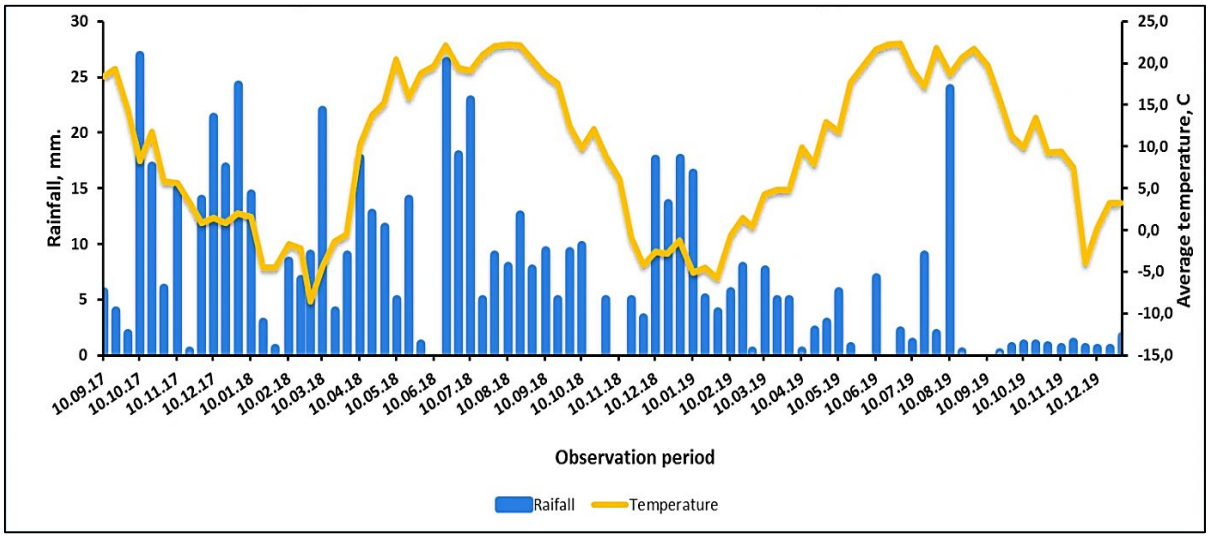

Figure 3. Weather conditions for the growing period of alfalfa in 2017-2019

In 2018 the spring began in early April, that is, a month later than in the previous year, and was characterized by rapid increase in temperature and fast snow melting. The flooding of microdepressions with alfalfa was observed within 10-15 days, which is well shown in the Sentinel-2 satellite image (Figure 2).

Assessment of moisture reserves in the soil layer 0-100 cm 3 weeks after the beginning of snow melting and, accordingly 1 week after evaporation from the surface of the water and absorption into the soil, showed that there was a significant redistribution of moisture among the morphological elements of depressions (Figure 3).

At the bottom of pothole (microdepression), the moisture reserves were about 3600 m^3 / ha, on the slopes they were 1000 m^3 / ha less, and on the plain - 1200 m^3 / ha less. At the same time, alfalfa plants at the microdepression bottom died, and on the slopes and on the plain they developed satisfactorily. During hot and dry May and June, the moisture reserves on the plain sharply decreased (by almost 1000 m^3 / ha), and on the slopes and lowering bottom - by 600-700 m^3 / ha. Under these conditions, alfalfa plants developed better on the slopes of the depressions than on the control, and weeds began to appear at the bottom. As a result, by the second harvest of alfalfa for green fodder, there was no harvest at the bottom of the depression, on the slopes the freshly cut green mass averaged 115 metric centner / ha, and in the control 99 metric centner / ha. Only the July rains (Figure 3) improved the state of vegetation.

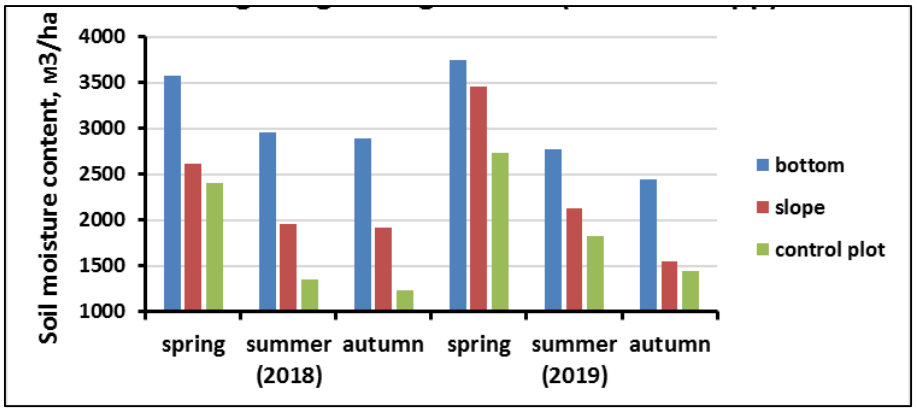

Figure 4. Dynamics of moisture reserves in the soil of the bottom, slope of the pothole (microdepressions) and on the plain (control) in 2018-2019.

The water regime of the soils of the experimental field changed significantly in 2019. After a warm winter, snowmelt began in early March with unfrozen soil and a gradual increase in temperature. Moisture on the plain and slopes was absorbed into the soil, and at the bottom of the depressions, snow accumulated over the 2019 winter still remained (Figure 2).

Figure 5. Physiological state of plants within the C-1 pothole, 19.06.2018 (from left to right, T1- bottom, T2 - slope, T3 - plain)

As a result, although there was no flooding of depressions, the moisture reserves in all morphological elements were large (Figure 4, 2019), which contributed to the good development of alfalfa. However, at the bottom of the depressions, alfalfa was completely replaced by weeds.

The condition of the vegetation cover is as follows: the bottom is alfalfa (cover 5-7%), the rest are weeds, the slope is cover 100%, height 55-60 cm; the plain - coating - 95%, height - up to 45 cm. During this period, the temperature regime was at the level of 21 ºC, and the amount of precipitation was approximately 25 mm. Already the first mowing of alfalfa amounted to approximately equal amounts on the plain and on the slopes of the lowering (42-45 t / ha of freshly cut green mass), and the weeds dominated in the lowering (Figure 5).

To illustrate the seasonal dynamics of alfalfa development in 2019, we present the traditional indicator of the vegetation index (NDVI) according to https://eos.com (Figure 6) and the results of the statistical processing of the results of its determination taking into account 4 cuttings of green mass during the growing season.

NDVI values for plants range from 0 to 1. In the middle of the season, the NDVI index can be used to determine how plants develop on the field. If the index values are medium and high (0.5-0.85), then, most likely, the agroecological state is within normal limits. If the index is low - it seems that something is missing from the plot, for example, moisture or nutrients.

Figure 6. Alfalfa vegetation index dynamics, 2019

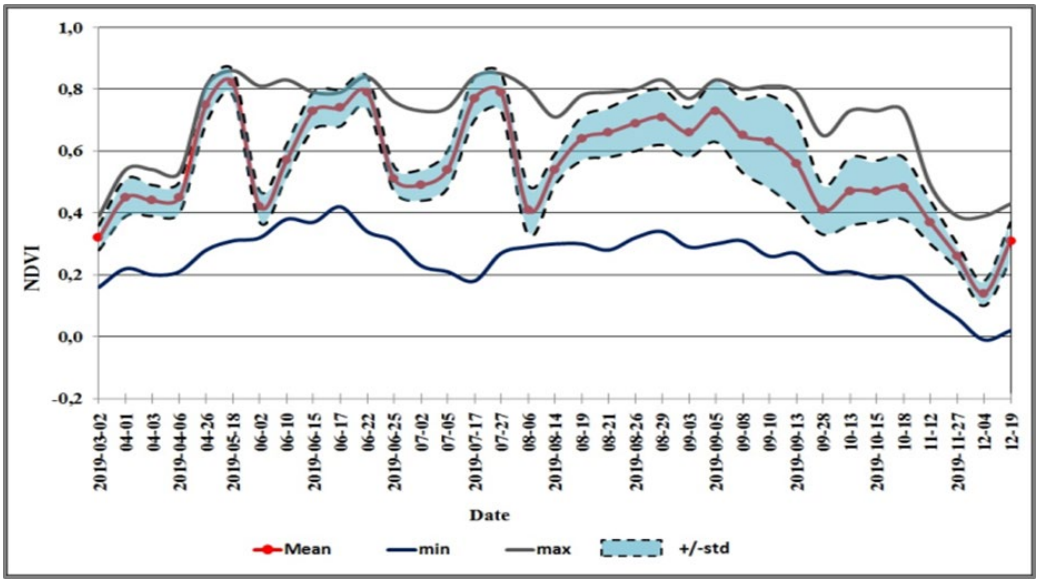

Figure 7. Annual dynamics of the vegetation index, taking into account 4 mowing of alfalfa (statistical analysis)

According to the NDVI index, recommendations are being formed for the differential application of nitrogen fertilizers. Based on the results of statistical processing (Figure 7), it is possible to identify

zones of high, medium and low vegetation for calculating the rate of fertilizers. Presumably, if the vegetation index in the plot is high, then the dose of fertilizers should be reduced by 10-30% of the average norm, if average, then increase - maximum by 20-25% of the average norm, if low, then first of all through field studies it is necessary to determine the cause of the poor state of the plants.

Conclusion

The results of the study indicate a high degree of heterogeneity of the soil cover of the Right-Bank Forest-Steppe and a peculiar water regime of soils on flat areas, in micro-depressions and even in nano-depressions. Based on our previous studies (Starodubtsev 2017; Starodubtsev *et al*., 2018; Vlasenko & Starodubtsev 2020) and the information provided in this article, we believe that spatial heterogeneity of the soil cover is an integral characteristic of its formation and functioning in the plain Forest-Steppe of Right-Bank Ukraine.

It is important to take into account the heterogeneity of the soil cover and the water regime of soils when conducting long-term (stationary) scientific research and when introducing precision farming systems. A two-year period of studying the features of the water regime and soil productivity during alfalfa cultivation showed that a significant redistribution of soil moisture occurs along the relief elements in the fields with microdepression. In spring, the moisture reserves in the meter-long layer on the bottom are 137-148% compared with the control, and on the slopes it is 108-126%, and the fluctuations in the values depend on the weather conditions of the year.

The yield of alfalfa green mass changes less significantly and ranges from 116 to 93% compared with the control. Spring flooding with thawed snow for more than 10 days leads to the complete death of alfalfa plants on the bottoms and its replacement by weed vegetation. That is, alfalfa, according to our two-year observations, is less resistant to flooding with thawed snow compared to winter wheat (Vlasenko & Starodubtsev, 2020)

References.

Starodubtsev VM, Ladyka MM, Chernyavska GK, (2013) Flooded soils of forest-steppe micro-depressions, their features and agroecological role. In.: IV All-Ukrainian Congress of Ecologists with International Participation (Ecology-2013). Collection of scientific articles. Vinnytsia: VNTU. pp: 420-422

Starodubtsev VM, Aniskevich KV, Urban BV, (2015) On estimation of soil cover spatial heterogeneity in plains of forest-steppe zone. *S World J. Agric.* **J21509**(9), 60-69. *http://sworld.com.ua/e-journal/j21509.pdf*

Starodubtsev VM, Aniskevich LV, Vlasenko I, (2016) Features of soil cover and water regime of soils on the plains of the Right Bank Forest-steppe. In: XV International conference "Development of science in the 20th century" (15.07.2016.). Part 1. Kharkiv, SIC "Znanie", pp. 152-156.

Starodubtsev VM, Basarab RM, Komarchuk DS, Vlasenko IS, (2018) Heterogeneity of typical chernozem productivity in Ukraine. In.: 10th International Soil Science Congress on "Environment and Soil Resources Conservation", Kazakhstan, pp. 332

Starodubtsev VM, Bogdanets VA, (2015). New vision for mapping and estimation of soil cover heterogeneity in plain Forest-Steppe zone. *S World J. Agric.* **J11509(7)**, 30-36 http://www.sworldjournal.com/e-journal/j11509.pdf.

Starodubtsev VM, Bogdanets VA. (2015) A new look at mapping and assessment of the heterogeneity of the soil cover of the plain forest-steppe. *Collection of scientific papers SWorld*, Issue №1 (38), p.89-94

Starodubtsev VM, Yatsenko SV, Pavlyuk SD, (2009) Influence of water regime of microfluidic forest-steppe on heterogeneity of soil cover and its use. In.: II All-Ukrainian Congress of Ecologists, Vinnytsya, Danylyuk, pp. 176-179.

The Practical Blog. Single Post. Field Day Recap: Profitability of Farming Prairie Potholes. (2017). *http://www.practicalfarmers.org/blog/2017/10/18/field-day-recap-profitability-farming-prairie-potholes-aug-31*/. Visited on 01.04.2018.

Vlasenko I.S., Starodubtsev V.M. (2020). Soil cover spatial heterogeneity in agricultural fields of Forest-Steppe zone. *Int. J. Ecosy. & Ecol. Sci. (IJEES).* **10**, 2. *https://doi.org/10.31407/ijees10.2*

J. Int. Environmental Application & Science, Vol. 15(2): 122-126 (2020)

Research Paper

Spectroscopic Investigation of *Syzygium aromaticum* L. Oil by Water Distillation Extraction

Krenaida Taraj[1,*], Adelaida Andoni [1], Fatos Ylli[2], Ariana Ylli[3], Riza Hoxha[1], Jonilda Llupa[4], Ilirjan Malollari[5]

[1]University of Tirana, Department of Chemistry, Faculty of Natural Sciences, University of Tirana, Blv. Zog I, 1001, Tirana, Albania; [2]Institute of Applied Nuclear Physics, P.O. Box 85, University of Tirana, Tirana, Albania [3]University of Tirana, Department of Biotechnology, Faculty of Natural Sciences, University of Tirana, Blv. Zog I, 1001, Tirana, Albania; [4]Laboratory of Food Chemistry, Department of Chemistry, University of Ioannina, Greece; [5]University of Tirana, Department of Chemical Engineering, Faculty of Natural Sciences, University of Tirana, Blv. Zog I, 1001, Tirana, Albania

Received March 23, 2020; Accepted May 04, 2020

Abstract: Water distillation is commonly used for obtaining essential oils from aromatic herbs. In the present work Clevenger apparatus is applied to obtain essential oil from *Syzygium aromaticum* L. Clevenger extraction represents an environmentally method for oil herb extraction as it employs water as solvent during the distillation process. Essential oils are highly valued. They are traditionally used in medicines and health remedies. The purpose of the present work is to obtain essential oil from clove plant and subsequently identify the chemical composition by means of spectroscopic techniques. Essential oil samples were analysed by spectroscopic techniques FTIR spectroscopy and UV-Vis. spectrophotometer. Both techniques indicated presence of eugenol as main chemical component in the oil of clove in excellent agreement with reported literature data.

Keywords: *water distillation, clove flowers; essential oil; oil extract; FTIR; UV-Vis.*

Introduction

Hydro-distillation is commonly used for the extraction of essential oils from plants. It is reported that hydro-distillation can be categorized into steam distillation and water distillation (Dilworth *et al*., 2017). In addition, hydro-distillation can be a combination of water and steam distillation (Dilworth *et al*., 2017). Hydro-distillation is one of the most preferred methods as it represents an eco-friendly process (Taraj *et al.*, 2019a). In addition, its application has a low cost.

The distinction between steam distillation and water distillation is that in steam distillation, steam extracts essential oils at temperatures to approx. 100°C, whereas in water distillation the plant is plunged into water and subsequently boiled (Dilworth *et al*., 2017). Oil extracts are composed of aromatic constituents and they are traditionally used in medicines and health remedies.

In the current work, *Syzygium aromaticum* L. is used to attain essential oil by use of Clevenger apparatus and by employing water as extracting solvent. The aim is to isolate the oil and next to identify the chemical composition by means of spectroscopic techniques. In this work, eugenol is found to be the main chemical constituent in clove oil. Eugenol is a common odour in many dental practices. Additionally, for comparison reason Soxhlet extraction using hexane as solvent was carried out as well.

It is reported that eugenol quantity in clove oil is up to 90% (Yadava and Saini 1994, Li 2001, Guan *et al*., 2007, Rana *et al*., 2011, Mohammed *et al*., 2016). Additionally, spectroscopic techniques such as FTIR spectroscopy and UV-Vis. spectrophotometer were used for the characterization of essential oil samples. FTIR and UV-Vis. analyses are well reported in the literature (Schulz *et al*., 2005; Schulz & Baranska 2007; Andoni *et al*., 2015; Ciko *et al*., 2016a; Ciko *et al*., 2016b; Gakis 2016; Soto-Barajas *et al*., 2018; Taraj *et al*., 2013; Taraj *et al*., 2017; Taraj *et al*., 2018a; Taraj *et al*., 2018b; Taraj *et al*., 2019a; Taraj *et al*., 2019b). Infrared spectroscopy (FTIR) is well-known as a fast and accurate investigative technique (Soto-Barajas *et al*., 2018). It is reported that FTIR can be successfully used for the qualitative differences between samples (Andoni, 2009; Andoni *et al*., 2009; Andoni, 2014; Andoni *et al*., 2015; Andoni *et al*., 2018; Rodrıguez *et al*., 2018; Soto-Barajas *et al*., 2018; Taraj *et al.*, 2019a). Additionally, FTIR and UV-Vis. spectra of clove oil samples indicated

*Corresponding: E-Mail: krenaida.taraj@fshn.edu.al; Tel: 0035542221737; Fax: 0035542221737

presence of eugenol as main chemical component in good agreement with reported data (Yadava & Saini, 1994; Mohammed *et al*., 2016).

Materials and Methods

Sampling and extraction methodology

The origin of *Syzygium aromaticum* L. used in this work is from local Albanian herb. The hydro-distillation extraction was carried out, in a round bottom flask, using Clevenger equipment. The amount of *Syzygium aromaticum* L. used for hydro-distillation was 15 g. The water-herb mixture underwent distillation process for 4 hours (Taraj *et al.*, 2019a; European Pharmacopoeia,1983).

As noted in the introduction section, for comparison reason, Soxhlet extraction was carried out as well. The amount of *Syzygium aromaticum* L. used for Soxhlet distillation was 10 g. Additionally, the Soxhlet extraction was allowed to run for 4 hours by using hexane as solvent. The oils were dissolved in hexane and further used for FTIR and UV-Vis analyses.

FTIR spectra were acquired by Nicolet 6700 spectrometer, manufactured by Thermo Electron. FTIR spectra were recorded by using KBr plates. Additionally, the interval of measurements was in the range mid Infra-Red (4000-400 cm^{-1}). OMNIC software was used for additional analyses. UV-Vis spectra measurements were recorded by 6800 UV-VIS Jenway spectrophotometer.

Results and Discussion

Table 1 displays summarized results for Clevenger and Soxhlet extractions. These values are in good agreement with reported results by Ciko *et al*. (2016a), Taraj *et al*. (2019a) and Taraj *et al*., (2019b) for the relevant extraction methods.

Figure 1 represents UV-Vis. spectra of *Syzygium aromaticum* L. essential oil attained by Clevenger extraction. Additionally, in the insert the chemical structure of the main chemical compound i.e. eugenol is displayed (Yadava & Saini, 1994; Mohammed *et al*., 2016). The oil yield was 1.2% for 15 g herb used for the extraction.

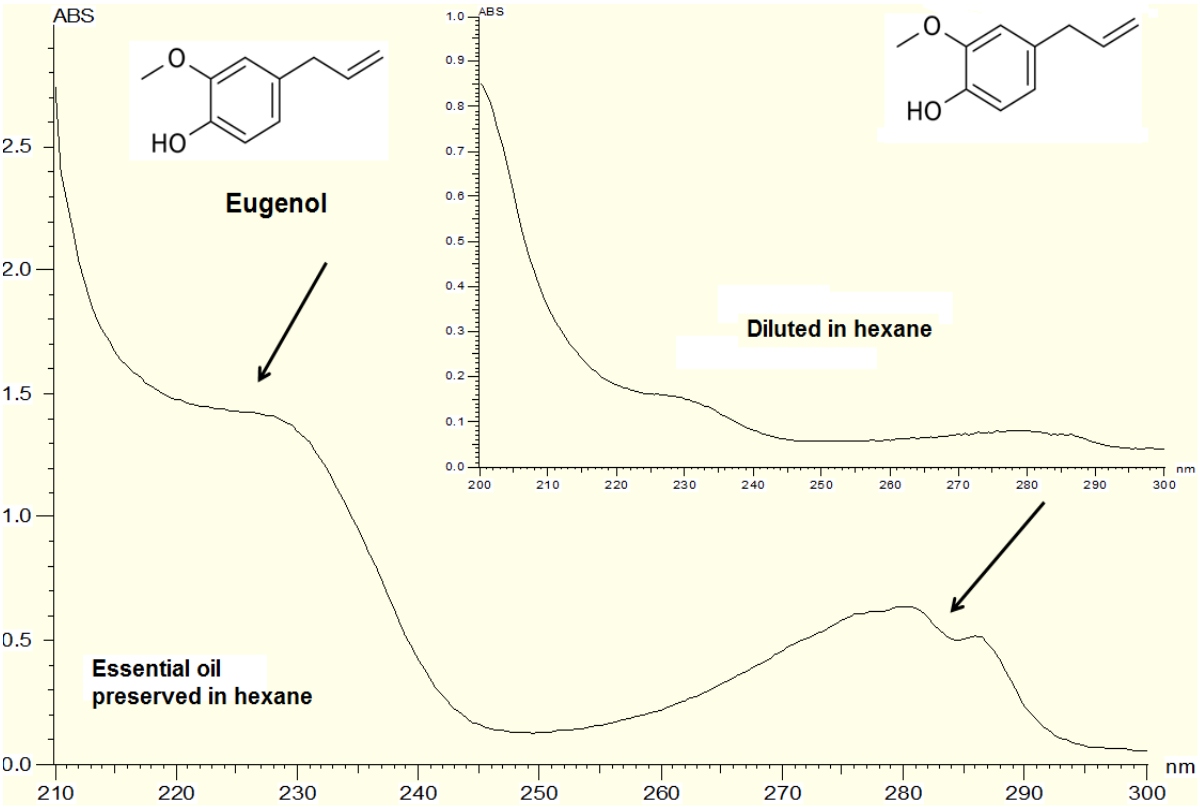

Figure 1. UV-Vis. spectra of *Syzygium aromaticum* L. essential oil obtained by Clevenger extraction.

Table 1: Tabulated results for the extractions of *Syzygium aromaticum* L.

Amount of *Syzygium aromaticum* L.	Extraction solvent	Extraction time	Extraction method	Yield of extract
15 g	Water	4 h	Clevenger	1.2%
10 g	Hexane	4 h	Soxhlet	12.5%

The UV-Vis. spectrum displays two absorption bands at 225-230 nm and at 270-290 nm. The absorption at 225-230 nm arises from the electronic transition of *n-π type of alcohol functional group -OH that links to the eugenol aromatic ring (Mohammed *et al*., 2016). Absorption band at 270-290 nm regards the electronic shift of *n-π type for C-O group that binds with eugenol aromatic ring (Mohammed *et al*., 2016).

Figure 2a displays FTIR spectrum for the extract of *Syzygium aromaticum* L. herb by Soxhlet extraction. Characteristic FTIR signals appear at 1637 cm^{-1}, 1606 cm^{-1} and 1513 cm^{-1}. It is reported (Yadava and Saini 1994, Smith 1999, Mohammed *et al*., 2016) that C-C vibrations of aromatic rings appear at 1630 cm^{-1}, 1604 cm^{-1} and 1508 cm^{-1}. Therefore, the wavenumbers at 1637 cm^{-1}, 1606 cm^{-1} and 1513 cm^{-1} belong to C-C aromatic rings vibrations of eugenol and eugenol acetate. In addition, C=C double bonds give rise to FTIR bands at 1640-1630 cm^{-1} (Smith, 1999).

The band at 1765 cm^{-1} is attributed to the ester group C-O or aromatic ketone group C=O which can be combined with more than one ring (Yadava & Saini 1994, Smith 1999, Mohammed *et al*., 2016). The peak at 1765 cm^{-1} is assigned to eugenol acetate presence. In addition, the intense FTIR bands in the interval 1300-1000 cm^{-1} belong to the C-O vibrations of ether and alcohol functional group of eugenol and eugenol acetate (Yadava & Saini 1994, Smith 1999, Mohammed *et al*., 2016). Other moderate bands appear at 794 cm^{-1} and 995 cm^{-1}. They belong to the groups CH_2 and C-H bonding vibrations, alkene monosubstituted, respectively (Yadava & Saini, 1994; Smith, 1999; Mohammed *et al*., 2016). Lastly, Figure 2b displays a Photo of *Syzygium aromaticum* L. oil extract. The oil appeared yellow in colour. Due to eugenol presence, the extract had a pleasant and spicy, clove like fragrance. The yield for the Soxhlet extraction was 12.5% for 10 g herb used.

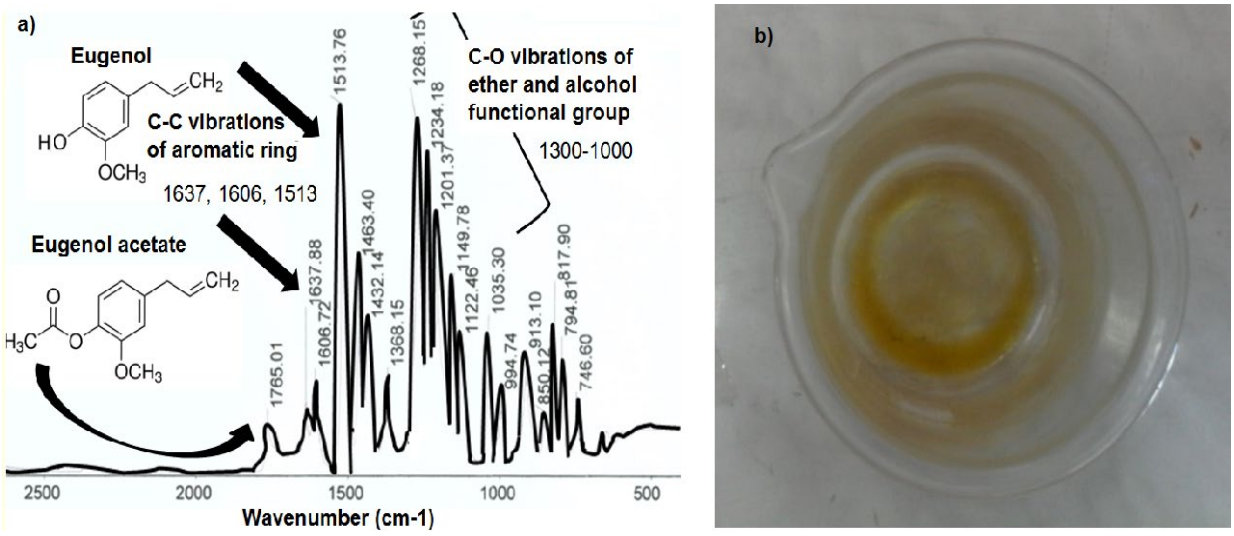

Figure 2: a) FTIR spectrum of *Syzygium aromaticum* L. extract obtained by Soxhlet apparatus. The main chemical compounds of *Syzygium aromaticum* L. oil extract i.e. eugenol and eugenol acetate are indicated in the inserts. b) Photo of *Syzygium aromaticum* L. oil extract.

Table 2 summarizes the most important FTIR bands (wavenumbers) identified in the essential oil and oil extract of *Syzygium aromaticum* L. compared with relevant data in the literature. It is evident that the obtained data are in good agreement with previous publications reporting IR spectra analyses of essential oil and oil extract from *Syzygium aromaticum* L. (Yadava & Saini 1994; Mohammed *et al*., 2016).

Table 2. FTIR and UV-Vis. assignments for the most characteristics bands of the oil extract compound for *Syzygium aromaticum* L.

Compound	FTIR (cm^{-1})	Assignments	UV-Vis. (nm)	Assignments
Eugenol	~1637, 1606, 1513 (this work), ~1650 (Yadava and Saini)	C-C of aromatic ring	~225-230 (this work), ~224 (Mohammed et al)	-OH
Eugenol acetate	~1637, 1606, 1513 (this work) 1650 (Yadava and Saini)	C-C of aromatic ring	~270-290 (this work), ~268 (Mohammed et al)	C-O
Eugenol	~1300-1000 (this work) 1070 (Mohammed *et al*)	C-O alcohol and ether		
Eugenol acetate	~1300-1000 this work)	C-O ether		
Eugenol acetate	~1765 (this work), ~1730 (Mohammed *et al*)	C=O ketone		

Conclusions

In this paper, distillation process was employed to attain essential oils from *Syzygium aromaticum* L. herb. Hydro-distillation was carried out by employing Clevenger apparatus. In addition to hydro-distillation extraction, Soxhlet extraction was utilized as well. FTIR spectroscopy and UV-Vis spectrophotometer were used as rapid techniques to analyze the extracts of *Syzygium aromaticum* L. Spectral analyses indicated presence of two chemical constituents i.e. eugenol and eugenol acetate in the oil extracts of *Syzygium aromaticum* L. This result was in good agreement with other relevant studies. The distinctive bands in the UV-Vis. spectrum were ~225-230 nm and ~270-290 nm, whereas the characteristic bands in the FTIR spectrum were in the intervals ~1637-1513 cm^{-1}, ~1300-1000 cm^{-1} and 1765 cm^{-1}.

References

Andoni AA, (2009) *Flat model approach to Ziegler-Natta olefin polymerization catalysts*. Eindhoven, Ph.D. Thesis. Technische Universiteit Eindhoven (Eindhoven University of Technology). The Netherlands. Ch. **7.** https://doi:10.6100/IR638773

Andoni A, Chadwick JC, Niemantsverdriet JW, Thüne PC, (2009) Investigation of Planar Ziegler-Natta Model Catalysts Using Attenuated Total Reflection Infrared Spectroscopy. *Catal. Lett*. **130**, 278-285. https://doi10.1007/s10562-009-0002-3

Andoni, A. (2014) High resolution electron energy loss spectroscopy for studying planar model catalyst: A test of NO on Rh (100). *Rev Roum Chim* **59** (3-4), 245-249.

Andoni A, Salihila J, Ylli F, Osmëni A, Taraj K, Çomo A, (2015) Extraction of essential oil from Albanian chamomile plant by water distillation method and its characterization by FTIR spectroscopy. *Int. J. Ecosys. Ecol. Sci* **5/3**, 321-324.

Ciko L, Andoni A, Ylli F, Plaku E, Taraj KA, (2016a) Study on Oil Extraction from Albanian Chamomile and Characterization by IR Spectroscopy. *J. Int. Environ. Appl. Sci*. **11** (2), 154-158.

Ciko L, Andoni A, Ylli F, Plaku E, Taraj KA, Çomo A, (2016b) Extraction of Essential Oil from Albanian *Salvia officinalis* L. and Its Characterization by FTIR Spectroscopy: a Soxhlet Method Extraction. *Asian J. Chem*. **28(6)**, 1401-1402. http://dx.doi.org/10.14233/ajchem.2016.19658

Andoni A, Delilaj E, Ylli F, Taraj K, Korpa A, Xhaxhiu K, Çomo A, (2018) FTIR spectroscopic investigation of alkali-activated fly ash: A test study. Zastita Materijala **59** (4), 539-542. doi:10.5937/zasmat1804539A

Dilworth LL, Riley CK, Stennett DK, (2017) *Pharmacognosy in Fundamentals, Applications and Strategies explores a basic understanding of the anatomy and physiology of plants and animals, their constituents and metabolites.* Chapter **5** - Plant Constituents: Carbohydrates, Oils, Resins, Balsams, and Plant Hormones. pp 61-80. Edited by S Badal, R Delgoda. https://doi.org/10.1016/C2014-0-01794-7

European Pharmacopoeia (1983) Part 1. Maisonneuve SA, Sainte Ruffine, p. **V**.4.5.8.

Gakis MIG, (2016) Comparative Study of the Chemical Components of plant species in the genus Sideritis L. (*S. scardica*, *S. perfoliata*, *S. raeseri*), M.Sc. Thesis, Department of Food and Human Diets, Group of Study and Natural Products Evaluation, Agricultural Univer. of Athens, Greece. http://hdl.handle.net/10329/6492 Last accessed 7 June 2018.

Guan W, Li S., Yan, R., Tang S, Quan C, (2007) Comparison of essential oils of clove buds extracted with supercritical carbon dioxide and other three traditional extraction methods. *Food Chem*., **101** (4), 1558–1564.

Lee, K-G. (2001) Antioxidant property of aroma extract isolated from clove buds [*Syzygium aromaticum* (L.) Merr. et Perry]. *Food Chemistry*, **74** (4) 443–448.

Mohammed KAK, Abdulkadhim HM, Noori SI, (2016) Chemical Composition and Anti-bacterial Effects of Clove *(Syzygium aromaticum)* Flowers. Int. J. Curr. *Microbiol. App. Sci* **5** (2), 483-489 doi: http://dx.doi.org/10.20546/ijcmas.2016.502.054

Rana IS, Rana AS, Rajak RC, (2011) Evaluation of antifungal activity in essential oil of the *Syzygium aromaticum (L.)* by extraction, purification and analysis of its main component eugenol. *Brazilian J. Microbiol.* **42**, 1269-1277.

Schulz H, Özkan G, Baranska M, Krüger H, Özcan M, (2005) Characterisation of essential oil plants from Turkey by IR and Raman spectroscopy. *Vib. Spectr*. **39**, 249–256. doi:10.1016/j.vibspec.2005.04.009

Schulz H, Baranska M, (2007) Identification and quantification of valuable plant substances by IR and Raman spectroscopy. *Vib Spectr* **43**(1), 13-25. https://doi.org/10.1016/j.vibspec.2006.06.001

Smith, B. Infrared Spectral Interpretation, A systematic approach, CRC Press (1999).

Soto-Barajas MC, Zabalgogeazcoa I, González-Martin I, Vázquez-de-Aldana BR, (2018) Near-infrared spectroscopy allows detection and species identification of *Epichlow* endophytes in *Lolium perenne.* J. Sci. Food Agric. **98** (13), 5037-5044. DOI: 10.1002/jsfa.9038

Taraj K, Delibashi A, Andoni A, Lazo P, Kokalari (Teli) E, Lame A, Xhaxhiu K, Çomo A, (2013) Extraction of Chamomile Essential Oil by Subcritical CO_2 and Its Analysis by UV-VIS Spectrophotometer. *Asian J Chem* **25** (13), 7361-7364. http://dx.doi.org/10.14233/ ajchem.2013.14642

Taraj K, Malollari I, Andoni A, Ciko L, Lazo P, Ylli F, Osmeni A, Çomo A, (2017) Eco-extraction of Albanian Chamomile Essential Oils by Liquid CO_2 at Different Temperatures and Characterisation by FTIR Spectroscopy. *J. Environ. Prot. Ecol*. **18 (1)**, 117-124.

Taraj K, Malollari I, Llupa J, Ylli A, Ylli F, Andoni A, Ciko L, (2018a) Water distillation extraction of Albanian *Sideritis raeseri* herb and characterisation by FTIR spectroscopy. "*5th Int. Conference on Small and Decentralized Water and Wastewater Treatment Plants*", August 26-29, 2018, pp. 468-472, E-proceedings ISBN 978-960-243-710-0, Thessaloniki, Greece.

Taraj K, Malollari I, Ylli F, Maliqati R, Andoni A, Llupa J, (2018b) Spectroscopic study on chemical composition of essential oil and crude extract from Albanian Pinus halepensis Mill. *J. Agric. Inform.,* **9**(1), 41-46. doi: 10.17700/jai.2018.9.1.440

Taraj K, Malollari I, Ciko L, Llupa J, Ylli A, Ylli F, Andoni A, (2019a) Water Distillation Extraction of Essential Oil from Sideritis Raeseri Herb, *Environ. Process.,* **6**(4), 1051–1058.

Taraj K, Ciko L, Malollari I, Andoni A, Ylli F, Ylli A, Plaku E, Llupa J, Borshi X, (2019b) Eco-extraction of essential oil from Albanian Hypericum perforatum L. and characterisation by spectroscopy techniques. *J. Environ. Prot. Ecol.,* **20** (1), 188-195.

Yadava RN, Saini VK, (1994) UV and IR Spectral Studies of Essential Oil of *A. indica*, *M. hortensis* and *E. triplinerve* Leaves. *Asian J. Chem*. **6(1)**, 77-80.

J. Int. Environmental Application & Science, Vol. 15(2): 127-134 (2020)

Research Paper

Assessing the Environmental Costs of Port Emissions: The Case of Trabzon Port

Aydın Tokuşlu*

Turkish Naval Forces, 06420 Ankara, Turkey,

Received April 03, 2020; Accepted May 15, 2020

Abstract: In this study, the exhaust gas emissions generated from ships in the Trabzon port were assessed as 906 t y^{-1} for NO_X, 409 t y^{-1} for SO_X, 52.160 t y^{-1} for CO_2, 54 t y^{-1} for PM, 38 t y^{-1} for VOC based on ship activity-based method. General cargo and tanker vessels are accountable for the 87% exhaust gas emissions in the port, and container, bulk carrier, other vessels such as tugs, service boats follow it. Ship-borne air emissions are emitted at cruising mode (81%), followed by port mode (18%). Port emissions in the Trabzon port may have negative effects on the health of a minimum of 33.922 people living 1 km from the port area including other emissions (domestic heating, road traffic, and industry). The environmental cost of the port emissions for each pollutant has been estimated as $32 million and $47.039 per ship call. All kinds of emission sources in the harbour area should be detected and measures to decrease the emissions should be executed in this context. This is the first study to estimate the Trabzon port emissions in the Black Sea region.

Keywords: *Trabzon, environmental pollution, port, emissions, environmental costs*

Introduction

Marine ports are important economic activity centres where countries carry out their import and export activities. Although seaports are often associated with industrial commercial activities, they are usually situated in or near settlements, schools, etc. The reason for this is to benefit from the labour force of the region and to make an economic contribution to the region. Due to the proximity of the ports to residential areas, people living in that area face health risks due to the air pollution created by the ports. The most important source of port emissions is shipping. Hundreds of trucks, tractors, locomotives, load handling machines, etc. working in the port area are among the other sources of air pollution in the port area (NRDC, 2004). The diseases caused by air pollution are mainly respiratory and cardiovascular, asthma, bronchitis, premature death, and lung cancer. Many epidemiological studies have discovered that diesel exhaust gas emissions increase cancer risks, and they are responsible for 70% of the cancer risk from air pollution (CARB, 1998; Mauderly, 1992; Ulfvarson et al., 1991). Emissions from ships' diesel engines that may adversely affect human health include sulphur oxides (SOx), nitrogen oxides (NOx), and particulate matter (PM). Port related emissions have been investigated by many studies such as Alver *et al*. (2018), Goldsworthy and Goldsworthy (2015), Deniz and Kilic (2009), López-Aparicio *et al*. (2015); Popa and Florin (2014); Yang *et al*. (2007), Lonati *et al*. (2010), Saracoglu et al. (2013), Song (2014), Bayirhan *et al*. (2019), Mersin *et al*. (2019), and Tokuslu (2020) and concluded that emissions from shipping cause illness and they affect the quality of life of people living close to the port area.

Trabzon, in terms of air pollution, is one of the most polluted cities in Turkey (Türk & Kavraz, 2011). Previous studies such as Türk *et al*., (2008; 2011), Tezel *et al*. (2019), Yomralioglu *et al*. (2009), Topbaş *et al*. (2004), Uzunali (2004) and Çuhadaroğlu and Demirci (1997; 2000) have almost exclusively focused on the relationships between air pollution and meteorological factors, and emission-related health problems in the Trabzon region. Türk *et al*. (2008; 2011) investigated the effects of air pollution on human health in the city of Trabzon between 2005 and 2007, and they found that due to the use of low-quality coal for heating in residential areas, air pollution occurred at a high level in the winter period in Trabzon and had a serious effect on human health with the increase in the number of air pollution-related diseases. A traffic emission inventory was developed by Tezel et al. (2019) and the relationship between NOx and noise pollution from road traffic was measured in Trabzon. The results of the study indicated that percentages of the population exposed to traffic-related NOx and noise levels above the regulatory limits were 10% and 21%, respectively. Yomralioglu *et al*. (2009) examined 1.150

*Corresponding: E-Mail: aydintokuslu78@gmail.com; Tel: +90 506 6905844; Fax: +90 212 3980126

cancer cases in Trabzon province. Cancer density map was produced by using GIS, and correlations between cancer types and geographical factors were analysed. They found that breast cancer cases commonly occurred in residential areas that are generally situated on the coast and along valleys and within the low elevation class. Çuhadaroğlu and Demirci (1997) investigated the relationship between outdoor air quality and meteorological factors, such as wind speed, relative humidity ratio and temperature using the code SPSS. According to the results, for some months there was a moderate and weak level of relation between the SO_2 level and the meteorological factors in Trabzon city. Another study was performed by Çuhadaroğlu and Demirci (2000) and they explored the relationship between air pollution and wind speeds of different directions using the code SPSS. They found that there was a weak level of relation between air pollution concentrations and wind speeds in urban Trabzon.

No prior studies have examined port emissions in the port Trabzon. Port emissions are also one of the main pollutant sources of the city of Trabzon and should be considered in this context. To fill this gap, the main aim of this investigation is to calculate the ship-borne air emissions and assess the environmental costs of port emissions. This study will help to create a port emission inventory of the Trabzon port. This study focuses on only port emissions generated from ships and doesn`t engage with other city emissions (residential heating, road traffic, and industry).

Material and Method

Study Area

Trabzon port is located at the centre of the city of Trabzon and situated on the historical silk road on the route of Iran, Iraq, Russia, and Turkey (Figure 1). The port is one of Turkey's most important and busy port and surrounded by the cities of Rize, Giresun, Gumushane, and Bayburt on the eastern side of the Black Sea region. The Trabzon Port has been built to be able to berth all kinds of ships and serves 2.000 ships per year. Its capacity is 250.000 passengers, 2.000.000 tons of bulk dry cargo, 1.830.000 tons of general cargo, and 10,000 vehicles with 175.000 TEU containers. Trabzon Port has an open area that allows 2.500.000 tons of cargo to be stored annually and closed warehouses where 500.000 tons of cargo are stored annually. There is a 306.000 m^2 bonded area in the port. The port is operated by Trabzon Port Operations as of 2003 (Atliaş, 2019). The harbour has 9 docks that deliver loading and unloading activities between the vessels and the shore with a total length of 1.525 meters.

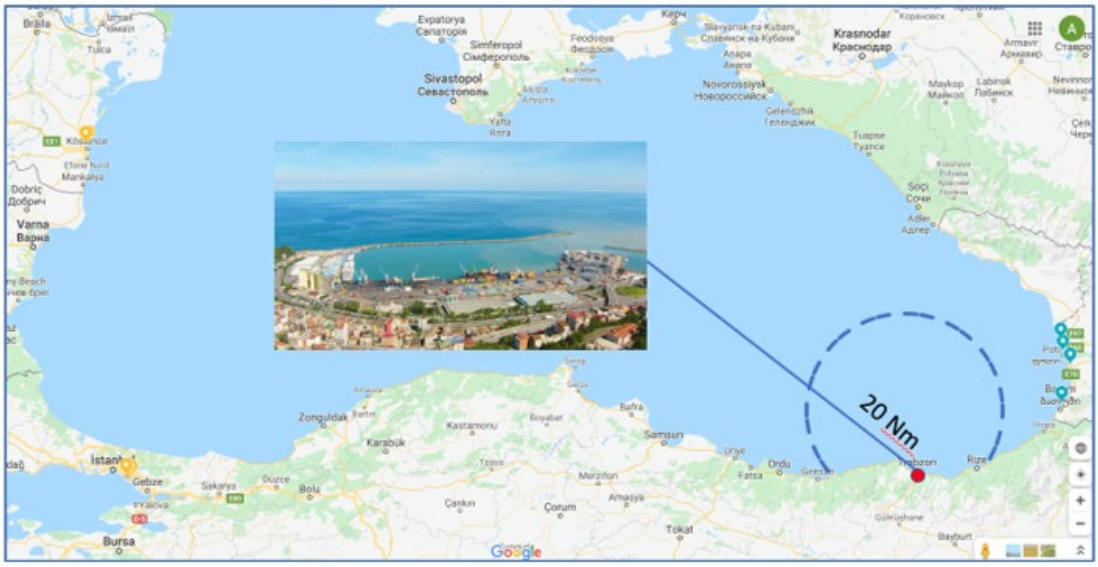

Figure 1. The Trabzon Port (Atliaş, 2019)

Calculation Method

In this research, the up-down approach was used to calculate the port emissions in the Trabzon port based on data. For calculation, Entec UK Limited methodology was preferred which is commonly used in literature for ship-borne emission assessments. The ship estimation equation (1) is stated as;

$$E_{cruising} = D * [[ME * ME\ LF\ ]+ [AE * AE\ LF\ ]\ ]* EF_{cruising}\ / V) \quad \text{(Equation 1)}$$
$$E_{manoeuvring} = T * [[\ ME * ME\ LF\ ]+ [AE * AE\ LF\ ]\ ]*\ EF_{manoeuvring}$$
$$E_{port} = T * AE * AE\ LF * EF_{port}$$

D is the ship navigating distance, ME is the power of the main engine, ME LF is the main engine load factor, AE is the power of the auxiliary engine, AE LF is the auxiliary engine load factor, EF is the emission factors according to operational modes (cruising, manoeuvring, port), V is the vessel speed and T is the times of manoeuvring and port activities.

The data in this research contains the type of vessel, tonnage, speed, operation times and these data were achieved from the port authority. Total navigating distance from the Trabzon port is 20 nm. Times during manoeuvring and port modes were calculated in hours (Entec, 2005). The average time for manoeuvring for all types of visiting vessels is 1 hour and port times of every vessel's calls were 38 hours for a tanker, 14 hours for the container, 52 hours for general cargo, bulk carrier and 27 hours for other vessels (research, ro-ro cargo, passenger, *etc*.) respectively. Table 1 presents the emission factors for each operational mode (Entec, 2002; 2005; 2007).

Table 1. Emission Factors According to the Type of Ships

Ship Types	**NOx**			**SOx**			**CO_2**			**VOC**			**PM**		
	C	M	P	C	M	P	C	M	P	C	M	P	C	M	P
Liquefied Gas	8	8.9	8.8	12.4	12.5	6.9	816	818	795	0.31	0.67	0.6	1.03	1.55	1.2
Chemical	14.6	11.9	11.6	11	12.2	5.7	650	715	698	0.55	1.04	1	1.34	1.6	1.2
Tanker	13.3	11.2	11	11.7	12.7	7.8	690	745	730	0.5	1.1	1.1	1.43	1.82	1.5
Bulk Carrier	15.9	12.6	11.5	10.6	11.9	1.6	627	698	690	0.59	1.3	0.5	1.61	1.84	0.5
General Cargo	14.5	11.9	11.4	10.9	12.1	1.2	649	715	691	0.54	1.03	0.5	1.28	1.59	0.4
Container	15.5	12.3	11.4	10.8	12	1.4	635	705	690	0.57	1.19	0.5	1.56	1.73	0.5
Ro-Ro Cargo	13.7	11.5	11.3	11.1	12.2	1.3	655	719	692	0.52	1.06	0.5	1.17	1.68	0.5
Passenger	11.9	10.6	11.2	11.8	12.6	1.5	697	747	696	0.46	0.97	0.5	0.81	1.71	0.5

C: Cruising, M: Manoeuvring, P: Port

Vessel speeds by vessel types are shown in Table 2 (Entec, 2005). The main engine load factors were %80 for the cruise, %20 for manoeuvring, %20 for port and auxiliary engine load factors were %30 for the cruise, %40 for manoeuvring, %50 for the port (EMEP/EEA, 2016a; EMEP/EEA, 2016b).

Table 2. Vessel Speeds

Type of Vessels	**Speed (knots)**
Liquefied Gas	16.90
Chemical	13.70
Tanker	14.00
Bulk Carrier	14.30
General Cargo	12.30
Container	19.30
Ro-Ro Cargo	15.40
Passenger	20.80
Fishing Vessels	13.90
Tug	12.90

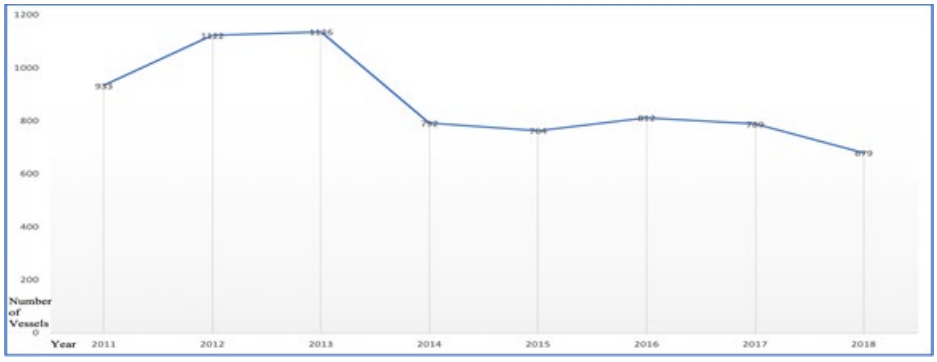

Figure 2. Ship Activities in the Trabzon Port (TDGCS, 2019)

The vessel activities in the port between 2011 and 2018 are illustrated in Figure 2 (TDGCS, 2019). In 2013, 1136 vessels visited the port and on average 878 vessels were hosted in the port during years. Generally, four types of vessels visit the port such as general cargo (70%), tanker (21%), bulk carrier (6%), container (1%), and other ships (2%) yearly (Figure 3).

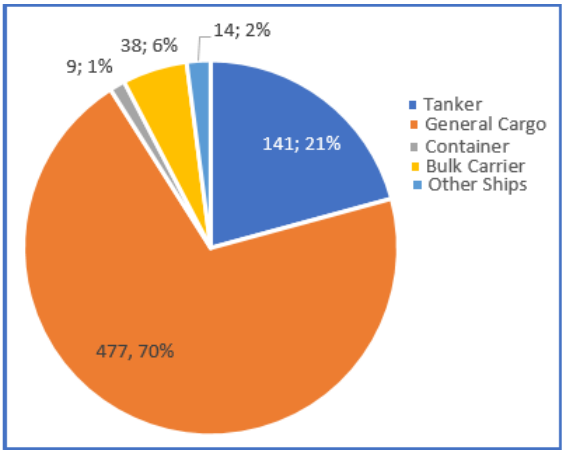

Figure 3. Types of Vessels Visiting the Trabzon Port

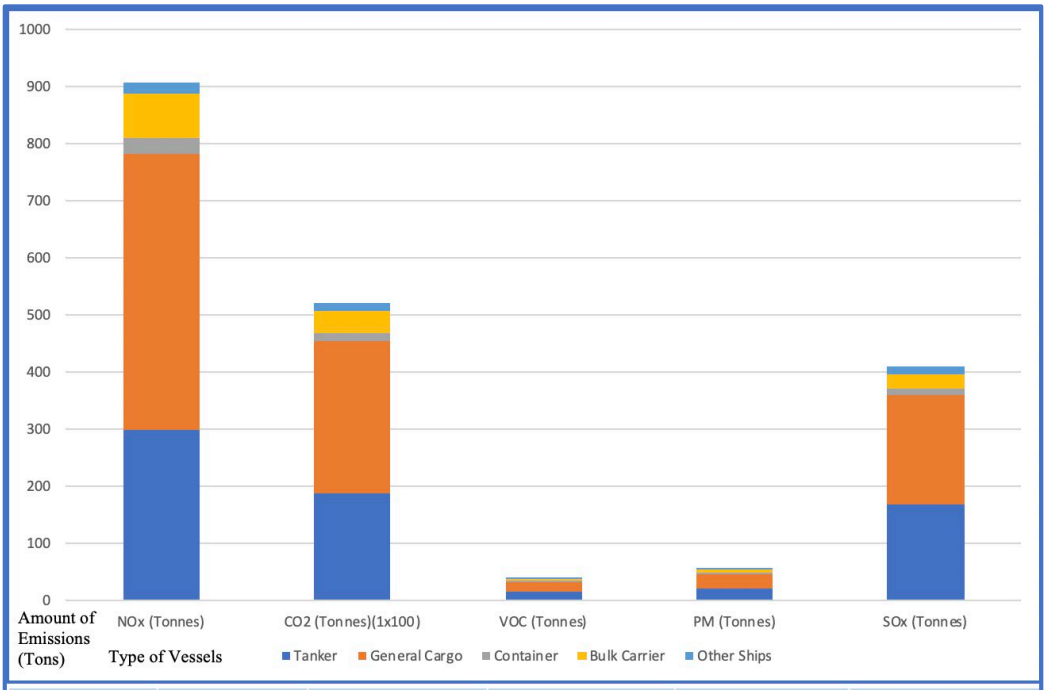

Type of Vessels	NOx (Tonnes)	CO2 (Tonnes)(1x100)	VOC (Tonnes)	PM (Tonnes)	SOx (Tonnes)
Tanker	298	187,55	14	22	167
General Cargo	485	265,86	19	24	192
Container	28	13,73	1	2	11
Bulk Carrier	77	39,13	3	5	27
Other Ships	18	15,33	1	1	12
TOTAL	906	521,6	38	54	409

Figure 4. Yearly Emissions According to Vessel Types

Results and Discussion

Port Emissions

In this study, port emissions in the Trabzon port during operational modes (cruising, manoeuvring, and port) were assessed as 906 t y^{-1} for NO_X, 52.160 t y^{-1} for CO_2, 409 t y^{-1} for SO_X, 38 t y^{-1} for VOC, 54 t y^{-1} for PM for 2018. Yearly shipping emissions according to vessel types are presented in Figure 4.

Tanker and general cargo vessels produce the maximum level of emissions in the port and they make 87% of all the total port emissions. Bulk carriers, containers, and other vessels emit the rest of 13% emissions. These results match those observed in earlier studies such as Saracoglu *et al*. (2013); Alver *at al*. (2018); Popa and Florin (2014); Deniz and Kilic (2009) that general cargo and tanker vessels are the main emitters in the studied ports.

The cruising mode emissions are much more than the port and manoeuvring modes emissions. Figure 5 presents the emission rates during the operational modes. Cruising mode emissions are responsible for 81% of all port emissions, port mode emissions are 18%, and manoeuvring mode emissions are 1% of it.

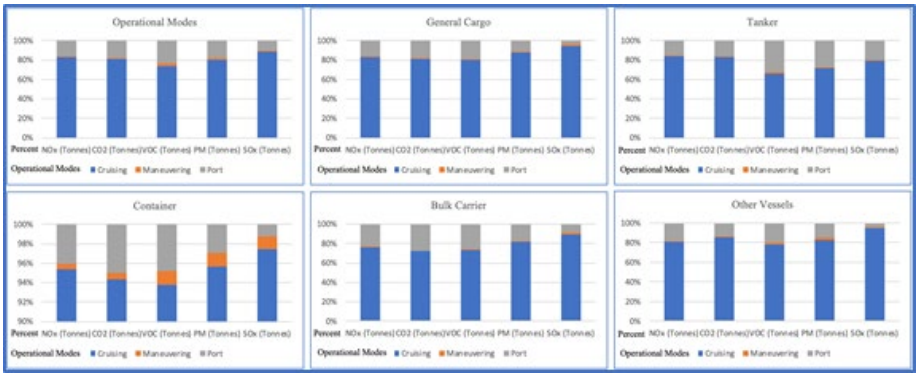

Figure 5. The Emission Rates During the Operational Modes

The Trabzon port emissions comparison with other ports emissions are presented in Table 3 and it can be assessed that the Trabzon port can be recognized as a minimum size harbour in the world-wide context.

Table 3. Comparison of Port Emissions

Ports	Year of Study	Hosted Number of Ships	NOx (ton y^{-1})	CO_2 (ton y^{-1})	PM (ton y^{-1})	SO_X (ton y^{-1})	Source
Ambarli Port, Turkey	2005	5.432	845	78.590	36	242	Deniz and Kilic, 2009
The Samsun Port	2015	2.504	728	-	64	574	Alver at al., 2018
Yangshan Port, China	2009	6.518	10.758	578.444	859	1.136	Song, 2014
The Port of Oslo, Norway	2013	3.004	759	56.289	18	260	Lopez-Aparicio et al., 2015
Port of Oakland, USA	2012	1.916	2.591	133.005	67	289	EIC, 2012
Izmir Port, Turkey	2007	2.806	1.923	82.753	165	1.405	Saraçoğlu et al., 2013
Las Palmas Port, Spain	2011	3.183	4.237	208.697	338	1.420	Tichavska and Tovar, 2015
The Trabzon Port	2018	679	906	52.160	54	409	This Study

Effects of Port Emissions on People

The population of Trabzon city is 807.903 according to the 2018 census conducted by Turkey Statistics Institute and the city has 18 districts. The port takes place in the Ortahisar district and this district is the biggest in the city with a population of 317.520 people. This district has 85 neighbourhoods. The neighbourhoods are divided into 5 zones according to distance from the port, starting from 0 km from the harbour area; **zone 1** (0-1 km from the harbour), **zone 2** (1-2 km from the harbour), **zone 3** (2-3 km from the harbour), **zone 4** (3-4 km from the harbour), **zone 5** (4-5 km from the harbour). There are 49 neighbourhoods within 5km from the Trabzon port which are under the threat of port emissions. The population to be affected by port emissions are shown in Table 4. At least 33.922 people living 1 km (zone 1) from the Trabzon port will be at risk due to harmful port emissions such as SO_X, NO_X, PM including other city emissions (residential heating, road traffic, and industry). As moved away from the port area, the number of people who will be exposed to emissions also increases. As seen

in Table 4, a maximum of 235.512 people will be in danger for any emissions, including port emissions. These results agree with the findings of other studies, in which Corbett et al. (2007); Eyring et al. (2009); NRDC (2004); Deniz and Kilic (2009) stated that the diesel engines of vessels, including other port vehicles, produce a large amount of air pollution that jeopardizes the health of people working in the port area and living near the port. All kinds of emission sources in the harbour area should be detected and measures to decrease the emissions should be executed in this context.

Table 4. Population to be Affected by Port Emissions

Zone 1 neighbourhoods	**Zone 2 neighbourhoods**	**Zone 3 neighbourhoods**	**Zone 4 neighbourhoods**	**Zone 5 neighbourhoods**
İskenderpaşa	Bahçecik	Çukurçayır	Aydınlıkevler	2 Nolu Beşirli
Boztepe	1 Nolu Erdoğdu	Üniversite	Soğuksu	1 Nolu Beşirli
Yenicuma	Kalkınma	3 Nolu Erdoğdu	Yeşiltepe	Karşıyaka
Gazipaşa	Kaymaklı	2 Nolu Erdoğdu	Fatih	Kutlugün
Cumhuriyet	2 Nolu Bostancı	İnönü	Toklu	Gölçayır
Değirmendere	Hızırbey	Yalı	Konaklar	Bengisu
Esentepe	Gülbaharhatun	Yenimahalle	Kanuni	Çilekli
Kemerkaya	Sanayi	1 Nolu Bostancı	Bulak	Aktoprak
Çömlekçi	Çarşı	Kurtuluş	Beştaş	
	Pazarkapı		Fatih Sultan	
	Ortahisar		Çamoba	
	Zafer			
Total Zone 1 Population	**Total Zone 1-2 Population**	**Total Zone 1-3 Population**	**Total Zone 1-4 Population**	**Total Zone 1-5 Population**
33.922	76.998	160.054	220.717	235.512

Environmental Costs

The environmental cost of the Trabzon port emission releases for each pollutant has been predicted for 2018 and was $32 million and $47.039 per ship call (Table 5). These results can be matched with further environmental costs. Berechman and Tseng (2010) analysed the environmental costs of Kaohsiung port as $123 million per year. Maragkogianni and Papaefthimiou (2015) assessed the releases of cruise vessels hosted by Greece ports such as Piraeus, Santorini, Mykonos, Corfu and Katakolo as €24.25 million. Song (2014) calculated the Shanghai Yangshan port`s social cost and eco-efficiency and the total social cost and eco-efficiency performance was found as $287 million, $36,528 respectively.

Table 5. Environmental Costs of the Trabzon Port

Pollutants	**NO_X**	**CO_2**	**VOC**	**PM**	**SO_X**	**Total Environmental Costs**
Environmental cost (Lee et al., 2010)	4.992 $/ton	26 $/ton	1.390 $/ton	375.888 $/ton	13.960 $/ton	-
The amount of port emissions	906 tons	52.160 tons	38 tons	54 tons	409 tons	-
Total environmental costs	4.522.752$	1.356.160$	52.820$	20.297.952$	5.709.640$	31.939.324$

Conclusion

The air emissions generated from ships in the Trabzon port were assessed as 906 t y^{-1} for NO_X, 409 t y^{-1} for SO_X, 52.160 t y^{-1} for CO_2, 54 t y^{-1} for PM, 38 t y^{-1} for VOC. General cargo and tanker vessels are accountable for the 87% exhaust gas emissions in the port, and container, bulk carrier, other vessels such as tugs, passenger vessels, service boats follow it. Ship-borne air emissions are emitted at cruising mode (81%), followed by port mode (18%). Port mode emissions are more than the manoeuvring mode (1%) since harbour handling activities are longer than the manoeuvring events. The following conclusions can be drawn from the present study that port emissions in the Trabzon port may have negative effects on the health of a minimum of 33.922 people living 1 km from the port area including other emissions (domestic heating, road traffic, and industry). All kinds of emission sources in the harbour area should be detected and measures to decrease the emissions should be executed in this context. This is the first study to estimate the Trabzon port emissions in the Black Sea region. The

present study made some remarkable contributions to literature about port emissions and supported other port emissions in the region.

Acknowledgments: *The author would like to thank the port authority for providing data.*

References

Alport Trabzon Liman İşletmeciliği AŞ (ATLIAŞ), (2019) Trabzon Port – *www.trabzonport.com.tr/* (retrieved on December 2019).

Alver F, Sarac BA, Sahin UA, (2018) Estimating of shipping emissions in the Samsun Port from 2010-2015. *Atmospheric Pollution Research,* **9** (2018) 822-828, *https://doi.org/10.1016/j.apr.2018.02.003*

Bayırhan İ, Mersin K, Tokuşlu A, Gazioğlu C, (2019) Modelling of Ship Originated Exhaust Gas Emissions in the Strait of Istanbul (Bosphorus). *International Journal of Environment and Geoinformatics*, **6** (3), 238-243. *https://doi.org/10.30897/ijegeo.457184*.

Berechman J, Tseng PH, (2010) Estimating the environmental costs of port related emissions: The case of Kaohsiung, *Transportation Research Part D* **17** (2012) 35–38. *doi: 10.1016/j.trd.2011.09.009.*

California Air Resources Board (CARB), (1998) *Draft Diesel Exposure Assessment*, A-7.

Corbett JJ, Winebrake JJ, Green EH, Kasibhatla P, Eyring V, Lauer A, (2007) Mortality from ship emissions: a global assessment, *Environmental Science & Technology* **41** (24), 8512–8518. *doi: 10.1021/es071686z*.

Çuhadaroğlu B, Demirci E, (1997) Influence of some meteorological factors on air pollution in Trabzon City, *Energy and Buildings*, **25**, 179-184, 1997

Çuhadaroğlu B, Demirci E, (2000) Statistical analysis of wind circulation and air pollution in urban Trabzon. *Energy and Buildings* **31** (2000) 49–53.

Deniz C, Kilic A, (2009) Estimation and assessment of shipping emissions in the region of Ambarlı Port, Turkey, *Environ. Prog. Sustain. Energy* 107-115. *http://dx.doi.org/10.1002/ep.10373*.

EMEP/EEA, (2016a) *International Maritime Navigation, International Inland Navigation, National Navigation (Shipping), National Fishing, Military (Shipping), and Recreational Boats*.

EMEP/EEA, (2016b) EMEP/EEA *Air Pollutant Emission Inventory Guidebook 2016.*

Entec, (2002) *Quantification of Emissions from Ships Associated with Ship Movements between Ports in the European Community*, European Commission, Final Report, Northwich, UK.

Entec, (2005) *European Commission, Directorate General Environment Service Contract on Ship Emissions: Assignment, Abatement and Market-based Instruments*, Task 1 - Preliminary Assignment of Ship Emissions to European Countries, Final Report, August 2005

Entec, (2007) *Ship Emissions Inventory Mediterranean Sea*, Final Report for Concawe.

Environ International Corporation (EIC), (2012) *Port of Oakland, Seaport Air Emissions Inventory*, Novato, California November 5, 2013.

Eyring V, Isaksen I, Berntsen T, Collins W, Corbett J, Endresen O, Grainger R, Moldanova J, Schlager H, Stevenson D, (2009) Transport impacts on atmosphere and climate: Shipping, *Atmospheric Environment* **44** (2010) 4735–4771. *http://dx.doi.org/10.1016/j.atmosenv.2009.04.059*.

Goldsworthy L, Goldsworthy B, (2015) Modelling of ship engine exhaust emissions in ports and extensive coastal waters based on terrestrial AIS data; An Australian case study, *Environmental Modelling & Software* **63** (2015) 45-60. *http://dx.doi.org/10.1016/j.envsoft.2014.09.009*.

Lee PTW, Hu KC, Chen T, (2010) External costs of domestic container transportation: short-sea shipping versus trucking in Taiwan, *Transport Reviews* **30**, 315-335.

Lonati G, Cernuschi S, Sidi S, (2010) Air quality impact assessment of at-berth ship emissions: Case-study for the project of a new freight port, *Science of the Total Environment* **409** (2010) 192–200. *doi: 10.1016/j.scitotenv.2010.08.029*.

Lopez-Aparicio S, Tønnesen D, Thanh TN, Neilson H, (2015) Shipping emissions in a Nordic port: Assessment of mitigation strategies, *Transportation Research Part D* **53** (2017) 205–216. *http://dx.doi.org/10.1016/j.trd.2017.04.021*.

Maragkogianni A, Papaefthimiou S, (2015) Evaluating the social cost of cruise ships air emissions in major ports of Greece, *Transportation Research Part D*. **36** (2015), 10-17. *http://dx.doi.org/10.1016/j.trd.2015.02.014*

Mauderly JL, (1992) *Diesel exhaust, Environmental Toxicants: Human Exposures and Their Health Effects,* ed. M Lippman (New York: Van Nostrand Reinhold).

Mersin K, Bayırhan İ, Gazioğlu C, (2019) Review of CO_2 Emission and Reducing Methods in Maritime Transportation, *Thermal Sciences*, 1-8.

Natural Resources Defense Council (NRDC), (2004) *Harboring Pollution: Strategies to Clean up U.S. Ports.* NewYork, USA: The Natural Resources Defense Council.

Popa C, Filorin N, (2014) *Shipping Air Pollution Assessment. Study Case on Constanta Port*, 14th International Multidisciplinary Scientific GeoConference SGEM 2014. *doi:10.5593/sgem2014/b42/s19.067*

Saraçoglu H, Deniz C, Kilic A, (2013) An investigation on the effects of ship sourced emissions in Izmir port, Turkey, *Sci. World J.* 2013 *http://dx.doi.org/10.1155/2013/218324*.

Song S, (2014) Ship emissions inventory, social cost and eco-efficiency in Shanghai Yangshan port, *Atmos. Environ.* **82**, 288-297. *http://dx.doi.org/10.1016/j.atmosenv.2013.10.006*.

Tezel MN, Sari D, Ozkurt N, Keskin SS, (2019) Combined NOx and noise pollution from road traffic in Trabzon, Turkey. *Science of the Total Environment* **696** (2019) 134044. *https://doi.org/10.1016/j.scitotenv.2019.134044*.

Tichavska M, Tovar B, (2015) Port-city exhaust emission model: An application to cruise and ferry operations in Las Palmas Port, *Transportation Research Part A* **78** (2015) 347–360. *http://dx.doi.org/10.1016/j.tra.2015.05.021*.

Topbaş M, Can G, Kapucu M, (2004) Effects of local decisions on air pollution in Trabzon, Turkey during 1994-2000, *Turkish Journal of Public Health* **2** (2), 80-84, 2004

Tokuslu A, (2020) Analyzing the Energy Efficiency Design Index (EEDI) Performance of a Container Ship. *International Journal of Environment and Geoinformatics (IJEGEO)*, **7(2)**: 114-119. *DOI: 10.30897/ijegeo*

Turkish Directorate General of Coastal Safety (TDGCS), (2019) *Port Statistics*, web page: *https://atlantis.udhb.gov.tr/istatistik/istatistik_gemi.aspx*, (retrieved on December 2019).

Türk YA, Kavraz M, Türk MH, (2008) *Trabzon Kentinde Hava Kirliligi ve İnsan Sagligina Etkileri*, (In Turkish), Hava Kirliliği ve Kontrolü Ulusal Sempozyumu-2008, 22-25 Ekim 2008, Hatay.

Türk YA, Kavraz M, (2011) *Air Pollutants and Its Effects on Human Healthy: The Case of the City Trabzon*. In AM. Moldoveanu (Ed.), Advanced Topics in Environmental Health and Air Pollution Case Studies (pp.251-268).

Ulfvarson U, Alexandersson R, Dahlgvist M, Elkolm U, Bergstrom B, (1991) Pulmonary function in workers exposed to diesel exhausts: The effect of control measures," *American Journal of Industrial Medicine*, Vol. **19**, 3 (1991): 283–289.

Uzunali D, (2004) *Air pollution maps based on the data collected between 1998 and 2002 for the center of Trabzon City*, (In Turkish), M.Sc. Thesis, Department of Mechanical Engineering, Karadeniz Technical University.

Yang DQ, Kwan SH, Lu T, Fu QY, Cheng JM, Streets DG, Wu YM, Li JJ, (2007) An emission inventory of marine vessels in Shanghai in 2003, *Environ. Sci. Technol.* **41**, 5183-5190. *http://dx.doi.org/10.1021/es061979c*.

Yomralioglu T, Colak EH, Aydinoglu AC, (2009) Geo-Relationship between Cancer Cases and the Environment by GIS: A Case Study of Trabzon in Turkey. *Int. J. Environ. Res. Public Health 2009*, **6**, 3190-3204; doi: *10.3390/ijerph6123190*.

J. Int. Environmental Application & Science, Vol. 15(2): 135-140 (2020)

Research Paper

Improvement of Fungal Oil Production from Apple Processing Industry Wastewater

H. Duygu BİLGEN*, Süreyya DÖŞLÜ ÇETİNKAYA

Mersin University, Engineering Faculty, Department of Environmental Engineering, 33343, Mersin, TURKEY

Received April 04, 2019; Accepted June 12, 2020

Abstract: Turkey has an important place in the world ranking in terms of apple production area and apple processing products. During the process, apple processing industries produce high amounts of fruit washing water with high Chemical Oxygen Demand (COD) and acidic properties, which are highly suitable for use as a fungal substrate. It is also known that fungal oils produced by oleaginous fungi from wastewater is also suitable to produce low-cost biodiesel as an alternative fuel. In this study apple processing industry wastewater was used as an alternative substrate for *Mucor circinelloides* and the C/N/P ratio was changed to improve fungal lipid production. Maximum oil content of dry fungal biomass was 17.7 %. Composition of fatty acids from the fungal oil were also analyzed and gas chromatography analyses showed that the major fatty acid was oleic acid (C18:1, 31.62 %) which is very suitable for biodiesel production. Results of the study indicated that fungal oil produced from the low-cost substrate apple processing industry wastewater can be useful as an alternative source for different industries especially in the bio-energy for the future.

Keywords: Apple processing industry, wastewater, fatty acid, fungal oil, *Mucor circinelloides*, value-addition.

Introduction

Rapid population growth and rapid industrial development have led to an increase in new food products and agricultural practices, and consequently the rapid depletion of natural resources. Therefore, the increase of industrial and agricultural wastes and the decrease of fossil fuels constitute the most important environmental problems (Owusu & Asumadu-Sarkodie, 2016). To minimize the environmental damages of these wastes, on the other hand, to find alternative energy sources is the focus of recent researches. Biofuels, on the other hand, are an alternative fuel source for reducing dependence on fossil fuels. Biofuels have many advantages, such as energy independence, reduction of greenhouse gas emissions and economic sustainability. It is known that the oils of various plants are used in the production of biodiesel which is a type of biofuel. However, the use of primary foods and favorable agricultural land for biodiesel production has recently led to controversy.

It is known that microbial oils (single cell oils) can be produced by many microorganisms and these oils have a very high potential as a raw material for biodiesel production. In addition, microorganisms are not affected by changing seasonal and climatic conditions, having a high amount of oil content in the cells. Microorganisms can be produced in large quantities in a short time compared to plants, which makes biodiesel production superior to microbial oils (Xue, 2006). In recent years, oil accumulating fungi have been seen as a preferred raw material for the sustainable biodiesel industry (Sankaran *et. al*., 2010; Khot *et al*, 2012; Bhanja *et.al*., 2014; Amoozegar; 2019).

Among the oil-producing fungi, the genus *Mucor* is of great biotechnological importance since they can accumulate high levels of triacylglycerol in the mycelium. Concerning lipid-producing *Mucor spp*, several previous studies in the literature have reported that *Mucor circinelloides* offer polyunsaturated fatty acids-rich lipids that can be used as alternative raw materials to obtain biodiesel (Annie, 2018).

The production of new food products and fruit juices from fruits leads to the formation of by-products or waste water containing high amounts of organic matter. Ucar *et al*. (2016) reported that the demand for apple products increases gradually both in the Turkey and the world. Countries with highest production of apples include China (49.10%), United States (5.05%), Turkey (3.87%), Poland (3.82%), and Italy (2.74%). Because of suitable climate, apple production in Turkey increases year by year resulting in significant amount of wastewater production from their processing industries. It is not possible to discharge this wastewater into the receiving environment without treatment, representing a significant

* *Corresponding: E-Mail: hduygubilgen@gmail.com; Tel: +903243610001/7102 Fax: +903243610032*

financial burden on industries. However, due to the presence of polysaccharides, nitrogen, phosphorus, various minerals and organic acids, it is possible to convert this wastewater into a suitable medium for the growth of fungi. The utilization of wastewater compounds by fungi can result in wastewater sufficiently clean to meet the discharge and/or recycling criteria while simultaneously increasing biomass yield and oil composition, the extent of which depending on the environmental conditions and species selected (Puyol *et al*., 2017).

There are various studies on the use of fungal oils in biodiesel production. However, the use of industrial waste streams as a substrate for the production of fungal oil for subsequent biodiesel production has been limited.

Materials and methods

Wastewater supply and analysis

In this study, wastewater of apple processing industry (Anadolu Etap Agriculture and Food Products Industry) located in Mersin, Turkey was used as a substrate in fungal oil production.

Chemical Oxygen Demand (COD), pH, conductivity and Total Nitrogen (TN) analyzes were performed in order to characterize the wastewater supplied. TN analyzes were performed with Hach brand LCK138 nitrogen kits with a measuring range of 1-16 mg / L. COD analyzes were performed both with Hach brand LCK514 kits with a measuring range of 100-2000 mg / L and standard methods (5220 C) (Standard Methods, 2005). Total Phosphate (TPO_4^{3-}) analyzes were performed according to the phosphorolybdenum blue method with Hach brand LCK348 test kits. All analyzes performed for the characterization of wastewater were carried out in 3 replicates (Table1).

Renewal and inoculation of fungal cultures

0.1mL of *M. circinelloides* spore stocks in glycerin stored at -85 ºC were used as the inoculum to inoculation of Potato Dextrose Agar (PDA) plates at aseptic conditions and incubated at 31 ^{0}C for 5 days (Mitra et al., 2012). At the end of the incubation period, agar fragments were cut to about 1 cm^2 from the solid culture of the fungi and inoculated into flasks containing sterilized Potato Dextrose broth. The flasks were incubated for 2 days in an orbital shaking incubator at 31 ºC and 150 rpm.

Incubated *M. circinelloides* biomass in the flasks was separated from the liquid phase by filtration under sterile conditions and washed twice with sterile isotonic serum (0.09% NaCl solution). Therefore, the carbon source that is likely to come from the pre-culture medium is removed. Then the fungal biomass was rinsed with sterilized de-ionized water to remove any salt from the NaCl solution. The washed fungal biomass was placed into 250 mL Erlenmeyer flask containing 100 mL of sterile deionized water and homogenized under sterile conditions for 135 seconds at 13500 rpm to produce fungal inoculation solution for oil production experiments.

Determination of fungal biomass and oil yields

Homogenized *M. circinelloides* mycelium suspensions were then oven dried at 80 ºC for 24 h. All of the experiments were performed in triplicate. Yields and coefficients were determined according to equations below (Carota et al., 2017; Chan et al., 2018):

The biomass yield was expressed as grams of dry biomass per liter of Apple Processing Industry Wastewater (g/L). Oil yield (ΔP) was calculated according to Eq. (1) (g/L):

$$\Delta P = \Delta X \times (C_L/100) \quad (1)$$

where ΔX is the biomass yield (g/L) and C_L is the intracellular oil content (%).

Optimization of growth and oil production conditions

Optimization of carbon /nitrogen /phosphorus (C/N/P) ratios of wastewater was investigated in order to increase fungal oil production. For this purpose, wastewater has been prepared in three different C/N/P ratios, 100/18/1, 100/10/1 and 100/5/1. Urea, D-Glucose, K_2HPO_4 and KH_2PO_4 were added to provide necessary ratios. The pH of wastewaters with different C/N/P content was then adjusted to 6.00, the optimum pH of *M. circinelloides* fungi, by addition of 1 M NaOH solution. Wastewaters with different C/N/P ratios were added to the 4L volume reactor and autoclaved with glass reactor at 121 ºC for 15 minutes.

After sterilization, 100 mL of homogenized fungal biomass was inoculated into the reactor under aseptic conditions and incubated for 48 hours at 31 ºC, 200rpm agitation and the addition of oxygen from the bottom of the reactor with a diffuser. At the end of the incubation period, fungal biomass was harvested from wastewater and oven dried 60 ºC for 24 hours.

Intracellular fungal-oil extraction using high-power ultrasonication

The oven-dried fungal cells were subjected to ultrasonication for 30 min with a maximum power output of 400W and frequency of 40 kHz (Mercury) in the presence of toluene and methanol (1:1, v:v) to disrupt the cell wall of fungus and extraction of the intracellular oil (Christi et al, 2010; Mitra et al., 2012). After the ultrasonic bath, the biomass was filtered (whatman no. 1) into the flask and washed with methanol-chloroform (2:1, v:v) solutions. The flasks were then kept in an oven at 60 ºC until the organic solvents became volatile. After that step, the flasks were kept in desiccator for 30 minutes and the extracted oils were weighed (Mitra et al., 2012).

Analytical methods for fatty acid analysis of fungal oil

Fatty acid profiles of microbial oils were performed by a Agilent 7890A gas chromatograph equipped with HP Innowax column (30 m length, 0.25 mm internal diameter, 0,25µm film thickness) and a flame ionization detector. The operating conditions were as follows: detector temperature at 330 ºC and initial oven temperature at 140 ºC held for 5 min then raised to 250 ºC at a rate of 10 ºC /min, then held at 250 ºC for 15 min. Carrier gas was helium (20 cm/sec), injection mode 1 µl, 280 ºC, split 100:1. Chromatographic peaks and retention times were identified by the comparison to a fatty acid methyl ester (FAME) standard mixture and individual peaks were quantified by means of external standards and their corresponding calibration curves.

Conclusion

Determination of optimum C/N/ P ratio of wastewater

According to the results of the determination of dry fungal biomass, 1 mL homogenized mycelial suspension contained 9.32 g/L fungal dry mass. In the studies to determine the optimum C/N/P content of the wastewater, it was observed that the development of mycelium was favored when using a C/N/P ratio of 100/10/1.

In regards to the biomass yield and composition, the amount of wet and dry fungal biomass harvested from wastewater with different C/N/P ratio and the mass of the oil extracted from the dry fungal biomass are given in Table 2. Picture depicting the various biomass oil yields are shown in Figure1.

Figure 1. Oils from fungal biomass developed in wastewater with different C/N/P ratios (left:100/5/1; middle:100/10/1; right:100/18/1).

As described in Table 2, the highest oil production yield (17.7%) was achieved with the use of wastewater with a 100/10/1 ratio. Previous studies indicated that the fungal oil yield of the oleaginous fungi growth in different substrates were obtained between 12% and 24% by different researchers. Vicente et al. (2009), investigated the effects of temperature, pH and solvents used for extraction on fungal oil yield and reported yield values ranging from 15.3% to 19.9%. Chan et al. (2018) reported that *M. circinelloides* oil yield reached 24% of dry biomass and 2.20 g/L whey permeate, at 168 h incubation period.

Table 1. Characterization of apple processing industry wastewater

Chemical Oxygen Demand (COD)	**2400 mg/L**
Total Nitrogen (TN)	428 mg/L
Total Phosphate (TPO_4^{3-})	2.47 mg/L
pH	4.70
Temperature	23°C
Suspended solid	740 mg/L

Table 2. Wet and dry fungal biomass harvested from wastewater with different C/N/P ratio and amount of obtained fungal oil.

Wastewater with different C/N/P ratio	**Wet Fungal Biomass (g/L)**	**Biomass Yield (ΔX)**	**Oil yield (ΔP)**	**C_L (%)**
100/5/1	184.180	7.898	0.408	5.17
100/10/1	330.406	17.072	3.015	**17.67**
100/18/1	165.386	10.609	0.698	6.58

The oil yield observed in our study is in agreement with the values reports in the literature using other substrates, although is below the maximum value reported. However, apple processing wastewater is considered as a good alternative for producing single cell oil due to its availability and low cost. The process herein developed can be further scaled up to pilot-and industrial-scale.

Fatty acid profile of fungal oil

The chromatogram of the fungal oil obtained from *M. circinelloides* growth in apple processing industry wastewater shown in Figure 2. Fatty acid types and contents (%) of the obtained oil are also given in Table 3.

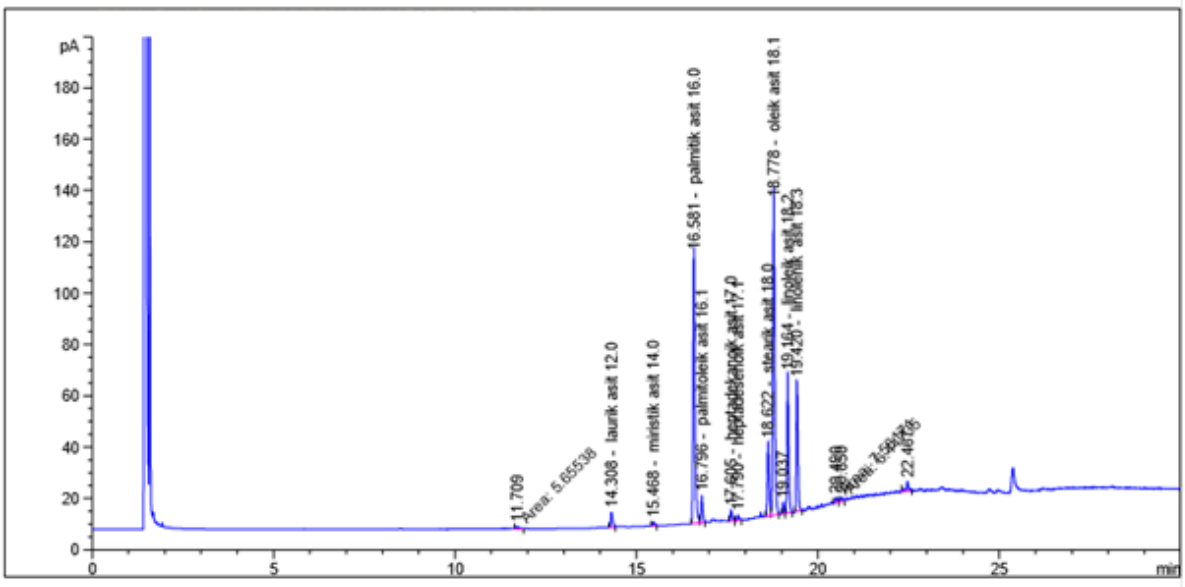

Figure 2. Fatty acid profile of fungal oil obtained from *M. circinelloides* growth in apple processing wastewater.

When the fungal lipids are examined, it is known that the most common linolenic acid (C18: 3) is the precursor of omega-6 fatty acids. Linoleic acid is converted to gamma linolenic acid (GLA), an important food supplement in the body. Therefore, the fungal biomass is known to be a rich source of gamma linolenic acid (Ratledge, 2004).

Table 3. Fatty acid composition and contents (%) of the fungal oil obtained from the cultivation of *M. circinelloides* in Apple Processing Wastewater.

Fatty acid types	Fatty Acid Standard Number	Content (%)
Oleic acid	C18:1	31.62
Palmitic acid	C16:0	27.74
Linoleic acid	C18:2	12.24
Linolenic acid	C18:3	11.64
Stearic acid	C18:0	7.34
Palmitoleic acid	C16:1	2.34
Lauric acid	C12:0	1.53
Heptadecanoic acid	C17:0	1.07

The high content of oleic acid which is one of the monounsaturated fatty acids of the fungal oil obtained in the study shows that this oil can be a preferred substrate for biodiesel production (Durett et. al., 2008; Sit-up et al., 2013; Sitepu et al., 2014). Moreover, linolenic acid (11.64 %), was also reported to have beneficial effects for the prevention and treatment of inflammatory disorders, diabetes, cardio-vascular disorders, cancers and some other diseases (Horobbin, 1992; Fan and Chapkin, 1998; Lu and Zhu, 2015; Kim et al., 2012).

Acknowledgement: *This study is part of a research project (2017-2-AP3-2387) funded by Mersin University, Department of Scientific Research Projects. The authors would like to thank Anadolu Etap Agriculture and Food Products Industry for providing wastewater.*

References

Amoozegar MA, Safarpour A, Noghabi KA, Bakhtiary T, Ventosa A, (2019) Halophiles and Their Vast Potential in Biofuel Production, *Front. Microbiol.* **10,**1895, 1-17.

Annie L, Laurence MC, Stéphanie MS, Emmanuel C. Jean-Luc J, Georges B, Erwan C, (2019) Comparative analysis of five Mucor species transcriptomes, *Genomics*. **111**, 1306-1314.

Bhanja A, Minde G, Magdum S, Kalyanraman V, (2014) Comparative Studies of Oleaginous Fungal Strains (*Mucor circinelloides* and *Trichoderma reesei*) for Effective Wastewater Treatment and Bio-Oil Production", *Biotech. Res. Int*., **2014**, 1-7.

Carota E, Crognale S, D'Annibale A, Gallo AM, Stazi SR, Petruccioli M, (2017) A sustainable use of ricotta cheese whey for microbial biodiesel production, *Sci Total Environ*., **584**,554–560.

Chan GL, Cohen LJ, Ozturk G, Hannebelle M, Taha AY, de Moura Bell JMLN, (2018) Bioconversion of cheese whey permeate into fungal oil by *Mucor circinelloides*, *J. Biol. Engin.,* **12**:25, 1-14.

Christi WW, Han X, (2010) Lipid Analysis- Isolation, Separation, Identification and Lipidomic Analysis, The Oily Press Lipid Library, **24**, eBook ISBN**:** 9780857097866.

Durrett TP, Benning C, Ohlroogee J, (2008) Plant triacylglycerols as feedstocks for the production of biofuels, *Plant J.*, **54**, 593-607.

Fan YY, Chapkin RS, (1998) Importance of dietary gamma-linolenic acid in human health and nutrition. *J. Nutr.*. **128**, 1411–1414.

Horrobin DF, (1992) Nutritional and medical importance of gamma-linolenic acid, *Prog Lipid Res*. **31**, 163–194.

Khot M, Kamat S, Zinjarde S, Pant A. Chopade B, RaviKumar A, (2012) Single cell oil of oleaginous fungi from the tropical mangrove wetlands as a potential feedstock for biodiesel, *Microbial Cell Factories*, **11**, 71-84.

Kim DH, Yoo TH, Lee SH, Kang HY, Nam BY, Kwak SJ, Kim JK, Park JT, Han SH, Kang SW, (2012) Gamma linolenic acid exerts anti-inflammatory and anti-fibrotic effects in diabetic nephropathy, *Yonsei Med J*. **53**, 1165–1175.

Lu H, Zhu Y, (2015) Screening and molecular identification of overproducing gamma-linolenic acid fungi and cloning the delta 6-desaturase gene, *Biotech.l Appl Biochem*. **62**, 316–322.

Mitra D, Rasmussen ML, Chand P, Chintareddy VR, Yao L, Grewell D, Verkade JG, Wang T, van Leeuwen JH, (2012) Value-added oil and animal feed production from corn-ethanol stillage using the oleaginous fungus *Mucor circinelloides*, *Biore. Tech*. **107**, 368–375.

Owusu PA, Asumadu-Sarkodie S, (2016) A review of renewable energy sources, sustainability issues and climate change mitigation, *Cogent Engin.*, **3**, 1-14.

Puyol D, Batstone DJ, Hülsen T, Astals S, Peces M, Krömer JO, (2017) Resource Recovery from Wastewater by Biological Technologies: Opportunities, Challenges, and Prospects, *Front. Microbiol*. **7**, 1-23.

Ratledge C, (2004) Fatty acid biosynthesis in microorganisms being used for Single Cell Oil production, *Biochimie*. **86**, 807–815.

Sankaran S, Khanal SK, Jasti N, Jin B, Pometto AL, Van Leeuwen JH, (2010) Use of filamentous fungi for wastewater treatment and production of high value fungal byproducts: a review, *Cri. Rev. in Environ. Sci. & Tech.*, **40**, 400–449.

Standard Methods for the Examination of Water and Wastewater, (2005) American Public Health Association/ American Water Works Association/Water Environment Federation (APHA/AWWA/WEF), 21st Washington DC, USA.

Sitepu RI, Jin M, Fernandez JE, da Costa Sousa L, Balan V, Boundy-Mills KL, (2014) Identification of oleaginous yeast strains able to accumulate high intracellular lipids when cultivated in alkaline pretreated corn stover, *Appl. Microbio. Biotech*. **98**, 7645-7657.

Sitepu RI, Sestric R, Ignata L, Levin D, German JB, Gillies LA, Amanda LAG, Boundy-Miles KL, (2013) Manipulation of culture conditions alters lipid content and fatty acid profiles of a wide variety of known and new oleaginous yeast, *Biore. Tech*. **144**, 360-369.

Uçar K, Engindeniz S, Markovic T, Kokot Z, (2016) Analysis of Changes in Apple Production in Turkey, In: 27th International Scientific-Expert Congress of Agriculture and Food Industry, pp:147-151, Bursa-Turkey.

Vicente G, Bautista LF, Rodríguez R, Gutiérrez FJ, Sádaba I, Ruiz-Vázquez RM, Torres-Martínez S, Garre V, (2009) Biodiesel production from biomass of an oleaginous fungus, *Biochem. Eng. J*. **48**, 22–27.

Xue F, Zhang X, Luo H, Tan T, (2006) A new method for preparing raw material for biodiesel production, *Process Biochem*. **41**, 1699-1702.